

Engineering Hybrid Polymer Materials for Enhanced Biosensing

Engineering Hybrid Polymer Materials for Enhanced Biosensing

By Yang Lu, BASC

A Thesis Submitted to the School of Graduate Studies in Partial Fulfilment of the
Requirements for the Master's Degree of Biomedical Engineering

McMaster University © Copyright by Yang Lu, September 2020

TITLE: Engineering Hybrid Polymer Materials for Enhanced Biosensing

AUTHOR: Yang Lu, BASC (University of Toronto)

SUPERVISOR: Professor Todd R. Hoare

NUMBER OF PAGES: 185

LAY ABSTRACT

Electrochemical biosensors are analytical devices that convert the signal of a biological reaction into an electrochemical signal and are used in a range of clinical, pharmaceutical, agricultural, and food applications. Since their first development, scientists have put many efforts into designing smaller, more accurate, and more automated biosensors. One approach for achieving these goals is through the integration of various types of polymers. Magnetic microgels, crosslinked three-dimensional polymer networks containing entrapped magnetic materials, are demonstrated to help achieve these goals by carrying higher quantities of biological components relative to two-dimensional surfaces while being separable easily with a magnet after the sensing reaction is complete. To satisfy the end-use, magnetic microgels with optimal size, stability, magnetization properties, and functionality were designed in this project.

Another general focus in the area of biosensors is to achieve detection of targets without the need to pre-process the source sample (e.g. blood, urine, saliva, etc.) prior to analysis. However, most in-field biosensors have to work with untreated clinical samples and thus generate noisy or low-resolution signals. Polymer can play an important role in reducing this interfering signal by preventing the interfering molecules from approaching the detector. While coating the detector with a highly water-loving polymer can minimize such interference, such polymers are typically non-conductive and as such also block the desired signal from target binding. Therefore, thin layer polymer coatings were designed and optimized to repel interfering molecules without influencing the detection of targets.

ABSTRACT

Biosensors, as a potential diagnostic tool contributing to next-generation medicine, have been continuously researched and optimized to achieve improved performance with lower cost. Among them, electrochemical sensors coupled with multi-functional polymers have attracted particular attention because of their ability to provide real-time, quantitative, and highly-sensitive analysis. For example, appropriate polymers can enhance the bioavailability of an immobilized biomolecule or recognition elements and/or facilitate lower limits-of-detection when used as a coating.

In this thesis, magnetic microgel beads and ion-conductive polymers were fabricated to serve as anti-fouling bioactive immobilization platforms. Magnetic microgel beads are routinely used in biosensing and bioseparation applications given their high surface area for immobilization (and thus high capacity to capture biomolecules) coupled with their facile separation from suspension using a magnetic field. However, current magnetic beads are typically based on silica or polystyrene and thus have relatively poor protein-repellent properties, leading to enhanced binding of non-target molecules and thus reduced signal:noise ratios. In response, magnetic microgel beads based on the highly protein-repellent polymer poly(oligo(ethylene glycol) methacrylate (POEGMA) were fabricated using a semi-batch inverse emulsion polymerization. The resulting microgel beads have a narrow size distribution centred around $\sim 5 \mu\text{m}$, a low level of aggregation, and high colloidal stability, all at a low cost. Effective magnetic separation can be achieved within five minutes, while the inherent protein-repellent properties of POEGMA

significantly reduce non-specific protein adsorption. Upon using carbodiimide chemistry to tether a methylene blue-linked DNAzyme to the microgel bead that is selectively cleaved in the presence of *E. coli*, a 6.3-fold higher signal was measured upon exposure to *E. coli* in buffer and a 97-fold higher signal retention was achieved in clinical urine (based on the electrochemical detection of released methylene blue from capture probes) relative to that achieved with Dynabeads[®], a leading commercial magnetic bead.

To reduce non-specific adsorption on gold electrodes without compromising the conductivity and thus signal:noise of the electrochemical device, three types of water-soluble polymers were synthesized and tested for their anti-fouling performance and conductivity when coated on gold electrodes. POEGMA polymer functionalized with (2,2,6,6-tetramethylpiperidin-1-yl)oxyl (TEMPO) failed to show sufficient conductivity, while POEGMA polymer functionalized with thiol groups that bound directly to the gold electrode maintained sufficient ion conductivity but reduced the DNA signal at the desired voltage (as generated by hybridization between cleaved probes from DNAzyme and capture probes grafted on electrodes). The possible explanation is that the capture probes were not immobilized on polymer efficiently because of the reversibility of imine bonds formed between amine labelled probes and aldehyde groups from polymer. Zwitterionic polymer poly[2-(methacryloyloxy)ethyl]dimethyl-(3-sulfopropyl)ammonium hydroxide] (PDMAAPS) functionalized with thiol groups enhanced the conductivity of the electrode (showing a lower resistance to ion

conductivity even compared to the bare electrode), although further optimization is still required to realize higher DNA signals for clinical applications.

Overall, both magnetic beads microgels and conducting non-fouling polymers enabled significantly improved performance of electrochemical biosensors for *E.coli* detection.

Magnetic microgel beads show potential for commercialization in the future.

Acknowledgements

Throughout my Master's studies in McMaster University, I was surrounded and supported by many great people, but I want to first express my sincere appreciation to my supervisor, Dr. Todd Hoare, who offered me chance to study and work in such a wonderful place and always motivates, understands, and inspires me. I also want to thank Dr. Leyla Soleymani and Dr. Yingfu Li for providing me valuable suggestions and guidance to my projects.

I would like to thank every member in Dr. Hoare's group. It has been a great pleasure to work with all of you, especially Pan who mentored me on the polymer synthesis and provided lots of help. I also want to thank members from other research groups, especially to Richa Pandey from Dr. Leyla Soleymani's group who helped me conduct all of the electrochemical testing on the polymer as well as to Zijie Zhang and Dingran Chang from Dr. Yingfu Li's group, who synthesized DNazymes and prepared *E.coli* crude intracellular matrix. I can't finish this project without your help. I want to thank Dr. Robert Pelton, Dr. Alex Adronov, and facility members in Biointerfaces Institute for providing me access and training for instruments. To the entire School of Biomedical Engineering, thanks for always being so helpful. By participating all kinds of interesting departmental activities, I not only gained valuable experience and knowledge in research, but also met lots of new people and made friends with them.

Finally, I want to express my special thanks to my parents. Thank you for your unconditional love and supports, allowing me to chase my dream without any burdens. It's you who encourage me to improve every day and be a better person.

LIST OF FIGURES

Figure 1.2.1 Illustration of the hysteresis loop for materials with collective magnetism.

Figure 1.2.2 Difference between the hysteresis and magnetization observed between superparamagnetic and ferromagnetic materials. [1]

Figure 1.2.3. Illustration of the different structures of polymer magnetic beads.

Figure 1.2.4 Illustration of the three phases of the emulsion polymerization process and the corresponding kinetics. [2]

Figure 1.2.5 Illustration of the different stages of dispersion polymerization.

Figure 1.2.6. Illustration of cross flow filtration and dead-end filtration strategies for membrane emulsification. [3]

Figure 2.1 Schematic illustration of POEGMA-co-MAA magnetic microgel beads crosslinked by EDGMA with iron oxide particles physically encapsulated inside the polymer matrix.

Figure 2.2 Schematic illustration of magnetic microgel bead preparation and application.

Figure 2.3 Particle size distribution of magnetic microgel beads produced based on the protocol of Keiwet et al. [4]

Figure 2.4 Mechanical properties of magnetic microgel beads as measured using the MicroSquisher.

Figure 2.5 Magnetic beads produced by adjusting the pH of water phase to ~ 7 and using a mechanical stirrer.

Figure 2.6 Comparison between 5 wt% MAA functionalized magnetic particle and 30 wt% MAA functionalized magnetic particles.

Figure 2.7 Optical microscope images for magnetic beads synthesized with different surfactant concentration.

Figure 2.8 Base-into-acid conductometric titration curve.

Figure 2.9 (a). Thermogravimetric analysis for 30 wt% MAA functionalized magnetic beads. (b). Electrochemical assay measuring the current associated with the methylene blue labeled DNA probe released from *E.coli* DNAzyme.

Figure 2.10 Particle stability over a one month period as tracked by changes in (a) electrophoretic mobility and (b) particle size.

Figure 2.11 Illustration of two different possible pathways of magnetic microgel degradation.

Figure 2.12 Anti-fouling/protein repellency test for POEGMA magnetic microgel beads and commercial Dynabeads.

Figure 2.13 Electrochemical test comparing the performance of magnetic microgel beads (pMB) prepared with low and high degrees of MAA functionalization with commercial magnetic beads (cMB).

Figure 2.14 Electrochemical test comparing the performance of magnetic microgel beads (pMB) and magnetic microgel beads (cMB) with *E.coli* CIM of different concentrations.

Figure 2.15 Electrochemical test comparing the performance of pMB and cMB in buffer and in urine. The electrochemical signal was quantified by the redox current from released methylene blue following the hybridization of DNA barcodes with capture probes.

Figure 2.16 Fluorescence test showing the loading and cleavage efficiency of magnetic microgel beads (pMB) compared with commercial Dynabead magnetic beads (cMB) loaded with different amount of *E.coli* DNAzymes.

Figure 2.17 Limit of detection for designed electrochemical biosensors based on the use of magnetic microgel beads as an aRCD immobilization platform by performing the test in buffer and in undiluted urine.

Figure 3.1 Illustration of the reaction pathways for synthesizing (a) POEGMA-Ald and (b) POGMA-Ald-MAA.

Figure 3.2. Chemical structures of (a) TEMPO-grafted POEGMA-Ald and (b) TEMPO-grafted POEGMA-Ald-MAA.

Figure 3.3 Synthesis pathway for grafting thiols to POEGMA-Ald-MAA.

Figure 3.4 Cyclic voltammetry of nanostructured gold electrodes coated with POEGMA-Ald-MAA polymer grafted with different degrees of TEMPO compared to the bare electrode.

Figure 3.5 Illustration of the interaction between polymer and gold electrodes.

Figure 3.6. Cyclic voltammetry result for nanostructured gold electrodes coated with POEGMA-Ald-MAA polymer functionalized with different degrees of thiolation compared to an uncoated electrode.

Figure 3.7 Square wave voltammetry result for the redox current of methylene blue produced by the hybridization between methylene blue labelled DNA probes (barcodes) and capture probes immobilized on thiolated polymers.

Figure 3.8 Cyclic voltammetry result for nanostructured gold electrodes coated with a 15 mol% thiolated POEGMA-Ald-MAA polymer with 30 mol% aldehyde functionalization compared to a bare gold electrode.

Figure 3.9 Square wave voltammetry result for the redox current of methylene blue produced by the hybridization between methylene blue labelled DNA probes (barcodes) and capture probes immobilized on a 15 mol% thiolated POEGMA-Ald-MAA polymer with 30 mol% aldehyde functionalization.

Figure 3.10 Cyclic voltammetry result for nanostructured gold electrodes with zwitterionic polymer and sulfonic acid acrylic polymer comparing to that without polymer coating.

Figure 3.11 Anti-fouling test for thiolated POEGMA polymers coated on a polystyrene surface.

Figure 3.12 Anti-fouling test for various thiolated POEGMA polymers and thiolated zwitterionic polymer coated on a sputter-coated gold electrode interface by using FITC-labelled BSA as model protein.

Figure S.1 XPS scan for gold surface before the polymer coating (left) and after polymer coating (right).

LIST OF TABLES

Table 1.1 Summary of the change in magnetization with an applied magnetic field and the temperature susceptibility for different types of magnetic materials.

Table 2.1 Summary table for sequence of amine-labeled *E. coli* DNAzyme probes (aRCD).

Table 3.1 Summary of molecular weight and PDI of POEGMA-Ald and POEGMA-Ald-MAA polymers synthesized.

Table 3.2 Summary of ¹H-NMR result on the degree of aldehyde copolymerization and degree of 4-amino TEMPO grafting to aldehyde groups.

Table 3.3 Summary of base-into-acid conductometric titration results for the degree of MAA copolymerization and the degree of 4-amino TEMPO grafting to the carboxyl groups.

Table 3.4 Summary of the molecular weight, degree of thiol functionalization, and molar ratios of free thiols for thiolated POEGMA-Ald-MAA polymers synthesized.

LIST OF ABBREVIATIONS

RCD	RNA cleaving DNzyme
MB	Magnetic beads
pMB	Polymer magnetic beads
cMB	Commercial magnetic beads (MyOne carboxylic acid TM modified Dynabeads)
CIM	Crude intracellular matrix
INP	Iron oxide nanoparticles
PEG	Poly(ethylene glycol)
PEO	Poly(ethylene oxide)
POEGMA	Poly(oligo(ethylene glycol) methacrylate)
DMAPS	[2-(Methacryloyloxy)ethyl]dimethyl-(3-sulfopropyl) ammonium hydroxide
MAA	Methacrylic acid
OA	Oleic acid
SDS	Sodium dodecyl sulfate
W/O	Water in oil
O/W	Oil in water
AAEM	(2-acetoacetoxy) ethyl methacrylate
NSA	Non-specific adsorption
SAM	Self-assembled monolayer

Table of contents

Contents

Chapter 1: Introduction and Literature review	1
1.1 DNAzyme based electrochemical sensor	1
1.1.1 RNA cleaving DNAzymes	1
1.1.1.1 Selecting RNA cleaving DNAzyme for biosensing	2
1.1.1.2 Translating RNA cleaving DNAzyme to bio-recognition elements	3
1.1.2 Electrochemical biosensor	4
Part I. Magnetic Beads	5
1.2.1 Magnetic properties/magnetism	6
1.2.2 Synthesis of magnetic beads	11
1.2.2.1 Synthesis of iron oxide nanoparticles (INP)	12
1.2.2.2 Synthesis of polymer magnetic beads (pMB)	15
1.2.2.2.1 Conventional synthesis routes	16
1.2.2.2.2 Special synthesis routes or fabrication methods	29
1.2.3 Surface modification	34
1.2.3.1. Surface modification of iron oxide nanoparticles (INP)	34
1.2.3.2. Surface modification of polymer magnetic beads (pMB)	37
1.2.4 Applications	40
Part II. Anti-fouling coating for electrochemical biosensor	46
1.3.1 Understanding adsorptions on electrochemical biosensor	47
1.3.2 Mechanisms and strategies of reducing fouling/NSA	48

1.3.3 Surface modifications to reduce biofoulants/NSA	50
1.4 Objectives	53
Chapter 2: Multifunctional Ultra-Low Fouling Magnetic Microgel Beads for DNAzyme Immobilization	
2.1 Introduction	55
2.2 Objectives	57
2.3 Experimental Section	59
2.3.1 Materials	59
2.3.2 Iron Oxide Nanoparticles (INP) Synthesis	60
2.3.3 Magnetic Microgel Synthesis	61
2.3.4 Mechanical testing	62
2.3.5 Size characterization	63
2.3.6 Conductometric base-into-acid titration	64
2.3.7 Thermogravimetric analysis	65
2.3.8 Magnetization	65
2.3.9 Electrophoretic mobility	66
2.3.10 Protein Anti-Fouling Property	66
2.3.11 Loading efficiency test	67
2.4 Results and Discussion	72
2.4.1 Optimization and characterization of POEGMA microgel beads	72
2.4.2 Degree of surface functionalization	82
2.4.3 Iron oxide content	84

2.4.4 Colloidal stability	86
2.4.5 Reduction of Non-specific Protein Adsorption/anti-fouling test	88
2.4.6 Loading efficiency test.....	90
2.5 Conclusion	95
 Chapter 3: Water-Soluble Conductive Polymer Coating to Reduce Non-specific Adsorption on Gold Electrode Surface	
3.1 Introduction	97
3.2 Objectives	99
3.3 Experimental Section	99
3.3.1 Materials	99
3.3.2 Synthesis of polymer backbone	100
3.3.3 TEMPO-conjugated POEGMA	102
3.3.4 Conjugation of thiol groups to POEGMA-Ald-MAA	103
3.3.5 Synthesis of zwitterionic DMAPS-Ald-MAA	104
3.3.6 Synthesis of anionic POEGMA-Ald-MAA-AMPS	105
3.3.7 Gel Permeation Chromatography	105
3.3.8 Base-into-acid conductometric titration	106
3.3.9 Ellman’s assay	106
3.3.10 Nuclear Magnetic Resonance	107
3.3.11 Protein anti-fouling test	107
3.3.13 Electrochemical test	108
3.4 Results and Discussion.....	109

3.4.1 POEGMA polymer with TEMPO grafting	109
3.4.2 Thiolated POEGMA polymer	116
3.4.3. Charged Polymer	124
3.4.4 Protein anti-fouling test	126
3.5 Conclusion	129
Chapter 4: Conclusions and Recommendations	131
Appendix	136
Reference	137

Chapter 1: Introduction and literature review

1.1 DNAzyme-based electrochemical sensors

DNAzymes are single-strand DNA sequences that have catalytic functions to cleave substrates with the help of cofactors. Because of their high stability, ease of functionalization, and (more importantly) their recognition and cleavage ability, they can serve as the bio-recognition elements of biosensors. Specifically, RNA cleaving DNAzymes (RCD) are the most widely-studied type of DNAzyme and are used in the design of the biosensor discussed in this thesis given their highly specificity towards its target, such that even a single base mismatch decreases its catalytic activity. Such specificity renders RCDs to be an ideal candidate for the bio-recognition element of biosensors. There are various types of DNAzyme-based biosensors that incorporate detection of the analyte via fluorescence, colorimetry, surface-enhanced Raman scattering, chemiluminescence, luminescence, electrochemiluminescence, and electrochemistry-based methods [5]. Among them, DNAzyme-based electrochemical biosensors have attracted particular attention because they are less susceptible to interference signals compared to other methods and report a straightforward and real-time relationship between the electrochemical signal and the biochemical reaction.

1.1.1. RNA cleaving DNAzymes (RCD)

DNAzymes, or also called deoxyribozymes, are single-strand DNAs that are able to fold into three-dimensional structures and catalyze chemical transformations like enzymes. Unlike RNA-based enzymes naturally present in biological systems, DNA-based enzymes are typically selected and constructed from a single-stranded DNA library. RNA cleaving DNAzyme (RCD) is the first catalytic DNA that was discovered by Breaker and Joyce in 1994 via an *in vitro* selection process. They isolated a Pb^{2+} dependent catalyst from over 10^{14} molecules with an N50 randomized stretch and screened their ability to cleave a substrate containing a single embedded ribonucleotide. The DNAzyme acts as a phosphodiesterase, which cleaves the ribonucleotide by activating the 2' hydroxyl group of ribonucleotides to attack a nearby phosphodiester bond. [6].

1.1.1.1 Selecting RNA cleaving DNAzyme for biosensing

The two most effective and complete DNAzyme motifs, 8-17 and 10-23, were isolated by Santoro et al. through *in vitro* selection process [7]. The general *in vitro* selection procedure of an RCD is based on its function to cleave substrates through transesterification. These DNAzymes generally have two constant regions (which bind substrates) with a random sequence in the middle that is screened and selected from a DNA library by ligating the DNA pool to a substrate. The *cis*-acting DNAzymes are cleaved into smaller pieces, such that they separate from other DNAzymes on gel electrophoresis by traveling more quickly. The selected pool then goes through another round of selection after amplification by polymerase chain reaction. This

cleavage/amplification process is repeated until DNAzyme populations with strong cleavage activities are found [8].

8-17 and 10-23 DNAzymes are different in their catalytic activity. 10-23 can cleave all purine-pyrimidine base pairs, but 8-17 DNAzymes were found initially to only cleave N-G base pairs. However, recently Li and coworkers were able to identify three variants in 8-17 DNAzymes to help them catalyze all dinucleotide junctions. Both 10-23 and 8-17 have smaller catalytic cores and stronger catalytic activities than other RCD. Although 10-23 DNAzymes are more often used for catalyzing the cleavage of messenger RNA, 8-17 DNAzymes are more broadly used for biosensor detection due to their versatility in using different cofactors and capability to cleave all dinucleotide junctions [9].

1.1.1.2 Translating RNA cleaving DNAzyme to bio-recognition elements

DNAzymes form bio-recognition elements by hybridizing the enzyme strand with its substrate strand and folding into a three-dimensional structure. The substrate is cleaved at a ribonucleotide site into two pieces when target compounds or ligands are present.

Usually one part of the cleaved fragment remains bound to the enzyme strand and the other is released from the duplex due to the reduction in the melting temperature of the Watson-Crick base pairs after cleavage. The released fragments can be labelled with reporter molecules for improving ease of detection, which is extremely helpful for real-time diagnostic purposes [10]. For example, fluorophores or quenchers on substrates help

to enable fluorescence-based assays while methylene blue carried by the substrate generates an effective signal in an electrochemistry-based assay.

1.1.2. Electrochemical biosensors

Biosensors are constructions or devices that translate biological events into readable signals; in the case of electrochemical biosensors, the signal is electrochemical. The first electrochemical sensor was introduced by Clark et al. in 1960s to detect blood glucose based on an amperometric readout [11]. Since then, numerous electrochemical biosensors have been developed for various applications.

There are three common methods to quantify the electrochemical signal: amperometry, conductometry, or potentiometry. Amperometry measures the reduction or oxidation current of electroactive species at the electrode surface, with the concentration of electroactive species directly related to the current density. Conductometry relies on the changes in the properties of the electrolytic solution according to the chemical reaction happening at the boundary layer; in this approach, there is no chemical reaction on the electrode surface at all [12]. Potentiometric sensors utilize the measurement of the potential difference between an indicator electrode and a reference electrode, created based on the non-uniform ion distribution on the surface of indicator electrode upon interaction with the analyte [13].

Early stage detection of biochemical reactions requires immobilization of biomolecules on the electrode via different types of chemical modifications on the biomolecule and/or the electrode surface. For example, amine-labelled biomolecules can be covalently grafted to carboxylated electrode surfaces through carbodiimide chemistry while thiolated biomolecules can bind directly to a gold electrode through Au-S coordinative bonds [14]. However, inefficient immobilization greatly reduces the selectivity and specificity of electrode and the biological activity of the biomolecules.

One of the key challenges with performing electrochemical biosensors is to avoid biological fouling or the interference of the electrochemical signal from the probe with other components of the sample. The main focus of this thesis is to develop two different approaches to address this issue: the fabrication of polymeric magnetic beads and the development of conductive anti-fouling surface coatings. Prior literature on both these topics will be extensively reviewed in the following sections.

Part I. Magnetic beads (MB)

Magnetic beads refer to either magnetic nanoparticles or composites of magnetic nanoparticles and polymer coatings that can be rapidly and easily separated by external magnetic field. Employing functional nano- or micromaterials such as magnetic beads as immobilization sites helps enhance signal and the overall performance of biosensor because they provide larger surface areas relative to a flat 2D electrode and thus enable increased loading densities of biomolecules [15]. Iron oxide is usually preferred relative to other magnetic materials in fabricating magnetic beads because of its high saturation

magnetization and low cost. Iron oxide magnetic beads have been applied widely in many fields, but this section will discuss primarily on their synthesis, modifications, and applications in biomedical area [16].

1.2.1 Magnetic properties/magnetism

The magnetism of materials originates from the magnetic moments created by polarization of their electrons, which generally consists of the orbital motions around the nucleus and the self-spin around their own axis. Substances are classified based on their magnetic susceptibility χ , defined by the collective interactions between electrons when external magnetic fields are applied based on the relationship:

$$M = \chi H_0$$

where H_0 characterizes the magnetic field intensity and M represents the magnetic moment per unit volume. There are three major types of magnetism with regard to various behaviors of χ : diamagnetism, paramagnetism, and collective magnetism [17][18].

Diamagnetic materials: Diamagnetic materials possess negative magnetic susceptibility in that the applied magnetic field induces an increase in the electron orbital moments in opposite directions and decreases the moments in parallel (according to Lenz's law), such that the magnitude of the magnetism is proportional to that of applied magnetic field.

Although diamagnetism is a general property of all matter, it could be easily overpowered by the effects of unpaired electrons, which align to the same direction of external

magnetic field and get attracted. So this phenomenon is only observable in pure diamagnetic materials with zero net magnetic moment [19].

Paramagnetic materials: Most metals are categorized as paramagnetic materials that have a positive magnetic susceptibility due to unpaired electrons in their partially filled orbitals aligning in the same direction as the applied magnetic field. However, the induced dipole moment disappears immediately after the magnetic field is removed. In addition, according to the Curie-Weiss Law, the magnetic susceptibility is inversely proportional to absolute temperature T because the thermal fluctuations randomize the direction of magnetic moments.

Materials with collective magnetism: Collective magnetism includes ferromagnetism, ferrimagnetism, and antiferromagnetism, all of which are permanent magnetic moments that remain present in the absence of external magnetic field. Ferro-, ferri-, and antiferromagnetic materials have much stronger magnetic susceptibility compared to diamagnetic and paramagnetic materials due to short-range exchange interactions of unpaired electrons between orbitals. The magnetism of such materials is characterized by magnetic domains, the collective magnetic moments of many individual atoms in the same direction. Each domain has its own net magnetism but orients randomly relative to its neighboring domains[20][21]. Magnetic domains of ferromagnetic materials align in parallel to each other to result in positive magnetic susceptibility; in contrast, magnetic domains of ferri- and antiferromagnetic materials are in opposition to each other. For

antiferromagnetic materials, the macroscopic external moment equals zero because the magnitude of each domain's magnetic moment is the same; however, a ferrimagnetic material retains an overall negative magnetic susceptibility given that different domains have different magnetic moments [22]. Increases in temperature result in randomization of the magnetic moments for these materials such that above a critical temperature (the Currie temperature T_C for ferri-/ferromagnetic materials or the Néel temperature T_N for antiferromagnetic materials) they lose their collective magnetism and become paramagnetic [17][23].

Superparamagnetism is a special form of ferri- or ferro-magnetism that is usually attributable to nanomaterials that consist of a single magnetic domain; as such, all magnetic moments in the nanomaterial can align in the same direction, with the direction of magnetization switching randomly under the influence of temperature. In the absence of external magnetic field, if the time between two switches of the magnetization direction of the nanomaterials is longer than the regular relaxation time for materials with collective magnetism, these materials are said to be in their superparamagnetic state [24].

Ferri-, ferro-, and antiferromagnetic materials have intrinsic saturation magnetism (M_s), defined as the maximum magnetization could be achieved in a magnetic field, and also have magnetic field memory even when the magnetic field is removed, a phenomenon of remnant magnetization (M_r) called hysteresis. As illustrated below, once ferri- and ferromagnetic materials reach saturation magnetization (line a), an oppositely oriented magnetic field is required to bring the induced magnetism back to its saturation

magnetization again but in the reverse direction (line b). A closed loop called a hysteresis loop forms if the direction of the magnetic field flips for the second time (line c); however, the strength of magnetic field (termed as coercivity, H_c) needed to achieve the maximum magnetization is larger than that needed for saturation magnetization at the beginning. Iron oxides are the most commonly used magnetic materials for magnetic beads fabrication because they have relatively high magnetic saturation value.

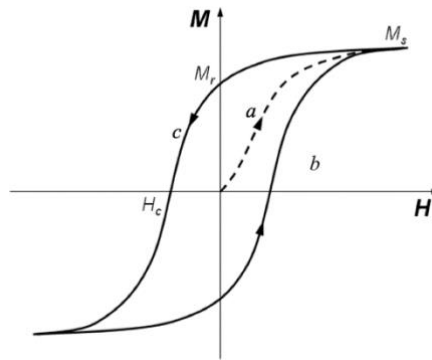


Figure 1.2.1 Illustration of the hysteresis loop for materials with collective magnetism.

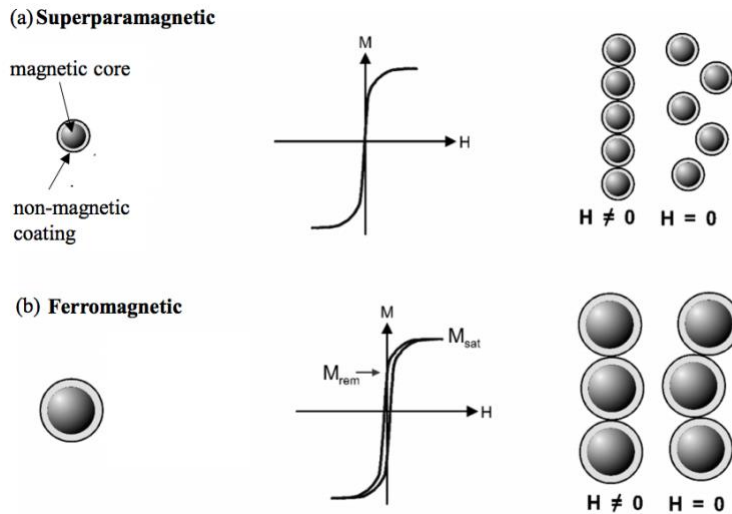
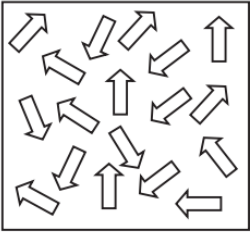
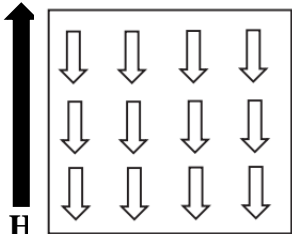
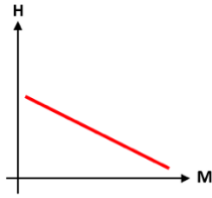
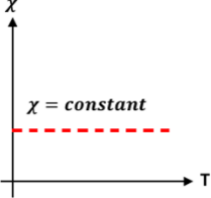
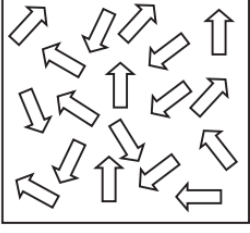
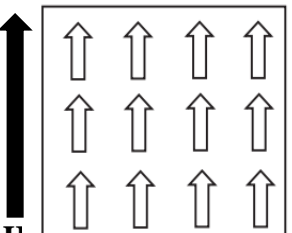
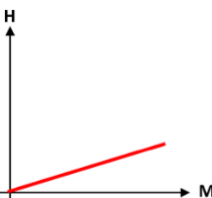
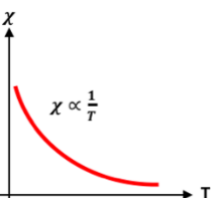
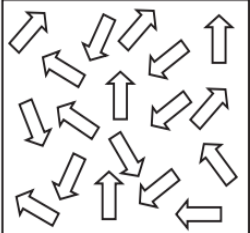
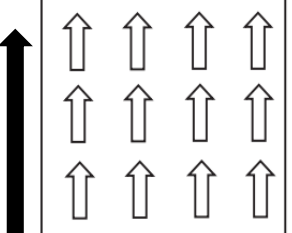
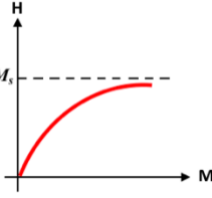
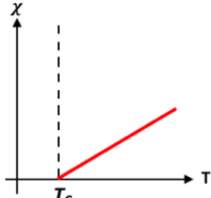
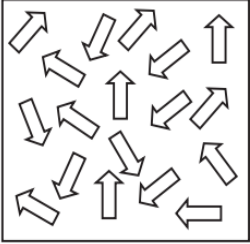
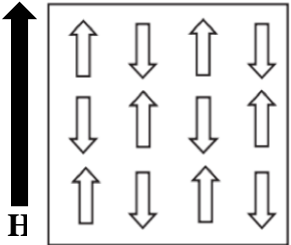
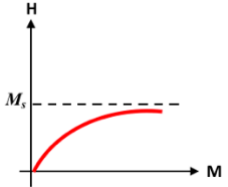
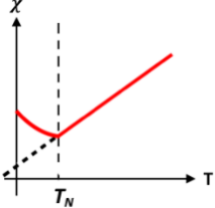
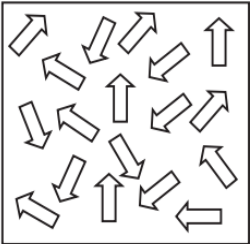
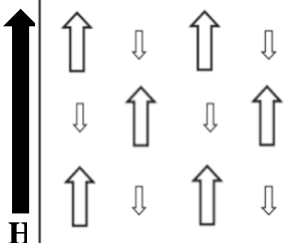
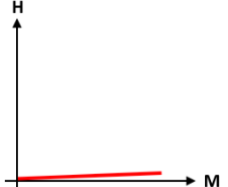
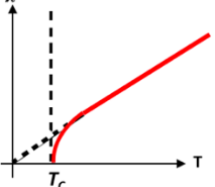


Figure 1.2.2 Difference between the hysteresis and magnetization observed between superparamagnetic and ferromagnetic materials. [1]

Table 1.1 Summary of the change in magnetization with an applied magnetic field and the temperature susceptibility for different types of magnetic materials

Type of Magnetism	Without Magnetic Field ($H=0$)	With Magnetic Field ($H \neq 0$)	Magnetization of the Materials	Temperature Susceptibility
Diamagnetic	 <p>(zero net magnetic moment)</p>	 <p>(weak net magnetic moment)</p>		 <p>$\chi = \text{constant}$</p>
Paramagnetic	 <p>(Random orientation but with net magnetic moment)</p>	 <p>(weak net magnetic moment)</p>		 <p>$\chi \propto \frac{1}{T}$</p>
Ferromagnetic	 <p>(Each arrow represents net magnetic moment of that domain)</p>	 <p>(Magnetic moment of neighboring domains are in parallel)</p>		 <p>T_c</p>

<p>Antiferromagnetic</p>	 <p>(Each arrow represents net magnetic moment of that domain)</p>	 <p>(Magnetic moment of neighboring domains are antiparallel and with the same magnitude)</p>		
<p>Ferrimagnetic</p>	 <p>(Each arrow represents net magnetic moment of that domain)</p>	 <p>(Magnetic moment of neighboring domains are antiparallel and with different magnitudes)</p>		

1.2.2 Synthesis of magnetic beads (MB)

Both iron oxide nanoparticles (INPs) and polymer magnetic beads (pMB), composites of INPs and polymers, have been used widely for biomolecule separations [25]–[28]. The INPs used are normally in the size range of few nanometers, but polymer magnetic beads are relatively larger, with a size range from hundreds of nanometers to over 100 micrometers [16]. The capacity to achieve different particle sizes with similar magnetization renders them more suitable for certain applications, depending on which factors are more crucial. For example, smaller particles have relatively higher surface

area:volume ratio and can thus carry more biomolecules compared to larger ones per unit mass of particles. However, smaller particles are magnetically separated more slowly because of larger viscous forces acting on the particles relative to the limited magnetization of small amount of magnetic materials they carry [29].

Regardless of the size and types of magnetic beads, they must be able to stably conjugate biomolecules to be used as carriers. Although proteins with a high concentration of carboxyl groups or pairs of carboxyl groups and thiol groups have been reported to be immobilize directly to INPs through chelation interactions with ferrite [30], magnetic particles are usually coated with polymer to (1) introduce extra functional groups for interaction with biomolecules and (2) increase the stability and biocompatibility of the magnetic beads, since long-term exposure to air leads to the oxidation of ferrite and ultimate loss of their magnetic properties [31].

1.2.2.1 Synthesis of iron oxide nanoparticles (INPs)

INPs provide the basic magnetism to polymer magnetic beads, and their size and morphology also relate closely to the synthesis technique used to fabricate the INP. Coprecipitation is the most straightforward and widely-used method to prepare both ferric oxide and ferrous oxide particles in water. INPs are most commonly synthesized from mixtures of aqueous Fe^{2+} and Fe^{3+} in solution upon the addition of base such as hydrogen peroxide in either an inert or open environment [32][33]. Alternatively, oxidizing amorphous ferrous hydroxide solution in the presence of nitrate ions can also be used to obtain Fe_3O_4 nanoparticles [34]. In both cases, the morphology, compositions, and size of

particles are tuned by adjusting the pH, temperature, ratio of $\text{Fe}^{2+}/\text{Fe}^{3+}$ in salt solution, and the type of base used. Although the cost of producing such particles is low, INPs prepared from these precipitation-based methods usually have very broad size distributions.

Alternately, microemulsion-based synthesis can produce nearly monodisperse iron magnetic particles due to the role of surfactants at the water-in-oil interface in limiting the nucleation and growth of the nanoparticles. For example, Gupta and Wells prepared poly(ethylene glycol) (PEG) modified iron oxide nanoparticles with size of ~40-50 nm and narrow size distributions through microemulsion polymerization [35].

Monodispersed iron oxide nanoparticles prepared from chemical precipitation were dispersed together with polymerizable methoxy-PEG monomer and the crosslinking agent N,N'-methylene(bis)acrylamide in the aqueous core of aerosol-OT/n-Hexane micelles under N_2 . The free radical polymerization starts inside the micelle solution once the initiator ammonium persulfate was added. The synthesized particles show strong superparamagnetism, making them especially useful in biomedical applications.

However, yield and agglomeration are major concerns with microemulsion polymerization, as is the need for removal of the organic phase and residual surfactant.

Another common way to prepare iron oxide nanoparticles is thermal decomposition. In this method, non-magnetic iron precursors are decomposed in boiling organic solvent in the presence of surfactants to generate pure metals that are further oxidized to INPs. For

example, Sun et al. produced monodispersed INPs with sizes between 3 to 20 nm by decomposing iron (III) acetylacetonate in phenyl ether and alcohol [36]. Hyeon et al. simplified the synthesis protocol to one step by using precursors with cationic iron centers and were able to produce monodispersed particles of size ~13 nm [37]. However, this method is hard to scale up because of strict requirements on reaction conditions and expensive reagents. Hydrothermal synthesis, a process similar to thermal decomposition, also requires high temperature and pressure under autoclave conditions under which metal salts are hydrolyzed to particles by water, at which point INPs precipitate out from solution once they are formed. Autoclaving time can be tuned to control particle size and shape, with short autoclaving times typically resulting in particles with smaller sizes and narrower size distributions [38][39]. INPs produced from this method have high crystallinity and good dispersibility with environmentally-friendly reaction conditions; however, the heating and cooling process takes time, especially for large scale reactions [40].

INPs with special structure features can also be produced by a method called polyol synthesis, in which iron salts are oxidized under alkaline conditions in polyol solution. Although this method does not provide as good of control over particle size as do the previous methods, particles prepared with this method show excellent hyperthermia performance because their special morphology gives them very high heat capacity. For example, Hugounenq et al. prepared flower-shaped INPs in polyol of around 11 nm that exhibit higher specific loss power (SLP) compared to other INPs at this size range [41].

Other synthetic techniques such as sol-gel reaction, electron beam lithography, microwave irradiation, glass crystallization, and gas phase deposition were also reported for synthesizing magnetic nanoparticles used for other areas such as recording, pigments and catalysis but not typically for biomedical applications [42].

1.2.2.2 Synthesis of polymer magnetic beads (pMB)

Polymer magnetic beads are hybrids of polymer with iron oxide nanoparticles and typically consist of one of three main composite structures (Figure 1.2.3): (i) INPs are embedded inside the polymer matrix, either homogeneously or heterogeneously (left); (ii) each INP is coated with a layer of polymer to create a polymer shell-magnetic core structure (middle); or (iii) polymer core-magnetic shell structures are formed in which INPs are coated at the outside of a polymer particle (right). INPs can be prepared simultaneous to polymerization or (more often) prepared beforehand and combined with polymer during polymerization, a process called in-situ polymerization. Finally, pre-formed INPs and polymer can be mixed directly to produce beads using a range of different fabrication techniques.

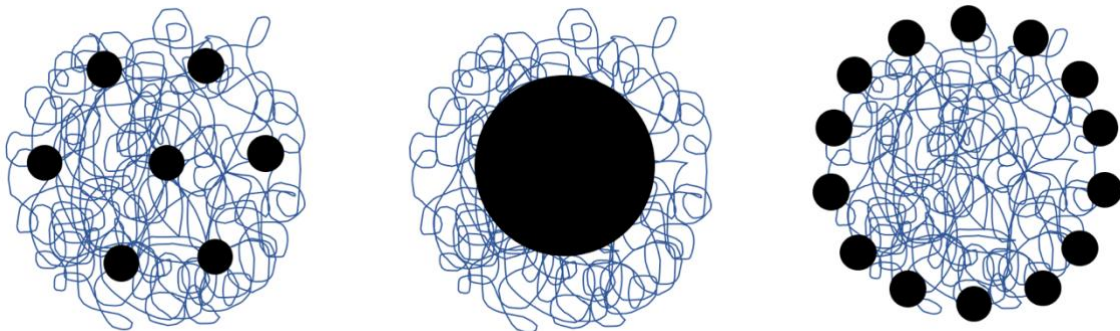


Figure 1.2.3. Illustration of the different structures of polymer magnetic beads.

1.2.2.2.1 Conventional synthesis routes

Emulsion polymerization. *In situ* emulsion polymerization is frequently used to create polymeric magnetic beads with different morphologies. Multiple mechanisms can be employed to leverage emulsions to prepare polymer magnetic beads, including conventional emulsion polymerization (water/oil W/O or oil/water O/W), microemulsion polymerization, miniemulsion polymerization, surfactant-free emulsion polymerization, or seeded emulsion polymerization [43]–[46].

Emulsion templating. Polymer magnetic beads are most commonly synthesized using an emulsion-templated process consisting of a dispersed phase, a continuous phase, surfactants, initiators, and sometimes additives such as stabilizers. The dispersed medium is either organic solvent or water depending on the hydrophobicity of monomers, most commonly referred to as direct or inverse emulsion polymerization, respectively. For direct emulsion polymerization, hydrophobic monomers are added to a pre-stirred hydrophilic continuous phase containing iron oxide nanoparticles, which are usually treated with surface stabilizers such as oleic acid (OA) or sodium dodecyl sulfate (SDS) to prevent the phase separation or particle aggregations [47]. However, for inverse emulsion polymerization, hydrophilic monomers are miscible with iron oxides such that the surface treatment of iron oxides is optional [16]. For both polymerization process, the free radical polymerization occurs inside the droplets of the dispersed phase to form the polymeric particle. For example, Okassa et al. formed uniformly-distributed INP-poly(lactide/glycolide) (PLGA) composites using modified double emulsion

polymerization (W/O/W) for loading hydrophilic drugs; in this case, INPs were pre-functionalized with oleic acid to increase their compatibility with hydrophobic PLGA, after which organic mixtures of OA-INPs and PLGA (W/O emulsion) were emulsified via sonication in an aqueous polyvinyl alcohol continuous phase to form the final particles [48]. Pre-formed polymers can also be crosslinked inside inverse emulsion droplets to form microbeads. For example, magnetic chitosan beads can be simply synthesized by crosslinking chitosan chains with glutaraldehyde inside pre-formed emulsion droplets of INPs and chitosan mixtures [49].

Emulsion polymerization. Alternately, a formal emulsion polymerization strategy can be used to form polymeric magnetic beads. Emulsion polymerization is generally described as occurring in a series three steps: initiation, propagation, and termination [2]. At the beginning of initiation phase, both surfactant-containing micelles and small monomer droplets are present in the continuous phase. Radicals produced via thermal or photocleavage of an initiator (which is soluble in the continuous aqueous phase) initiates polymer growth in solution to start the polymerization. The rate of initiation (R_i) is dependent on the initiator concentration and rate of initiator dissociation, given by the equation below:

$$R_i = 2fK_i[I]$$

Here, K_i is the rate constant for initiation, f is the initiation efficiency, and $[I]$ is the initiator concentration. During the propagation phase, the rate of polymerization remains

roughly constantly with monomers supplied by monomer droplets, with the instantaneous monomer concentration limited by the monomer solubility. During this phase, the rate of propagation (R_p) is determined by the monomer concentration in the continuous aqueous phase:

$$R_p = K_p[M \cdot] [M]$$

Here, K_p is the rate constant for propagation, $[M \cdot]$ is the concentration of polymer radicals, and $[M]$ is the concentration of monomers in solution. Finally, in the last stage, the monomer droplets are fully consumed leaving only monomer-swollen polymer latex and a small amount of dissolved monomer in the continuous phase, at which point the rate of polymerization decreases gradually. Polymerization eventually stops when all monomers are used up via termination, disproportionation, recombination, and/or chain transfer reactions. The whole process is illustrated in Figure 1.2.4.

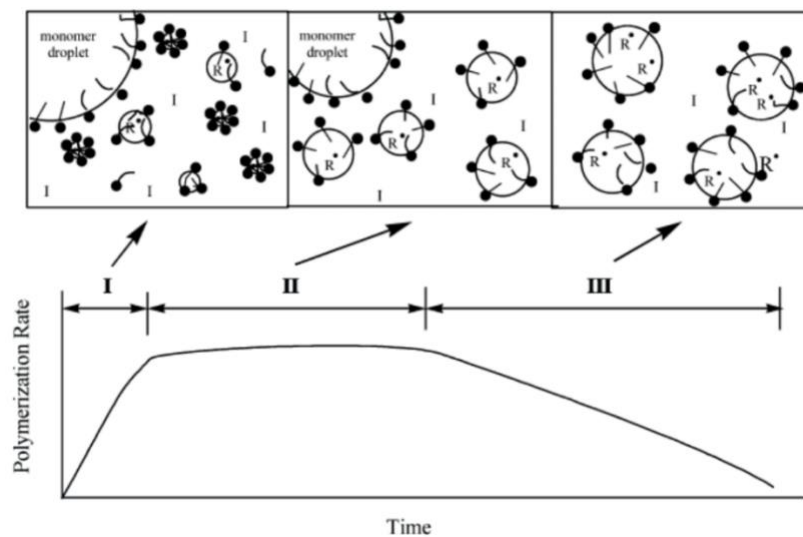


Figure 1.2.4 Illustration of the three phases of the emulsion polymerization process and the corresponding kinetics [2].

Multiple examples of polymer magnetic beads fabricated using emulsion polymerization have been reported. Kniajanski et al. synthesized highly INP-loaded polystyrene magnetic beads with a narrow size distribution using direct emulsion polymerization and treating INPs with both (2-acetoacetoxy) ethyl methacrylate (AAEM) and oleic acid (OA). OA at the INP surface formed bilayers, with the OA carboxyl groups of the first layer anchored on the INPs surface and that of the second layer pointed outward to enhance particle hydrophilicity. AAEM functioned as chelating ligands to anchor the polymer on the surface of iron oxides to reduce particle aggregation. However, in some cases in which AAEM is more active than the monomer, it could self-polymerize and result in phase separation during magnetic bead synthesis [44]. Polystyrene beads with bigger sizes could also be produced by reducing the concentration of OA while still keeping INPs from aggregating by adding non-surfactant co-ligands such as AAEM.

Surfactant-free emulsion polymerization in which the charge from the initiator (typically a persulfate) provides sufficient electrostatic colloidal stabilization can also be used to produce magnetic beads that are easy to purify but have good mechanical and water-resistance properties [50]. While this approach can increase aggregation between particles to lead to inhomogeneous encapsulation, Pich et al. found that the encapsulation of INPs into polystyrene via surfactant-free O/W emulsion polymerization could be enhanced by pre-treating iron oxide with OA to make the INP surface more hydrophobic [51].

A semi-batch or seeded process can enhance the stability of emulsion polymerization by managing the nucleation step, which varies with the random formation of radicals and further influences the particle growth. As its name suggests, seeded emulsion polymerization involves the introduction of pre-particles at the start of the polymerization step that serve as nuclei from which the particles can be grown, resulting in a final latex with a controlled particle number and size. Jamshaid et al. prepared submicron magnetic core-polymer shell beads starting with an O/W polystyrene-MAA emulsion seed crosslinked with divinylbenzene (DVB) and prepared using the carboxyl-bearing initiator 4,4'-azobis(4-cyanopentanoic acid) (ACPA). Seeded emulsions were further functionalized with MAA during the following emulsion polymerization process to facilitate even higher loading densities of cytochrome c and HRP enzymes. The seeded process allowed for denser but still uniform MAA functionalization on bead surface, demonstrated by gradually increasing the polymer shell thickness with higher fed MAA monomer concentration [52]. Alternately, the INPs can be used as the seeds provided the polydispersity of the initial INP suspension is sufficiently low. Montagne et al. demonstrated this route by shearing oleic acid treated INP fluids and first size-sorting them with magnetic field. A carboxyl group-containing polymeric surfactant was then coated on ferrofluid droplets by continuously washing these droplets in such polymer solution to enhance INP colloidal stability, after which the INP seeds underwent emulsion polymerization in the presence of styrene, divinyl benzene, and the water-soluble initiator potassium persulfate to generate homogeneous magnetic core-polystyrene shell beads with a narrow size distribution [53].

Microemulsion polymerization produces much smaller particles in the size range of 1-10 nm at rapid reaction rate [54] Microemulsions are thermodynamically stable suspensions that require much higher surfactant concentrations to stabilize compared to traditional emulsions because of their large interface areas. The reaction mechanism, and resulting kinetics, of microemulsion polymerization are also quite different from emulsion polymerization. For example, the second phase of traditional emulsion polymerization in which a constant rate of polymerization is observed is not present during microemulsion polymerization since monomer droplets are absent in microemulsion polymerization process [55]. The large interface area of the resulting materials make it useful in many fields such as cleaning fluids, oil recovery, and liquid membrane separation. Combining this particle-forming method with different polymerization methods, such as living radical polymerizations, polymer particles with unique morphology, structures, and properties can be generated. The main disadvantages of this process is that with the large amount of surfactant used, the solids content (e.g. magnetic materials) will be relatively low [56][57].

In comparison, the mechanism of miniemulsion polymerization is only slightly different from conventional emulsion polymerization, resulting in particle sizes in the size range of 50-1000 nm [58]. For example, particle nucleation for microemulsion polymerization is primarily through radicals entering into the monomer droplets, because the interface area of miniemulsion is relatively larger than conventional emulsions; as a result, little

surfactant is available to form micelles or to stabilize new polymer particles [59].

Compared to traditional emulsion polymerization, the complexity of both miniemulsions and microemulsion polymerization add cost in terms of the need for additional high-shear equipment, reagents, and energy consumption relative to traditional emulsion polymerization process [60]. Ramírez et al. synthesized homogeneous polystyrene magnetic beads using a two-step miniemulsion polymerization. Oleic acid-coated INPs were first prepared and aggregated in water using SDS as surfactant; following, mixtures of INPs aggregates and monomers were pre-emulsified and sonicated followed by the addition of initiator to start the polymerization. The INP aggregates formed during the first step enabled the formation of beads with high magnetic content [61]. Csetneki et al. incorporated a co-stabilizer stearyl alcohol to polystyrene/INP composites produced by miniemulsion polymerization and synthesized beads with complete and homogenous encapsulation of INPs [62]. Deng et al. obtained magnetic polyacrylamide beads with size ~80-180 nm by using aerosol OT as surfactant and 2,2,0 -azobis(isobutyronitrile) (AIBN) as initiator in a microemulsion polymerization system, demonstrating control over the particle size by adjusting the concentration of crosslinkers and surfactant/water ratio [63]. Ramos and Forcada synthesized magnetic core-polystyrene shell beads using surfactant-free miniemulsion polymerization with highly aggregated INPs under high shear; however, beads with more homogeneously distributed INPs can be obtained by coating INPs with oleic acid first and utilizing hexadecane as an additional hydrophobic stabilizer [64].

Suspension polymerization. Direct suspension polymerization utilizes mechanical agitation and stirring to disperse hydrophobic monomer mixtures in a hydrophilic continuous phase (i.e. water) with the help of suspending agents, which stabilize monomer droplets from coalescence and prevent agglomeration of produced polymer particles. Most common examples include using water-insoluble monomers such as poly(vinyl chloride), polystyrene, and poly(methyl methacrylate acid). Similar to conventional emulsion polymerization, mechanical agitation or stirring is required to create aqueous monomer droplets in an organic continuous phase [65][66]. Each monomer droplet acts as tiny reactor within which free radical polymerization proceeds to create typically micron-sized beads or pearls. The polymerization in each droplet is theoretically similar to bulk polymerization, which involves initiation, propagation, transfer to monomer, and chain length-dependent termination process; However, magnetic beads produced from suspension polymerization typically have much broader size distributions than those produced via emulsion polymerization processes [67]. Ma et al. produced micro-sized magnetic poly (methacrylate-divinylbenzene) beads by agitating the monomer phase and the oil-soluble initiator benzoyl peroxide, stabilized by poly(vinyl alcohol) [68]. Similarly, a metal chelating ligand called *N*-methacryloyl-(L)-histidine methyl ester (MAH) was polymerized with ethylene glycol dimethacrylate (EGDMA), also using PVA as the interfacial stabilizer, to produce magnetic beads with size of 50–100 μm for separating cytochrome c [69]. Ménager et al. prepared micro-sized magnetic beads via inverse suspension polymerization by introducing mixtures of iron oxide ferrofluid, *N,N'*-methylenebisacrylamide (BAA), and hydrophilic acrylamide

monomer to a dodecane continuous phase under stabilization by Span 80 and mechanical stirring [45]. This system was used also by Müller-Schulte and colleagues to create magnetic poly(N-isopropylacrylamide) (poly(NIPA)) microgels with a size range of 10-200 μm by controlling stirring speed [46]. Recently, *in situ* suspension polymerization was applied for generating molecularly imprinted magnetic beads. The polymerization begins with a “template” molecules added to the polymer matrix; after the polymer is formed, the template is extracted afterward to leave cavity in the polymer with both shape complementarity and favorable chemical interactions for binding to the template. Zhang et al. used this method to prepare porous magnetic beads of size 80-250 μm using triazines as the template. Co-precipitated INPs were first treated with poly(ethylene glycol) 6000 to improve their stability and distribution inside polymer matrix. PEG-INPs, self-assembled methacrylic acid and atrazine, crosslinker methacrylic acid-co-trimethylolpropane trimethacrylate (TRIM), and initiator (AIBN) were then dispersed in styrene under vigorous stirring following by microwave heating-initiated polymerization. Atrazine was removed and cleaned by ultra-sonication after polymerization, leaving high-affinity atrazine binding cavities that could be used to adsorb it from other complex samples [70]. Similar approaches were also used by multiple groups to prepare INP-embedded magnetic beads for chemical separation, catalysis, and molecular sensing purposes [71]–[75]. Kan et al produced aspirin-templated beads with a magnetic core-polymer shell structure by modifying the surface of INPs with a double bond to support radical polymerization on each particle, enabling the direct formation of a TRIM shell anchored to the underlying particle [76].

Dispersion polymerization. Dispersion polymerization is another method for single-batch production of micron-size monodisperse polymer beads, but it suffers from problems such as wide size distribution, large sizes, and low magnetic content. This strategy is distinguished by the monomers and initiators used for synthesis being soluble in the selected solvent but resulting polymers being insoluble. As a result, polymers/macroradicals precipitate out at the early stage of polymerization and nucleate into primary particles, which are usually surrounded and protected by stabilizers. Subsequent polymer initiated precipitates on to these nuclei to grow the particles into spherical beads with sizes typically in the range of 0.1-10 μm . Selected stabilizers are usually polymers or oligomers with low solubility in the dispersing medium but high affinity to the polymers [77][78].

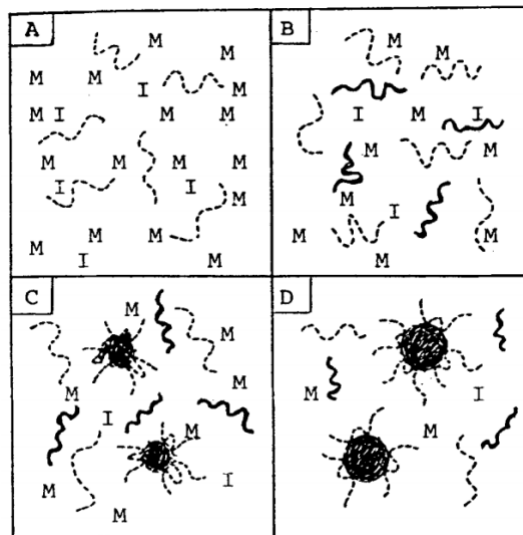


Figure 1.2.5 Illustration of the different stages of dispersion polymerization. M represents monomer and I represents the initiator.

For example, magnetic poly(glycidyl methacrylate) (PGMA) beads were prepared by Horák et al. via *in situ* dispersion polymerization of INPs in the presence of glycidyl methacrylate and ammonium persulfate in ethanol. Poly(vinylpyrrolidone) was pre-adsorbed on iron oxide nanoparticles to minimize aggregation following polymerization[79], with the highest iron content achieved being 24 wt%; however, parts of iron oxide in needle form protruded through polymer coating, therefore influencing the beads' performance. The protrusion problem was improved by Ma et al. through preparing PGMA beads first with dispersion polymerization and then co-precipitating iron salts (Fe^{2+} and Fe^{3+}) inside the beads afterwards. Although the synthesized magnetic beads were with spherical in shape, exhibited a smooth surface, and demonstrated a narrow size distribution, the iron oxide content achieved was still only ~24 wt%, which is much lower than that of beads prepared with other methods [80].

Membrane emulsification. Membrane emulsification uses the shear of fluid flow through membrane pores to produce emulsion droplets. Dead-end filtration and cross flow filtration are two different ways of using membranes to create droplets, as shown schematically in Figure 1.2.6. For dead-end filtration, pre-formed emulsions are directly pressed through the micropores to form droplets, such that droplet size is solely dependent on the pore size. For cross flow filtration, the dispersed phase is sheared into droplets while passing through membrane and is sheared to detach from membrane by cross flow of the continuous phase, such that the droplet size can be tuned by flow rate. Membrane emulsification can produce monodisperse particles with controlled sizes under

low energy input compared to traditional emulsification techniques [81], [82]. To form stable water-in-oil emulsions droplets, the membrane outlet needs to be hydrophobic to avoid the adsorption and retention of dispersed phase; conversely, a hydrophilic membrane is preferred for synthesizing oil-in-water emulsions [83]. Omi et al. prepared uniform oil-in-water emulsions by continuously pushing a SDS-stabilized INP and poly(styrene-co-acrylic acid) mixture through a porous glass membrane followed by evaporation of solvent. Magnetic microspheres with different sizes were obtained using membranes with different pore sizes. The selection of the dispersing medium is essential to produce beads, as switching the dispersing medium from toluene to chloroform resulted in the production of beads with much broader size distributions based on the higher viscosity and polarity of chloroform promoting sticking of the droplets to the outlet surface, thus affecting the formation of the next droplets [84].

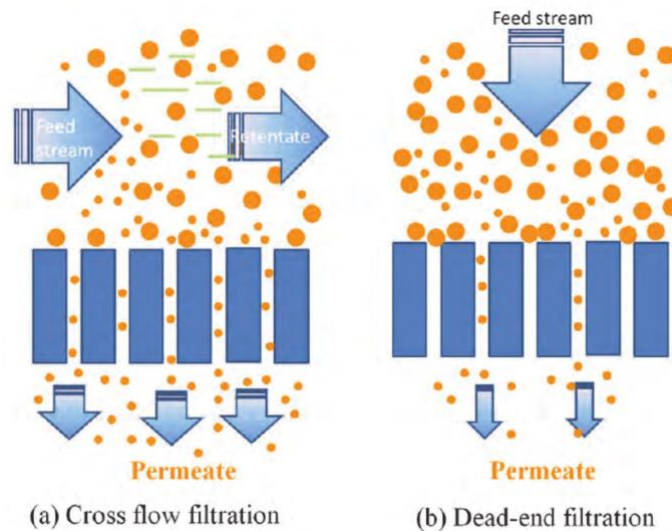


Figure 1.2.6. Illustration of cross flow filtration and dead-end filtration strategies for membrane emulsification. [3]

Microfluidics. Microfluidic devices operate in a manner somewhat similar to membrane emulsification in that monomer droplets of uniform sizes are produced inside microchannels under a continuous flow process followed by solidification of droplets with either polymerization or adjustment of temperature. However, given the high reproducibility of the shear field generated in a microfluidic device and the sequential nature of droplet generation, particles produced by microfluidics typically have highly controlled sizes/shapes and extremely narrow size distributions [85].

Polydimethylsiloxane (PDMS) devices are typically used for microfluidic particle fabrication. For example, Hwang et al. prepared monodispersed poly(ethylene glycol) diacrylate (PEGDA)-based spherical and non-spherical magnetic hydrogels by using a PDMS fabricated T-junction microfluidic device. During the synthesis, the aqueous phase containing iron oxides, PEGDA, and photoinitiators is pinched into droplets by an impinging flow of mineral oil within a PDMS channel to create monodispersed emulsion droplets, followed by photopolymerization initiated with a mercury lamp. Magnetic microgels with the desired morphology (spherical versus non-spherical) were obtained by confining the synthesis in microchannels with different geometries. This approach helps generate polymer particles with different compositions, structures, and properties (e.g. anisotropic) in a highly efficient ways [86]. However, the production of smaller microparticles using microfluidics is much more challenging given the need for smaller channel sizes that result in much higher pressure drops associated with pumping the dispersed and continuous phases through the device. In addition, a single microfluidic

chip produces only a very small number of beads per unit time, requiring complicated multiplexing to achieve usable particle yields. As such, although microfluidics is a superior technique for the generation of homogeneous magnetic beads, restrictions persist with current technologies.

1.2.2.2.2 Special synthesis routes or fabrication methods

Other methods have been reported to create polymer magnetic beads with special morphologies or properties.

Surface-initiated polymerization. The efficiency of anchoring polymer chains on INPs to create magnetic core-polymer shell beads can be improved by directly grafting initiators on the surface of the INP, a so-called “grafting-from” approach. This approach is particularly useful for the generation of ultra-small stable magnetic beads. For example, Schmidt et al. obtained well-dispersed and superparamagnetic beads with a size of 9.7 nm by performing ring-opening polymerization of lactones on INPs coated with glycolic acid, which provided hydroxyl groups as initiation sites [87].

Pickering emulsions. Pickering emulsions represent a special class of emulsions in which solid particles rather than surfactants act as the particle stabilizers at the water-oil interface. Comparing to traditional surfactants, solid particles are better at preventing coalescence, typically enabling the production of more stable emulsions. Solid particles with certain properties can also be chosen to tailor the porosity, conductivity, and

magnetic responsiveness of the prepared emulsions [88]. O/W Pickering emulsions have been applied to synthesize polymer core-magnetic shell morphologies using pre-synthesized INPs as the Pickering stabilizers. Prepared Pickering emulsions are easily solidified to polymer particles with various types of polymerization methods, such as Pickering emulsion polymerization [89], Pickering suspension polymerization [90], or atom transfer radical polymerization [91]. When applied in biomedical or *in vivo* applications, certain food-grade solid particles such as soy glycinin can be used to reduce the toxicity and increase the biocompatibility [92]. However, INPs at the polymer beads surface may subject to corrosion without the protection of polymer and can be desorbed from the particle surface in the presence of other surface-active agents, Peng et al. addressed the former problem by silica coating the iron oxide nanoparticles to stabilize and separate W/O emulsions [93]. The introduction of an external magnetic field may also destabilize the emulsion systems [94].

Deposition method. INPs can be directly deposited on polymer beads or polymer can be deposited on INPs through electrostatic adsorption or layer by layer (LBL) deposition methods. As an example of the former case, Singh et al. converted negatively charged polystyrene beads to positively charged beads by coating them with poly(diallyldimethyl) ammonium chloride (PDAMAC), enabling efficient adsorption of negatively charged magnetic nanoparticles to the beads; subsequently, to minimize the influence of exposed INPs on biomolecules and protect INPs from corrosion in biomedical applications, another layer of PDAMAC was then adsorbed on top of the magnetic particle layer.

Hollow core capsules can subsequently be prepared if desired by dissolving or calcining the polystyrene core [95]. This method is widely adaptable for creating magnetic bead structures using INPs as the base particle. For example, Thünemann et al. synthesized magnetic core-polymer shell beads by layer-by-layer depositing polyethylenimine (PEI, cationic) and poly(ethylene oxide)-block-poly(glutamic acid) (PEO-PGA, anionic) sequentially on an INP core. The thickness of polymer coating, charge, and hydrophobicity of the outer layer are all easy to control based on the number of layer-by-layer adsorption steps performed [96]. The disadvantages of this method are that only small number of magnetic particles can be loaded into beads (typically one INP/bead) and the LBL process is slow to perform.

Direct crosslinking. Magnetic beads could also be prepared by exploring the rapid crosslinking potential of some specific polymers in water. For example, the rapid ionotropic gelation observed between polyelectrolyte polymers and their counterions can be used to create microbeads by dropping a polymer solution into the ionic gelling bath; if INPs are included in the polymer solution comprising the drop, they also become entrapped in the formed gel bead. For example, cationic chitosan beads encapsulating INPs can be produced using phosphate anions, while anionic sodium alginate can be crosslinked with polyvalent cations such as Ca^{2+} [97]. Both “external gelation” and “internal gelation” can be used to synthesize magnetic beads [98]–[100]. In “external gelation”, crosslinking ions were externally added to the polymer solution; in

“internal gelation”, inactivated crosslinking ions are mixed with the polymer solution and are gradually activated by changing reaction conditions such as pH or temperature.

The convenience of generating microbeads using ionotropic gelation can also be used as a template to create other types of bead compositions/structures. For example, Xulu et al. created spherical interpenetrating networks by first creating Ca^{2+} /alginate microbeads using the method developed by Park et al [101] followed by free radical polymerization of N-isopropylacrylamide and INPs inside the network. The alginate-calcium network was then extracted by chelating the calcium using ethylenediaminetetraacetate (EDTA), leaving behind magnetic poly(NIPA) beads with intertwined channels [102].

Activated swelling. Activated swelling method is used to prepare one of the most well-known magnetic beads, Dynabead, and was first proposed by Ugelstad et al. in 1980s. This process involves first preparing highly porous polymer particles in dry form (typically starting with a nanoparticle seed), followed by in situ formation of magnetic materials inside the particles. Due to the low swelling ability of the pure polymer particles, they have to undergo many cycles of swelling and polymerization to produce large monodisperse particles, because only swelled or activated particles are more capable to absorb water-soluble monomer. Dynabeads consist of crosslinked polystyrene particles synthesized from a polystyrene latex seed followed by surface modifications to introduce reactive groups or to increase surface hydrophilicity to decrease non-specific adsorption [103][104]. For example, the type of Dynabeads called MyOne carboxylic

acidTM (used as the control for the work in this thesis) are coated with a layer of glycidyl ether at the outside of a polystyrene core to conceal the iron oxides, followed by the introduction of carboxyl groups using acrylic acid (AA) as functional sites. The active swelling method is good at preparing particles with size of 0.5-20 μm , with the final size and polydispersity of the magnetic beads produced depending on that of polymer latex used; given the high controllability of polystyrene latex formation, final products with very low polydispersity ($< 0.5\%$) are typically achieved [105]. However, as described, Dynabeads require multiple-step synthesis from the preparation of seed latex to the introduction of functional groups; in particular, because polystyrene is hydrophobic in nature with low surface free energy and wettability in water, surface functionalization following particle fabrication is required [106].

Spray drying. Solution process (SolPro) was first proposed by Hickstein et al. in 2009, who used a spray drying method to prepare magnetic beads specifically for protein separation; two components including co-precipitated INPs and ion exchange resins (extract proteins) were integrated in a polymer matrix, dispersed in organic solvent, and spray dried [107]. The spray drying method is used to create particles at micron size range, and different characters of beads such as shape, size, and structure can be altered dependent on the nature of polymer and operating parameters of spray dryer, including flow rate, nozzle size and distance, chamber volume and etc. [108]. While this process is among the most industrially scalable of those listed, the operating parameters can be hard

to optimize (particularly in the presence of nanoparticle additive) and the particle size distributions produced are typically among the broader of the reported methods.

1.2.3 Surface modification

Surface modifications are prevalent for both iron oxide nanoparticles or magnetic composite materials such as magnetic beads. However, surface modification for INPs is mainly used to improve their stability and facilitate their incorporation into the polymer bead with minimal aggregation, while surface modification of polymer magnetic beads is usually used to introduce functional groups for promoting the immobilization or interaction of the beads with biological ligands.

1.2.3.1. Surface modification of iron oxide nanoparticles (INPs)

Iron oxide nanoparticles without any surface treatment tend to aggregate to each other via magnetic interactions, significantly reducing their colloidal stability. When INPs are used directly as carriers of biomolecules, this aggregation influences their loading efficiency by decreasing the nanoparticle surface area. When combined with polymer, aggregated INPs influence the size, size distribution, morphology, stability, and performance of final products. For effective and homogeneous encapsulation of INPs into polymer matrix, surface modifications are required to tune their hydrophobicity so that they can more uniformly disperse in the targeted solvent or polymer matrix.

Common coatings for INPs include various surfactants, polymers, or inorganic materials. The most common surfactants include sodium dodecylbenzene sulfonate (SDS), oleic acid (OA), sodium oleate (SO), and sorbitan esters (Spans). [109]. Both mono-layers or double-layers of surfactants have been reported to form on the particle surface, depending on the surfactant used. For example, oleic acid, usually used as a stabilizer for INPs in emulsion polymerization, tends to form a monolayer with the polar group pointing toward the nanoparticles and the tail pointing to the surrounding medium, rendering INPs more hydrophobic and thus more dispersible in organic media. However, to improve stability for particles dispersed in aqueous medium, bilayer coatings employing both primary and secondary surfactants are usually used, with the polar head of primary surfactant interacting with the INPs but that of secondary surfactant pointing to medium; for example, Shen et al. reported the synthesis of a magnetic fluid with a particle size of 9.3 nm stabilized with bilayers of alkanolic acids that remained highly stable in aqueous suspension [110].

Relative to surfactants, modification of INPs with polymers further provides functionalization sites for subsequent modification as well as other benefits, like anti-fouling properties. Different synthetic or natural polymer coatings have been used for INPs in various applications, including poly(ethylene glycol) (PEG), poly(vinyl alcohol) (PLA), poly(ethylene imine) (PEI), polylactide, alginate, starch, dextran, chitosan, and others [111]–[114]. However, the success of polymer modification is dependent on the strength of the initial polymer-INP interaction, as otherwise the polymer can desorb (particularly in complex biological media) and the benefits of polymer modification are

lost. PEG, for example, is the most widely used coating for INPs because of its good biocompatibility, water solubility, and protein-repellent properties but exhibits poor adhesion in the absence of the use of a primary surfactant to pre-coat the particles or a surface reactive PEG derivatives such as ethoxy-PEG, complicating the synthesis process [115][116]. García et al. reported that stable iron oxide suspensions can be prepared using unmodified PEG by fulfilling three requirements: 1. the mass ratio of PEG to iron oxide particles has to be at least 1.5 to ensure good dispersion; 2. short chain PEG is preferred because long chain PEG cannot extend effectively on particle surface; 3. the medium is desalted so that methylene segments of PEG can better undergo hydrophobic interaction to form a multi-layer compact structure [117]. Similarly, Paul et al. demonstrated that reduced dextran-stabilized INPs had smaller sizes and better size distributions [118]. Saikia et al. showed that carboxymethylated starch-chitosan-coated INP has excellent stability (as enabled by the polyelectrolyte complexes formed between oppositely charged carboxymethylated starch and chitosan) as well as mucoadhesivity and biocompatibility (based on the cationic nature of chitosan) [119].

Silica is also a commonly used coating for INPs based on its biocompatibility and its high density of silanol groups that can be easily functionalized to form stable magnetic suspensions in organic solvent and also facilitate conjugation of biofunctional ligands. Silica has been coated on INPs using many methods. For example, Tartaj et al. hydrolyzed and condensed a tetraethyl orthosilicate-based precursors on the iron oxide precursors followed by the use of sodium borohydride to reduce the precursors to iron crystals [120], Santra et al. prepared small but uniform magnetic silica particles by

confining the INPs and silica precursors in an emulsion droplet [121], and Liu et al. directly deposited pre-formed silica nanoparticles on pre-synthesized INPs [122].

1.2.3.2. Surface modification of polymer magnetic beads

Surface modification on polymer magnetic beads is mainly used to introduce functional groups for biomolecule interaction and can be achieved either through copolymerization of a stabilizing functional group or chemical modification on existing polymer. A variety of functional groups including carboxyl groups, amine groups, oligo(dT), streptavidin, avidin, protein A/G, silica, and sepharose (or other carbohydrates) has been used to modify the surface of the polymeric magnetic beads using multiple mechanisms [123]–[126]. For example, pre-synthesized polymer can be modified to introduce specific functional groups, typically by grafting a functional molecule to pre-existing functional groups on the surface. Carboxyl, amino, and hydroxyl groups on magnetic beads surface are most typically introduced through grafting monomers such as methacrylic acid (MAA) or acrylic acid (AA) to produce carboxyl-terminated beads [43], cysteamine or aminoethyl methacrylate to produce amino-terminated beads [127], and hydroxyl ethyl methacrylate (HEMA) to produce hydroxyl-terminated beads. Surface functional groups can also be converted using several methods; for example, carboxyl-terminated polymer beads can be prepared by incubating glutaric anhydride ($C_5H_6O_3$) with amino-terminated beads [121] or hydroxyl groups can be introduced to epoxy-terminated magnetic beads via the addition of 4-hydroxybenzhydrazide [128]. These functionalities are chemically stable, easy and cheap to generate, and applicable to the conjugation of many

biomolecules, typically following a pre-activation step; for example, carbodiimide-mediated grafting between carboxyl groups and amino groups benefits from pre-activation with N-hydroxysuccinimide (NHS) to form an activated ester [129][130]. Carboxyl or amine groups also maintain charge under physiological pH conditions to provide stabilization benefits via electrosteric repulsion, while beads with hydroxyl surface groups have higher surface hydrophilicity and thus undergo less aggregation and non-specific binding than unmodified beads.

Other common types of functional groups on magnetic beads, including tosyl, epoxy, or chloromethyl groups, do not require activation steps but enable more stable covalent conjugation between beads and biomolecules that can in some cases be more selective. For example, the reactivity of tosyl groups to sulfhydryl groups is enhanced at neutral pH while the reactivity of tosyl groups to amino groups is enhanced at higher pH; similarly, shifting from slightly basic to very basic conditions results in a preference for epoxy reactivity from thiol groups to amino groups [131].

Alternately, instead of covalent conjugation of bioactive ligands to polymeric magnetic beads, high-affinity non-covalent biological interactions can be used to functionalize bead interfaces if an appropriate bio-activated surface can be created. Functionalization of beads using streptavidin, avidin, protein A/G, and/or oligo(dT) can all be leveraged in this context, exploiting their high biocompatibility and strong and often specific binding

affinities. For example, protein A/G, combining two binding domains of IgG protein, can specifically anchor or bind to immunoglobulins, with both protein A and G are normally immobilized on beads together to reduce the pH dependency of binding [132].

Streptavidin-biotin interactions are the strongest non-covalent interaction in nature and are widely used for ligating biotin labeled antigens, antibodies, and nucleic acids [133].

Oligo(dT) are used for recognizing the poly(A) tail of messenger RNA to enable its surface binding and/or functionality as an adsorbent to separate mRNA from crude extracts of sample. While such interactions are high affinity, non-specific binding can still happen because some molecules such as biotins are naturally present and circulate in biological samples to interfere the binding of specific ligands [133].

Another type of surface modification called pseudo-biospecific affinity ligands have attracted considerable interest in recent years and is especially useful for ligation and bioseparation applications due to their low cost, high binding capacity, good biocompatibility, and high stability. Typical molecules used for such modifications include triazine dyes, metal chelates, or amino acids, which all recognize targets through electrostatic or Lewis acid/base interactions with hydroxyl, amine, or thiol-containing amino acids in proteins. Because of the similarity in interaction mechanisms between pseudo-biospecific affinity ligands and their targets, the optimal binding conditions (e.g. pH or temperature) are all very similar [134]. For example, in an affinity application, Ma et al. were able to separate bovine serum albumin protein (BSA) in a large scale directly from crude biological samples by coating iron oxide nanoparticles synthesized by co-precipitation with silica and grafting a condensation product of 3-

glycidoxypropyltrimethoxysilane (GLYMO) and iminodiacetic acid (IDA) on silica that provides high affinity binding of histidine-tagged bovine serum albumin in the presence of copper (Cu^{2+}) [135].

1.2.4 Applications

The main applications of magnetic beads in biological fields include *in vitro* bioseparation, *in vivo* drug delivery, magnetic resonance imaging, and hyperthermia therapy. In each case, it is necessary to choose magnetic beads with appropriate size, homogeneity, surface features, morphology, structure, and compositions for specific applications to achieve the best performance. Each of these applications and the considerations in selecting magnetic beads for such applications are discussed below.

Bioseparation. Magnetic separation, using external magnetic field to separate nano- or micron-size magnetic particles from a suspension, is one of the most well-developed and widespread applications of magnetic beads. Magnetic separation has many advantages over other traditional separation techniques. For example, separation can be performed directly in crude clinical samples such as blood or urine; indeed, magnetic separation is the only method that allows for recovery of small particles in the presence of debris and other interfering molecules. Mixing magnetic beads with different ligand affinities also allows for easy manipulation and separation of a large number of targets both time- and cost-effectively.

Functionalized magnetic beads can be applied in two different ways in bioseparation applications: (1) binding with target molecule(s) in a complex sample to separate the target(s) from other molecules [136][137]; or (2) carrying immobilized detection molecules (e.g. aptamers or bioreceptors) remain bound to the beads (and are thus removed upon magnetic separation) but release a signal probes into the solution upon exposure to the target molecule(s) [138]. In the first approach, the targets are then eluted from magnetic beads for future use after disposing the remainder of the suspension; in the second approach, the supernatant containing the signal probes is retained but the beads with the reaction residues are separated or removed magnetically to eliminate any interference with the detection of the signal probes.

A large body of research on separating antigens, antibodies, enzymes, inhibitors, cells, and nucleic acids using magnetic beads has been published [135], [139], [140]. Among them, superparamagnetic beads with relatively small particles size are preferred for nucleic acid separation given that these beads do not show residual magnetization after magnetic field is removed, giving them good dispersibility and high surface areas particularly important for nucleic acid extractions [141]. Surface functionality, however, is highly variable depending on the method chosen to link a nucleic acid ligand to the bead. Carboxyl-terminated and amine-terminated beads couple best to amine-terminated and phosphate-terminated DNA/RNA, respectively, while poly(dT) oligonucleotide-coated beads are best for mRNA separation.

The main applications of magnetic beads in nucleic acid separation include purifying RNA or DNA from a complex RNA/DNA library [142], purifying plasmid DNA from

crude lysates of sample [143], or specifically capturing certain RNA/DNA strands [144]. Despite the ease of using magnetic beads, in most cases the sample still requires pre-treatment prior to magnetic separation. For example, if RNA needs to be separated from a RNA/DNA mixture, the DNA first has to be degraded with DNase [141]; similarly, to separate plasmid DNA from chromosomal DNA, it is necessary to remove lipids and proteins in crude cell lysates first given that the concentration of plasmid DNA in cell lysates are extremely low and most contaminants are of similar size, charge, and hydrophobicity to plasmid DNA [143][145].

Depending on the application, particular product lines of commercial magnetic beads are recommended. Magnetic beads for nucleic acid separation include Dynabeads[®]DNA from Dynal, SPHERO magnetic particles from Spherotech, MGP from Roche Diagnostic, GenoPrep[™] DNA magnetic beads from GenoVision, MagneSil from Promega, and MagPrep[®]Silica from Merck KgaA. Examples of commercially available magnetic beads for mRNA extraction include BioMag[®] oligo (dT)20 from Bangs Lab, Dynabeads[®] oligo from Dynal, μ MACS oligo-dT from Miltenyi Biotech, MagaCell[™] oligo-dT₃₀ from Cortex Biochem, MPG[®] streptavidin oligo (dT)25 from PureBiotech, and MagneSphere[®] from Promega [141].

Drug delivery. Targeted drug delivery greatly increases therapeutic efficiency and lowers the cytotoxicity of drugs, which is especially critical for tumour chemotherapy due to the serious side effects induced by non-specific exposure of healthy cells to

chemotherapeutics. Magnetic beads aid in targeted drug delivery by enabling the accumulation of drug at targeted treatment sites using an applied magnetic field. If drugs are loaded inside the beads rather than just attached at the surface, then polymer magnetic beads also allow controlled drug release by regulating drug diffusion from the beads and/or slowly degrading to release encapsulated drugs. Beyond control over positioning and drug delivery, magnetic beads for drug delivery must satisfy other criteria: (1) the beads must minimize non-specific protein adsorption and fouling, typically requiring their coating with a highly water-binding cytocompatible polymer such as poly(vinyl alcohol) or poly(ethylene glycol) or with silica [67]; (2) the size of the beads is restricted to the 10 nm - 200 nm range [16], with beads with size <10 nm tending to be removed quickly through extravasation and renal clearance while beads with size >200 nm being more easily taken up by the lymphatic system; (3) the beads should be neutral or slightly negative in charge to preserve long circulation half-lives and minimal non-specific adsorption; and (4) the beads are typically spherical, as anisotropic particles tend to exhibit less tight binding/contact with endothelial cells [146]. However, anisotropic magnetic particles are still reported to be used in certain cases to solve specific problems. For example, small magnetic particles are generally required for drug delivery to tumours [147], and leading to a compromise in magnetic responsiveness; in contrast, using nanochains or nanoclusters of iron oxide particles, which retain one very small dimension (diameter) but have stronger magnetic responsiveness while retaining superparamagnetism and good colloidal stability (based on their length) [148]. Multiple functionalities can also be incorporated into a single magnetic bead to enable improved

controlled release. For example, Wang et. al designed doxorubicin-loaded iron oxide core-polypyrrole (PPy) shell magnetic beads for cancer therapy in which the iron oxide was used for magnetic targeting to tumours and PPy was selected as the polymer shell due to its ability to respond to near-IR irradiation to trigger on-demand drug release; surface modification of the bead with PEG improved its water solubility and extended its circulation half-life. This combined cancer therapy approach enables remotely-controlled drug release to destroy cancer cells with minimum cytotoxicity [149].

Magnetic resonance imaging (MRI). Magnetic resonance imaging is a non-invasive tool widely used for tissue and organ imaging. Different tissues and organs have different compositions and internal morphologies and thus possess dissimilar proton density and magnetic relaxation time under applied magnetic field and stimulations. The contrast achieved in MRI imaging depends on the proton spin density and the resulting longitudinal (T_1) and transverse (T_2) relaxation times upon exposure to a strong external magnetic field. It was found in the 1980s that superparamagnetic iron oxide nanoparticles can be used as contrast agent due to their role in shortening T_2 , thus increasing the concentration-dependent relaxivity r_2 to produce darkening effects due to signal reduction. Beyond their role in imaging, beads with certain surface chemistries are able to carry therapeutic drugs, imaging probes (e.g. fluorescein tags), or receptor chelators (e.g. antibodies) [150] to create theranostic nanoparticles with multiple utility for diagnosing and treating disease. Similar to magnetic beads used for drug delivery, iron oxide particles for MRI are typically coated with a passivation layer such as silica, starch,

or dextran and can range in size from tens of nanometres to few micrometers depending on the target application. For example, small magnetic nanoparticles are easily retained and accumulated in hypervasularized and narrow brain tumour vessels even with the presence of blood brain barrier to aid in the magnetic imaging of brain tumour[151] while micron-sized magnetic particles are preferred to provide higher contrast for endovascular imaging since they exhibit a more homogeneous magnetic field and show higher specificity to targets with less non-specific cell uptake and extravasation compared to small iron oxide particles [152]. In other cases, magnetic beads with positive charge are often preferred because of enhanced cell uptake effects [153]. For now, magnetic particles are most often used for MRI imaging for liver. Li et al. synthesized PEGylated and anticancer drug-loaded poly(lactide-co-glycolide) (PLGA) based magnetic nanoparticles for liver cancer therapy and imaging. The surface of magnetic beads was conjugated with folate receptors for prolonged circulation and enhanced uptake to liver tumour cells. This design of magnetic beads allowed gradual release of drugs in addition to the generation of clearer MR images given that shorter T2 was achieved with a higher iron oxide content [154].

Hyperthermia. Hyperthermia is a method to induce cancer cell death and/or increase cancer cell susceptibility to chemotherapy and radiotherapy by elevating the temperature of tumor sites to 40-43 °C. When a sufficient amount of iron oxide is present in the beads, the magnetic beads lose paramagnetism and gain permanent dipoles, resulting in a delayed response to external magnetic field whose by-product is heat (a phenomenon

called hysteresis [155]). Although extensive research has been done on the use of hyperthermia for cancer therapy, it is not used widely clinically because of its ineffectiveness when applied as a single treatment [156]. However, by using magnetic particles that can localize at least to some degree in the tumour and can undergo hysteresis losses to generate heat under an oscillating magnetic field, improved therapeutic efficacy has been observed [157]–[159]. Magnetic particles with small sizes and strong magnetizations are generally preferred given that more particles can accumulate at a fine area, absorb more energy from oscillating magnetic field, and elevate temperature more quickly.

Part II. Anti-fouling coatings for electrochemical biosensors

In most cases, electrochemical biosensors are required to perform measurements in complex clinical samples such as blood, urine, sweat, or saliva that contain a large number of interfering molecules (e.g. enzymes, cells, oligonucleotides, lipids) that result in high background signals, low stability, and ultimately poor sensitivity. Therefore, incorporating anti-fouling strategies in designing biosensors can alleviate non-specific adsorption (NSA) and improve their overall performance. There are many ways of reducing NSA that can be broadly separated into two strategies: actively removing fouling as required or passively blocking fouling in the first place, the latter generally by surface modifications. Surface modifications are the earliest and most well-studied anti-

fouling strategy, with a variety of bioactive and biocompatible polymers having been reported to effectively reduce NSA in numerous studies and models [160]–[163]

1.3.1 Understanding adsorption on electrochemical biosensors

Biofoulants include a broad range of molecules from what naturally presents inside clinical samples, including lipids, cells, polysaccharides, or proteins, as well as the byproducts of electrochemical reactions, both of which severely reduce the sensitivity and reliability of the biosensors when adsorbed at the electrode surface. In the case of electrochemical biosensors, electrochemically active compounds in clinical samples that can alter electrical conductivity should be paid extra attention, including common chemicals such as uric acid, salicylic acid, dopamine, and ascorbic acid in blood samples and urea, citric acid, glucose, and proline in urine samples [164].

Non-specific adsorption may be either chemical or physical. For physical adsorption, the adsorbed molecules block the electrode surface through non-covalent interactions such as van der Waals forces, hydrophobic interactions, electrostatic interactions, and/or hydrogen bonding [160]. Chemical adsorption is much stronger and more specific and involves the formation of at minimum a transient chemical bond. Biofoulants more commonly interact with the surface through the weaker physical adsorption route depending on the structure, size, charge, and (for proteins) isoelectric point of the foulant. Biofoulants with shape complementary to the electrode surface are easier to bind, while larger biofoulants interact more strongly to electrode surface and are less likely to detach

[165][166]. Furthermore, both the net charge and (for macromolecular foulants like proteins) the charge distribution of biofoulants can influence adsorption, with biomolecules at or near their isoelectric point most likely to adsorb [167][168].

Adsorption is a thermodynamically favorable process because the formation of any of the physical or chemical interactions described above lower the free energy of the system. Biomolecules such as proteins can further lower free energy by unfolding and stretching themselves to maximize their interaction with surface, reducing the degree of bound water to the protein and thus enhancing the overall system entropy [169]; more hydrophobic interfaces further drive higher protein dewatering and thus are more likely to foul than more hydrophilic interfaces that already contain an appreciable fraction of bound water [170][171].

1.3.2 Mechanisms and strategies for reducing fouling/NSA

Passive anti-fouling methods for electrochemical biosensors reduce non-specific adsorption by modifying the electrode surface. The main such strategy involves the physical or chemical immobilization of a layer of blocking molecules on the electrode surface. Attached blocking molecules reduce biofouling through hydrophilic interactions, steric hindrance, or electrosteric repulsion that reduces the probability of biofoulant adsorption at the interface. To be specific, hydrophilic compounds coated on electrodes bind to water molecules with hydrogen bonds to form hydration layers that suppress the hydrophobic interactions between biofoulants and the electrode surface. Steric hindrance

is a special characteristic of long chain hydrophilic polymers that can sterically exclude biofoulants from reaching the surface (typically via hydrogen bonding), while electrosteric repulsion occurs with polymers containing charged residues that can form strong hydration layers with water through ionic interactions [172].

As an alternative, active treatment involves the triggered removal of biofoulants from an electrode surface by applying mechanical force or acoustic waves to the electrodes. Such active treatment can reduce non-specific adsorption without influencing the binding of targets, because the binding affinity of targets is much higher than that of biofoulants.

Comparing to passive biofoulant removal strategies, active biofoulant removal approaches do not require pre-functionalization processes or have chemical stability issues; indeed, the created shear forces not only reduce non-specific adsorption but also promote specific binding of targets by enhancing target diffusion at the interface [160].

One type of mechanical force used in this system is hypersonic resonance, usually created by resonators. Pan et al. introduced a hypersonic resonator on gold electrodes built on a silicone substrate and, via the microvertexes produced upon activation, demonstrated effective lifting away of loosely adsorbed biofoulants on the substrate surface. This resonator removed biofoulants without contacting the substrate surface, indicating its potential to be used in other surface-based biosensors [173]. However, because shearing forces usually result from the mechanical vibration of the devices, active foulant removal methods work only for biofoulants that are already adsorbed on the transducer surface.

Also, at this stage, active foulants removal methods are implemented primarily for microfluidics-based system on small surface areas, while passive blocking can be broadly

applied in most surface-based sensors. Other factors such as device size, operation difficulties, or cost more broadly limit usage of active foulant removal methods [160].

1.3.3 Surface modifications to reduce biofoulants/NSA

The simplest approach to surface modification is to use a blocking agent that physically adsorbs to the electrode surface. A typical example of a blocking agent is the protein bovine serum albumin (BSA), which is often used as membrane backfiller in immunoassays to reduce non-specific binding of proteins. However, BSA coatings reduce the charge transfer efficiency in electrochemical assays and thus decrease the sensitivity of a biosensor. Sabaté et al. solved this problem by intercalating conductive nanomaterials such as gold nanoparticles inside a porous BSA coating, which helped with electron transfer between underlying electrodes and immobilized bio-recognition elements while also showing high protein repellency. Modified electrodes were able to retain over 80% of their original signal even after one month of exposure in clinical samples [174]. A similar approach was used by Gooding et al. to suppress biofoulant adsorption on an electrochemical immunosensor operated in whole blood for glucose monitoring through the fabrication of hybrid electrodes consisting of BSA and conducting nanowires crosslinked using glutaraldehyde. These nanocomposite electrodes showed similar conductivity to a bare electrode and were able to retain 93% of the electrode's sensitivity even after incubating inside blood for one month [175].

Chemical modifications are usually performed via hydrophilic polymer grafting. The most common example of a hydrophilic coating is poly(ethylene oxide) (PEG) or the

related oligo(ethylene glycol) (OEG)-based polymers that strongly hydrogen bond with water, such that their anti-fouling performance decreases with hydration level and the length of OEG chains [176][177]. More recently, zwitterionic polymers, overall neutral macromolecules that contain both positively charged and negatively charged residues (e.g. sulfobetaine methacrylate, phosphorylcholine, or carboxybetaine methacrylate (CBMA)) have been demonstrated to offer improved anti-fouling performance due to their ability to interact with water through both hydrogen bonding and ionic solvation to form an improved hydration layer [178][179]. With either monomer type, coatings in the form of either polymer brushes or self-assembled monolayers (SAM) can be applied to the electrodes, depending on the chemistry involved. Polymer brushes are usually formed via graft-to polymerization of a pre-formed polymer to a functional group on the substrate or graft-from polymerization from a surface-immobilized initiator site, in either case resulting in a polymer with one end attached to electrodes and the other end pointing to surrounding medium [172].

Alternately, self-assembled monolayers (SAMs) are dense molecule assemblies that adsorb spontaneously on substrate surface via coordination interactions. By far the most common SAM is the interaction between alkanethiols and gold surface given that the Au-S interaction is generally very stable and hydrophobic self-assembly of the alkane tails can result in dense and highly ordered coatings [180].

Although various types of self-assembled polymer have been demonstrated in the literature to be used for anti-fouling, bioconjugation, or biosensing purposes, few examples have been reported for carrying multiple functions in a single polymer. As one of the few examples, self-assembled monolayers of thioated calix[6]arene coated on a gold surface was used to recognize different types of bisphenols (BPs) [181]; thiolated polymer R-methoxy ω -mercapto-poly(ethylene glycol) (PEG-SH) coated on gold clusters was shown to stabilize the self-assembled surface and increase its aqueous solubility to enable biological sensing applications [182]; Self-assembled layer of thiolated 2-methacryloyethyl phosphocholine was demonstrated as effective anti-fouling coating for gold electrodes, but its possible influence on electrode conductivity was not reported [183].

More recently, derivatives of conducting polymers have attracted attention as a new strategy to reduce biofouling while still exhibit excellent conductivity. For example, Goda et al. synthesized thiolated poly(3,4-ethylenedioxythiophene) (PEDOT) with zwitterionic polymers, which exhibit both good anti-fouling properties and high conductivity. However, the coating procedure was complicated, requiring cycles of continuous cyclic voltammetry in a strict potential range of -0.6 to +1.1 to -0.6V in water, or -0.6 to +1.4 to -0.6V in acetonitrile with a scan rate of 0.1 V/S. [184]. Similarly, an immunosensor for antigen capture developed from self-assembled redox polymer Os(bpy)₂ClPyCH₂NH poly(allylamine) and an antibody on a gold electrode exhibited both good anti-fouling properties and charge propagation ability. However, the antibody

and polymer need to be deposited on gold surface layer by layer, which significantly complicates the coating process [185]. Lu et al. used a relatively simple strategy by directly immobilizing antibodies and redox hydrogel on the electrode surface, but there is no precise control to the thickness of the coating layer and distribution of components [186]. Therefore, a water-soluble polymer that can be easily coated on electrodes in a single step while enabling good charge transfer ability, good anti-fouling properties, tunable layer thickness, and the capacity for easy immobilization of ligands would offer significant benefits over existing technologies.

1.4 Objectives

Electrochemical biosensors developed as point-of-care diagnostic devices need to work in untreated clinical samples often characterized by a low concentration of targets but high concentrations of different interfering molecules. As such, for proper function of a biosensor, new materials-based strategies for reducing fouling but enhancing target binding (i.e. improving signal-to-noise ratios) are essential for the translation of such sensors into clinical devices. In this context, the overall aim of this research is to apply new materials chemistry to achieve higher sensitivity and lower limits of detection for *E. coli* DNAzyme-based electrochemical biosensors operating in clinically-relevant environments.

The first aim (Chapter 2) is to design poly(oligo(ethylene glycol) methacrylate (POEGMA) based ultra-low fouling magnetic microgel beads, which are used herein to immobilize an *E. coli* RNA cleaving DNzyme (RCD). Magnetic beads with inherent anti-fouling properties repel interfering molecules and prevent false-positive results; simultaneously, the high surface area coupled with the high degree of interfacial hydration of the POEGMA-based magnetic beads both provide more immobilization sites for bio-recognition elements and reduce steric barriers to the capture targets. Chapter 2 describes the synthesis and characterization of POEGMA magnetic beads using emulsion templating with semi-batch feeding of the aqueous phase, initiator, and surfactants. Multiple fabrication parameters were studied and optimized to achieve higher stability and reproducibility as well as targeted particle sizes, surface charges, and morphologies. We demonstrate the significantly enhanced performance of these magnetic microgel beads in the context of the loading and cleaving of *E. coli* RCD relative to commercial Dynabeads.

The second aim (Chapter 3) is to design a water-soluble conductive polymer coating to reduce non-specific adsorption on a gold electrode surface to enable a low limit of detection and long-term usage of the biosensor in clinical applications. Multiple different polymers were synthesized and screened for performance as electrode coatings as a function of their chemical composition, molecular weight, functional group content, with zwitterionic thiolated polymers identified in particular to not only maintain but actually enhance surface conductivity on a gold electrode.

Finally, Chapter 4 summarizes and discusses the results from this research work as well as future directions for this work, including a brief discussion on other potential applications of the current findings.

Chapter 2: Multifunctional Low-Fouling Magnetic Microgel Beads for DNAzyme

Immobilization

2.1 Introduction

High sensitivity is a key requirement of DNA based electrochemical biosensors designed for clinical applications, requiring the amplification of the DNA hybridization signal between targets and bio-recognition elements to achieve low limits of detection[187].

Micro/nanomaterials can benefit signal amplification by immobilizing a high density of bio-recognition elements by virtue of their large surface area [188][15]. Polymer magnetic beads are one of the most commonly used micromaterials as biomolecule carriers because they allow facile magnetic separation/purification and can be tuned for specific applications in different biosensing systems [16][25][31].

The effective design of polymeric magnetic beads for biosensing applications involves three steps: synthesis[44][103][107], surface modification[67][163], and bio-conjugation to biomolecule ligands [67][129]. Appropriate synthesis routes are important for producing particles with desired physical properties. Emulsion-templated polymerization represents a rapid, convenient, and cost-effective way to generate micron-size hydrophilic polymer particles containing embedded iron oxide nanoparticles[4]. Magnetic beads in this size range allow for quick separation due to the capacity of such beads to encapsulate high numbers of iron oxide nanoparticles (and thus maintain high magnetization) while minimizing viscous forces in relation to the suspending solution upon magnetic separation[29]. Since iron oxide nanoparticles disperse well inside the hydrophilic

monomers mixture, they are effectively encapsulated inside the polymer matrix formed by free radical polymerization [16]. Second, surface modification is typically used to introduce functional groups to magnetic beads to enable biomolecule conjugation and/or enhance the colloidal stability of the beads (e.g. charged groups for enhancing electrosteric repulsion). Functional groups can be incorporated on the surface of magnetic beads either during polymerization (via copolymerization of monomers containing the target functional group) [142] or after polymerization [126] (via grafting of the desired functional group to the magnetic bead). Finally, attachment of sensing ligands to the polymeric magnetic beads via a range of potential physical interactions (e.g. streptavidin-biotin) or covalent bonds (e.g. carbodiimide-mediated crosslinking between amines and carboxylic acids), often by leveraging the incorporated functional group(s) in the surface modification step [128][133][145].

Of all various fields in which magnetic beads have been applied, bioprocessing or bioseparation is most well-studied. Comparing to traditional separation and purification process that involve multiple steps such as filtration, centrifugation, sedimentation, and chromatography, magnetic separation enables capture and purification in a single rapid step, promoting continuous or semi-continuous processing [189] and thus reducing cost/increasing productivity of down-stream processing in the biotechnology, pharmaceutical, and/or medical fields, among others.

2.2 Objective

While multiple types of commercial magnetic beads are available for different biosensing applications, none of the commercial samples is a hydrogel microparticle, mainly due to the synthetic challenges in creating monodisperse, colloidally stable, and well-defined microgel particle populations via emulsion templating or other methods accessible on the micron length scale. In the case of magnetic beads, the incorporation of dense and magnetizable nanoparticles into the gel further reduces colloidal stability due to the tendency of iron oxide particles to self-aggregate. As such, there is a significant need to develop a more reproducible and controllable technique to create magnetic microgel beads that can take advantage of both microgels (low fouling, low mass transport resistance at the interface) and magnetic beads (fast separation) for biosensing.

In this chapter, the synthesis of poly(oligo(ethylene glycol) methacrylate (POEGMA)-co-methacrylic acid (MAA) magnetic microgel beads via semi-batch inverse emulsion templating is reported. The structure of the prepared magnetic microgel beads is depicted in Figure 2.1. The influences of several major fabrication parameters on the stability and physical properties of the magnetic microgel beads were investigated, including the viscosity of the continuous (oil) phase, the pH of dispersed (aqueous) phase, the concentration of iron oxide nanoparticles (INP), and the concentration of methacrylic acid (MAA) comonomer. The performance of the magnetic microgels as biomolecule carriers in an electrochemical-based biosensing system was then assessed and compared to a leading commercial polymer magnetic bead (Dynabead).

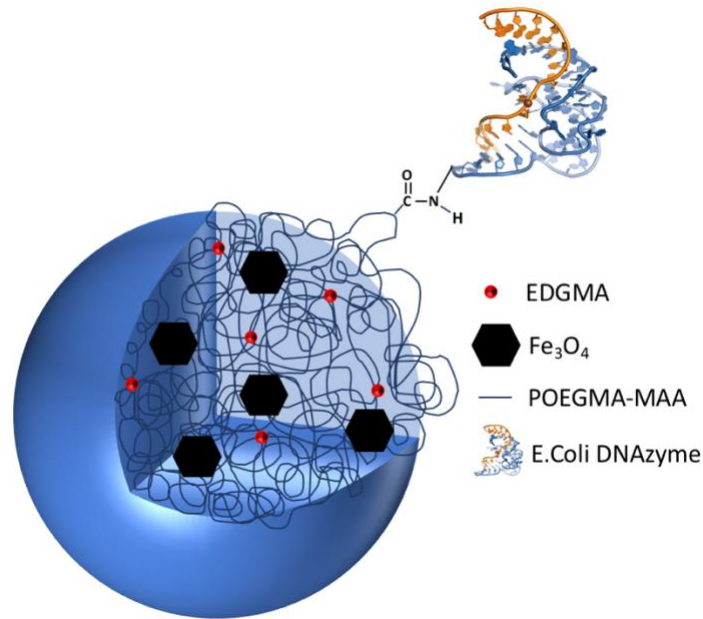


Figure 2.1 Schematic illustration of POEGMA-co-MAA magnetic microgel beads crosslinked by EDGMA with iron oxide particles physically encapsulated inside the polymer matrix. The carboxyl groups from the MAA monomer residues can be used to graft amine-labeled *E.coli* DNAzyme to the microgels via carbodiimide crosslinking.

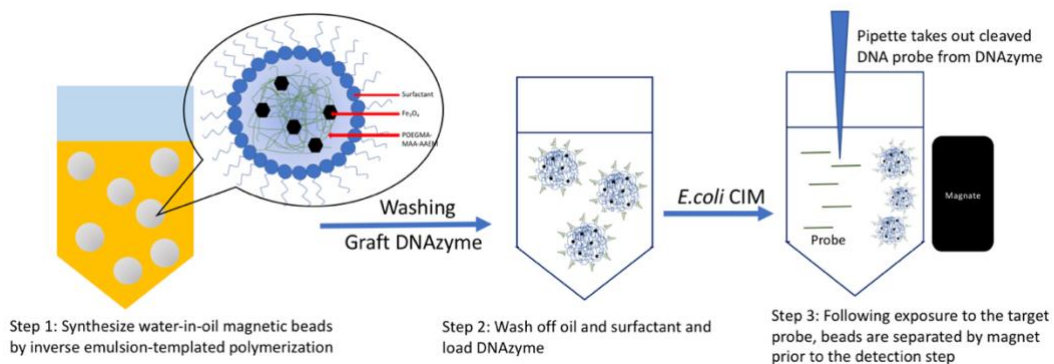


Figure 2.2 Schematic illustration of magnetic microgel bead preparation and application. Magnetic beads are washed with hexane and Milli-Q water to remove all of the templating oil prior to use. *E.coli* DNAzymes were then immobilized on magnetic beads via carbodiimide crosslinking. The addition of *E.coli* crude intracellular matrix (CIM) to a magnetic bead suspension triggers the cleavage of DNA signal probes from *E.coli* DNAzymes. The reaction residues (retained on the magnetic beads) can easily be removed using a magnetic field to leave behind only the cleaved probes that are electrochemically detected.

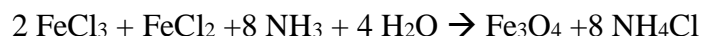
2.3 Experimental

2.3.1 Materials

Oligo(ethylene glycol) methyl ether methacrylate (OEGMA, $M_n \sim 500$), methacrylic acid (MAA, 99%), ethylene glycol dimethacrylate (EGDMA, 98%), ammonium persulfate (KPS, $\geq 99.0\%$), iron(III) chloride hexahydrate (97%), iron(II) chloride tetrahydrate (98%), ammonium hydroxide solution ($\geq 99.0\%$), *N*-hydroxysuccinimide (NHS, 98%), sorbitan oleate (SPAN[®] 80), Polysorbate 80 (TWEEN[®] 80), and silicone oil (5 cst or 50 cst) were purchased from Sigma Aldrich (Canada). Inhibitors in the OEGMA monomer, including 200 ppm BHT and 100 ppm MEHQ, were removed using an alumina oxide (Al_2O_3)-filled vertical glass column. Alumina oxide was purchased from Thermo Fisher Scientific (USA). *N*'-ethyl-*N*-(3-dimethylaminopropyl)-carbodiimide (EDC, commercial grade) was provided by Carbosynth (Canada). Milli-Q grade distilled deionized water (Milli-Q H₂O) was used for all experiments. 1.0 N and 0.1 N hydrochloride acid solution (HCl), and 1.0 N and 0.1 N sodium hydroxide solution (NaOH) for pH adjustment were purchased from VWR Analyticals (Canada). *N*-hexane (95%) and paraffin (95%) was purchased from Caledon Laboratory Chemicals (Canada). Bovine serum albumin ($\geq 96\%$, lyophilized powder), IgG from human serum (reagent grade, $\geq 95\%$, lyophilized powder), and fibrinogen from human plasma (50%-70% protein) were purchased from Sigma Aldrich (Canada). Standard Pierce 660 nm colorimetric assay reagent was purchased from Thermo Fisher Scientific (USA).

2.3.2 Iron Oxide Nanoparticles (INP) Synthesis

INPs were prepared using the co-precipitation method. Iron(III) chloride hexahydrate (3.04 g) and iron(II) chloride tetrahydrate (1.98 g) were dissolved at a 2:1 molar ratio in 12.5 mL Milli-Q H₂O. The solution was purged with nitrogen for 10 minutes, after which 6.5 mL ammonium hydroxide was added drop-wise under magnetic stirring at 800 rpm while maintaining nitrogen purging to create Fe₃O₄ INPs, as per the chemical scheme below. The resulting INPs were separated using a magnet over at least five purification cycles with Milli-Q H₂O, with the final product stored in Milli-Q H₂O at room temperature. The concentration of INP was determined by comparing the mass of INPs before and after drying them inside the oven at 80 °C overnight. The concentration was calculated by dividing mass of dried particles to that of particle suspension.



2.3.3 Magnetic Microgel Synthesis

Magnetic poly(ethylene glycol) methyl ether methacrylate (POEGMA)-based microgels were synthesized using an emulsion templating method. The continuous phase was prepared by mixing of 42 mL of paraffin oil and 1.5 mL of a surfactant mixture of Span 80 and Tween 80 in a 75 v%:25 v% ratio and was heated to 65 °C under 500 rpm mechanical stirring under a nitrogen purge for 20 minutes. The dispersed phase was prepared by dissolving of 2 g OEGMA₅₀₀ (inhibitors removed), 200 mg EGDMA, and 780 mg MAA in 5 ml Milli-Q H₂O. Pre-synthesized INPs were dispersed inside the

monomer solution via bath sonication for 10 minutes to prepare a 1.5 wt% INP suspension. After INPs were well dispersed, the pH of dispersed phase was adjusted to 7 with 1.0 N or 0.1 N NaOH. A three-stage semi-batch process was then used to prepare the magnetic microgels. In stage 1, 100 μL of initiator solution (prepared by dissolving 60 mg KPS in 600 μL Milli-Q H_2O), 2 mL of the dispersed phase, and 500 μL of surfactant were added to continuous phase dropwise during the first stage to start the polymerization. In stage 2 (initiated 20 minutes after stage 1), 250 μL of initiator solution, 2 mL of the dispersed phase, and 250 μL of surfactant were added dropwise to the continuous phase. In stage 3 (initiated a further 20 minutes after stage 2), 250 μL of initiator solution, 2 mL of the dispersed phase, and 250 μL of surfactant were added to the continuous phase. The reaction was then left to proceed for 2 hours at 65 $^\circ\text{C}$ with nitrogen purging under 500 rpm stirring. Following, the surfactants and continuous phase were extracted using hexane, after which the collected magnetic beads (in the aqueous phase) were magnetically washed with Milli-Q H_2O over 5 cycles and stored at 4 $^\circ\text{C}$ in water.

2.3.4 Mechanical testing

The formation of microgel was confirmed with mechanical testing using a Microsquisher (CellScale). Single polymer magnetic beads were probed using a cantilever system consisting of a 0.2032 mm diameter wire (enabling a force resolution of 0.604 μN and maximum force of 181 μN) to which is glued a 1cm x 1cm square platen. The deformation of magnetic beads was continuously monitored by an imaging system

through recording the difference between the current microbeam tip position to the initial tip position. Three specimens were tested over three cycles consisting of load, hold, recovery and rest phase. During the load phase, the compression plate applied force to the specimen and induced its deformation. Following that, the deformation or displacement of specimen was held for 10 seconds until the beginning of recovery phase, at which point the applied force was removed from specimen. The rest phase followed the recovery phase and represented the time between the end of one cycle and the beginning of the next cycle. The stiffness was calculated based on a modified Hertz model representing the nominal stress divided by the nominal strain value at 10% nominal compression of the sphere (Equation 1)

$$\begin{aligned}\phi &= \cos^{-1} \left[\frac{R-\delta}{R} \right] \\ a &= (R - \delta) \tan\phi f(a) = \frac{2(1+\nu)R^2}{(a^2+4R^2)^{3/2}} + \frac{1-\nu^2}{(a^2+4R^2)^{1/2}} \\ E &= \frac{3(1-\nu^2)F}{(4\delta a)} - \frac{f(a)F}{\pi\delta}\end{aligned}\tag{1}$$

F = applied force

R = sphere radius

δ = displacement

ν = Poisson's ratio (0.5)

E = Young's Modulus

2.3.5 Size characterization

The size of the magnetic microgels was characterized using a Mastersizer 2000 (Malvern Panalytical), a laser diffraction testing instrument. Magnetic microgels were suspended in Milli-Q H₂O and passed through a laser beam, causing laser diffraction at multiple angles. The light intensity at each position was measured by the detector and fit to Mie scattering theory to identify a particle size. The concentration of sample was calculated based on the rearrangement of Beer-Lambert law, which is expressed as Equation 2.

$$\alpha = \frac{-1}{b} \ln\left(\frac{I}{I_0}\right) \quad (2)$$

I = intensity of light at a distance b in the particle field of absorbance α

I_0 = intensity of light beam before it enters particle field

The size of the particle i can then be calculated based on particle radius r_i from Mie theory from equation below:

$$r_i = \sqrt{\frac{\alpha_i}{Q_i \pi n_i}} \quad (3)$$

Q_i = efficiency of light extinction

n_i = number of particles of radius r_i

Each sample was measured three times, with the average size based on particle surface area reported.

Inverted brightfield microscopy (Olympus) and scanning electron microscopy (SEM, Tescan) were used to visually confirm the results from the Mastersizer. For inverted brightfield microscopy, a drop of the magnetic microgel suspension was placed on glass

slide and observed directly with different objectives (10×, 20×, 40×). SEM was performed using an operating voltage of 10 kV under low vacuum mode. Samples were dried at room temperature on a carbon tape covered SEM stub prior to imaging.

2.3.6 Conductometric base-into-acid titration

The degree of methacrylic acid functionalization was determined by conductometric base-into-acid titration using a Burivar-I2 automatic buret (Mantech) running PC titrate software. 10-15 mg of magnetic microgel suspended in Milli-Q H₂O was magnetically washed with 3 mM NaCl solution over three cycles and resuspended in 3 mM NaCl solution. The magnetic microgel dispersion was purged with nitrogen for 20 minutes prior to titration, and the pH of magnetic bead solution was adjusted to 2.75. The system was set to inject 0.001 mL 0.1 M NaOH every 20 seconds until the solution achieved a pH of 11. The degree of MAA functionalization was calculated based on the amount of NaOH used to titrate the carboxyl groups.

2.3.7 Thermogravimetric analysis

Thermogravimetry (Mettler Toledo TGA/DSC 3+) was used to determine the content of iron oxide inside the magnetic microgels. Magnetic microgels suspended in water were freeze dried and vacuum dried to remove water prior to testing. Between 1-5 mg dried sample was loaded into a pre-weighed alux70 µL crucible. Three stages of heating were used: (1) heating from 25 °C to 100 °C at 20 K/min; (2) holding at 100 °C for 5 minutes; and (3) further raise the temperature from 100 °C to 800 °C at 10 K/min. The whole

process was conducted under argon environment with a flow rate of 30 mL/min. The mass was monitored continuously over time, with the iron oxide content of the magnetic microgels calculated by dividing the percentage of sample mass remaining after thermal decomposition by the total mass of sample.

2.3.8 Magnetization

The magnetization of the magnetic microgels was visualized using a magnetic separation test. Homogeneously dispersed magnetic beads were attracted to one side of the scintillation vials using a neodymium magnet. The time between the first exposure to magnet and complete isolation of magnetic beads from the suspension (as indicated by the change in color in the suspension from brown to clear) was recorded.

2.3.9 Electrophoretic mobility

The electrophoretic mobility, correlated to the surface charge density, was measured using a Brookhaven zeta potential analyzer running in phase analysis light scattering (PALS) mode. Magnetic microgels were magnetically washed and re-suspended in 0.1 M NaCl. Electrophoretic mobility measurements were then performed at a count rate ranging from 300 kilocounts/s to 700 kilocounts/s, with the average of six measurements was reported for each sample. The long-term stability of magnetic microgels was tested by continuously monitoring the electrophoretic mobility of three different batches of magnetic microgels over one month.

The size of magnetic microgels over time (correlated with both colloidal stability and any potential degradation) was monitored with a Mastersizer 2000 (Malvern Panalytical). Each sample was measured three times, with the average size and the standard deviation (as the error bar) of these repeat measurements reported. The long-term stability of the magnetic microgels was tested by continuously monitoring the average size changes of three independent batches of magnetic microgels over one month.

2.3.10 Protein Anti-Fouling Property

The anti-fouling property of magnetic microgels towards protein was tested and compared to that of Dynabeads under the same conditions. Four different proteins - bovine serum albumin (BSA), IgG, lysozyme, and fibrinogen - were selected for assessment. A 10 μL suspension of 1 mg/mL magnetic microgels was prepared by magnetically washing the beads and resuspending in $1\times$ PBS. 7.5 μg of each type of protein (10 μL of 750 $\mu\text{g}/\text{mL}$ protein stock) was incubated with 20 μg magnetic microgels for 1 hour with gentle shaking. The microgels were then magnetically separated and the supernatant was collected, followed by another two washing steps to remove loosely adsorbed protein. 10 μL of the supernatant was then added to 150 μL Pierce 660 nm assay reagent, shaken for 1 minute, and incubated for 5 minutes. The amount of protein remaining in the solution was determined for each sample using a Pierce 660 nm assay, with the colorimetric change of the Pierce assay reagent in the presence of protein measured using a plate reader (Tecan M200) operating at 660 nm wavelength. The concentration of residual (unbound) protein was calculated based on a

calibration curve prepared for each protein built by preparing the protein solutions with concentrations of 1000, 750, 500, 250, 125, 75, 50, 25, 10, 1 $\mu\text{g/mL}$.

2.3.11 Loading efficiency test

The loading efficiency of *E.coli* DNAzyme on magnetic beads was verified with both a fluorescence test and an electrochemical test. For both tests, *E.coli* K12 (MG1655) from a regularly maintained stock was used as a target to verify assays. The bacterial crude intracellular matrix (CIM) was prepared by centrifuging 1 mL of the bacterial dilution (10^8 CFU/mL) at $11,000 \times g$ for 5 min at 4°C . Following this, the cell pellet was re-suspended in 100 μL of Milli-Q H_2O and heated at 65°C for 10 min to release the RNA cleaving DNAzyme-activating target. The heat-treated cell suspension was then vortexed to dissolve the cell pellet completely and stored at -20°C .

The sequences of amine-terminated RNA cleaving DNAzyme (aRCD) used for both the electrochemical and fluorescence tests are as follows:

Table 2.1 Summary table for sequence of amine-labeled *E.coli* DNAzyme probes (aRCD).

Name	Electrochemical Test Sequence (5'-3')	Fluorescence Test Sequence (5'-3')
E.col DNAzyme Probes (aRCD)	5'-MBTTTTTTTGTGTGACT CTTCCTAGCTrATGGTTCG ATCAAGAGATGTGCGTCT TGATCGAGACCTGCGAC CGTTTTTTTTTTamin -3'	5'-FAMTTTTTTTGTGTGACT CTTCCTAGCTrATGGTTCG ATCAAGAGATGTGCGTCT TGATCGAGACCTGCGAC CGTTTTTTTTTTamin -3'
Aminated Part	GATGTGCGTCT TGATCGAGACCTGCGAC CGTTTTTTTTTTamin -3'	GATGTGCGTCT TGATCGAGACCTGCGAC CGTTTTTTTTTTamin -3'
Tagged Part	5'-MBTTTTTTTGTGTGACT CTTCCTAGCTrATGGTTCG ATCAAGA	5'-FAMTTTTTTTGTGTGACT CTTCCTAGCTrATGGTTCG ATCAAGA
Ligation Template	5'-CAAGACGCACATCTCTTG ATCGAACC-3'	5'-ATCAAGACGCACATCTCTT GATCGAACCA-3'
Capture Probe	5'-TAGCTAGGAAGAGTCAC ACAthiol-3'	N/A

2.3.11.1 Fluorescence assay to quantify DNAzyme cleavage efficiency

Amine-terminated RNA cleaving DNAzyme (aRCD) was prepared by T4 DNA ligase-mediated DNA ligation of a fluorescent substrate and DNAzyme in the presence of a ligation template. More specifically, *E.coli* specific RNA cleaving DNAzyme was first sequenced based on the *in vitro* selection technique [8]. Following that, a T4 nucleotide kinase reaction was performed on the aminated part of the DNA to add a 5' end

phosphate, which allows the phosphodiester bond formation between the tagged and aminated part of the DNA; this reaction is directed by the ligation template under the action of ligase enzyme. Subsequently, to graft the DNAzyme to the magnetic microgel beads, an aliquot of 5 μL of magnetic microgels with a concentration of 1 mg/mL was magnetically washed and re-suspended in MES buffer (pH 6, 25 mM). The carboxyl groups from the methacrylic acid residues were then activated by adding 15 μL of a solution consisting of EDC: NHS: MES buffer (10 mM:15 mM: 25 mM) to 5 μL of the magnetic microgel suspensions and incubating for 30 minutes at room temperature under gentle shaking. Following, the microgels were magnetically washed in the same MES buffer to remove unreacted EDC/NHS. Following, 20 μL of 0 μM , 0.1 μM , 1 μM , of 100 μM aRCD in 25 mM MES buffer were added and incubated with prepared magnetic microgels at 4 $^{\circ}\text{C}$ under gentle shaking in dark. After the reaction, aRCD conjugated magnetic beads were washed with 1 \times PBS (pH 7.4) and the amount of unbound DNAzyme in supernatant was measured using a plate reader (Tecan M200) operating at an excitation wavelength of 488 nm and an emission wavelength of 520 nm.

To assess the activity of the grafted aRCD conjugated magnetic microgels, 5 μg of the functionalized magnetic microgels (i.e. after removing all supernatant) was mixed with 20 μL *E.coli* CIM with a concentration of 10^6 CIM/mL buffer for 2 hours at room temperature under gentle shaking. Magnetic beads were then washed with 1 \times PBS (pH 7.4) and removed from the suspension magnetically, with the cleaved DNA probes in the

supernatant measured using a plate reader (Tecan M200) operating at an excitation wavelength of 488 nm and emission wavelength of 520 nm.

2.3.11.2 Electrochemical assay to quantify DNAzyme cleavage efficiency

The electrochemical characterization of *E.coli* DNAzyme loading efficiency was performed using polystyrene (PS)-templated electrodes. PS was first cleaned by rinsing with ethanol and Milli-Q H₂O followed by N₂ drying. PS was further masked with a vinyl sheet, which was peeled and cut according to the chip pattern designed. After a 100 nm gold film was sputtered on the exposed area of vinyl sheet, the mask was removed. Each gold sputtered chip was comprised of one working electrode and one Ag/AgCl reference electrode. A working electrode with a gold hierarchical structure was fabricated by electrodepositing a solution of 10 mM gold chloride (HAuCl₄) in 5 mM HCl using a CHI 420B potentiostat (CH Instruments, Austin, TX) with an operating voltage of -0.6 V (anodic negative) for 600 s. Before the immobilization of capture probes, the working electrode was rinsed with isopropyl alcohol and Milli-Q H₂O and activated electrochemically using cyclic voltammetry in 0.1 M H₂SO₄ (potential range: 0-1.5 V, scan rate: 0.1 V, cycles: 40). Following, 10 μL of a 1.5 μM single stranded thiol terminated capture probe solution was reduced with 10 μL of a 150 μM tris(2-carboxyethyl) phosphine (TCEP) solution (both in Milli-Q water) for two hours in the dark at room temperature and then deposited on the electrochemically activated working electrode for 18 hours. Following, 3 μL of 100 mM 6-mercaptohexanol (MCH) solution was deposited on the surface as a back-filler for 20 minutes in the dark at the room

temperature. The electrochemically active surface area of the gold nanostructured working electrode was assessed via cyclic voltammetry (CHI 420B, Austin, TX) in 0.1 M H₂SO₄ (potential range: 0-1.5 V, scan rate: 0.1V, cycles: 40). The area under the reduction curve was integrated to calculate the electrochemical charge involved in the redox process and was divided by the surface charge density involved in forming a monolayer of gold oxide (AuOx) (386 $\mu\text{C}/\text{cm}^2$)

The aRCD for electrochemical test was prepared by T4 DNA ligase-mediated DNA ligation of DNAzyme and methylene blue substrates in the presence of ligation template, using a process similar to that described for the preparation of fluorescently-labelled DNAzyme. A 5 μL aliquot of a 1 mg/mL magnetic microgel suspension was washed and suspended in MES buffer (pH 6, 25 mM) followed by activation in 15 μL of a EDC:MHS:MES solution (10 mM:10 mM:25 mM) for 30 minutes at room temperature under gentle shaking. Magnetic microgels were further washed in MES buffer (pH 6, 25 mM) to remove non-specifically adsorbed EDC/NHS. Following, 10 μL of 1 μM aRCD was added to 10 μL of a magnetic bead suspension and 80 μL of 25 mM MES (100 μL total volume), followed by incubation for 12-18 hours at 4 °C under gentle shaking in the dark. After the reaction was complete, aRCD-conjugated magnetic microgels were washed with 25 mM MES and 1 \times PBS and resuspended in 1 \times PBS for further use.

To assess the activity of the aRCD-conjugated magnetic microgels electrochemically, the microgels were incubated with 20 μL of 10 \times *E.coli* CIM for 30 minutes at room

temperature under gentle shaking. Magnetic microgels were then magnetically separated, and the methylene blue (MB) reduction signal of the hybridised MB-barcode with CP was measured by square wave voltammetry (SWV, CHI 420B, Austin, TX) over a voltage range of 0 V to -0.6 V (anodic negative) for 30 minutes at 37 °C. The background signal of electrode in the presence of bacteria but without any DNAzyme cleavage was assessed by spiking the bacteria CIM dilution in 1× PBS and performing the same electrochemical measurement using the chip.

The detection of the bacteria spiked in urine was carried out by diluting the bacterial CIM from undiluted urine with concentrations of 10^7 CFU/mL down to 1 CFU/mL using 1× PBS. All urine samples were received at Hamilton General Hospital's Clinical Pathology lab through culture on the Walk Away Specimen Processor (WASP) and handled according to the protocols approved by the Hamilton Integrated Ethics Board (HiREB). After evaluation through culture, throughout which the urine samples were stored at 4 °C, the samples were tested (within 5 days) on the e-DChip using the same protocol described above for samples tested in buffer.

2.4 Results and discussion

2.4.1 Optimization and characterization of POEGMA magnetic microgel beads

The preliminary microgel synthesis protocol was designed according to the published protocol by Kriwet et al. for poly(acrylic acid) microgel beads [4]. In this work, the original recipe of the oil phase contained 14 mL silicone oil and 500 μ L of a surfactant mixture comprised of 75 v% of Span 80 and 25 v% of Tween 80 while the water phase was comprised of 1 mL OEGMA475 and 400 μ L of EDGMA. The oil phase was first purged with nitrogen in an oil bath of 80 °C for 30 minutes under magnetic stirring, after which the water phase was added and the whole mixture was purged with nitrogen for another 30 minutes under stirring. Polymerization was initiated once the water-soluble initiator ammonium persulfate (0.16 wt%) was added to the reaction flask, and the whole reaction was allowed to proceed under magnetic stirring at 500 rpm for 2 hours.

However, as shown in Figure 2.3, magnetic beads produced by this method were severely aggregated with large particle sizes (\sim 300 μ m), too large for achieving high surface area bioactive sensors with high DNAzyme loading capacities; in comparison, most commercial magnetic beads used for bioseparation and biopurification (e.g. Dynabeads or Bang's beads) have sizes <10 μ m. This protocol was also observed to suffer from low reproducibility, consistent with a key documented challenge with the inverse emulsion polymerization system [65]. However, the mechanical properties of the microgel beads are appropriate for biosensing, with MicroSquisher testing indicating the magnetic microgels have a Young's moduli of \sim 6 kPa and good reversibility over multiple compression cycles (Figure 2.4). As such, the inverse emulsion templating method is a

feasible strategy to fabricate magnetic microgels but required further optimizations to improve its repeatability and reproducibility and achieve magnetic beads with minimum aggregation, high stability, and a target size of ~5-20 μm that offers a combination of high magnetization, reasonable colloidal stability, and high loading efficiency [190], [191].

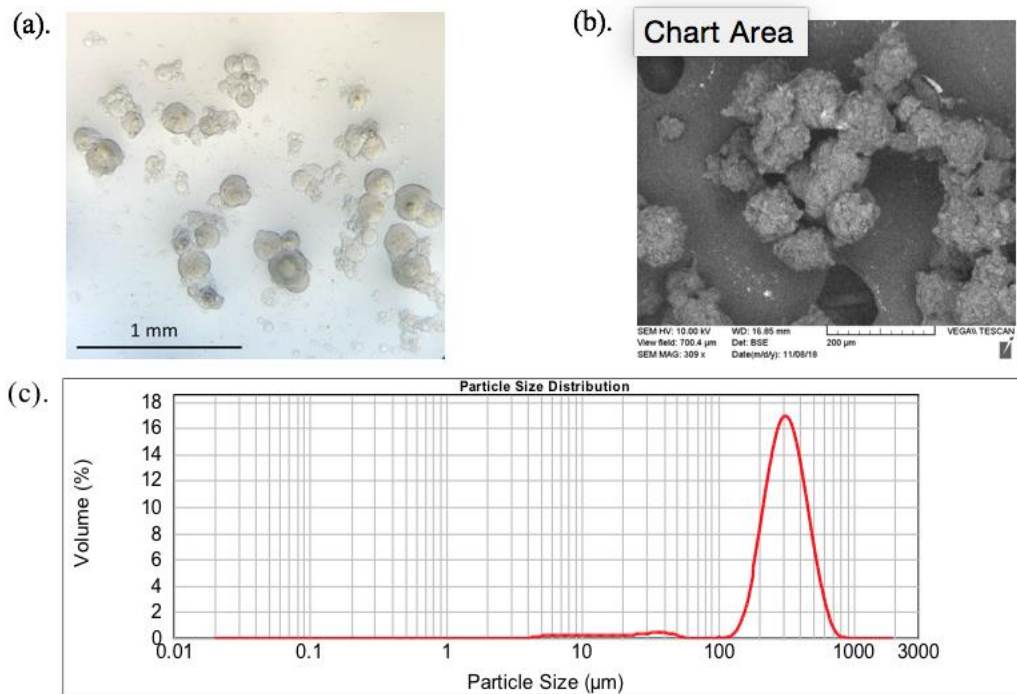


Figure 2.3 Particle size distribution of magnetic microgel beads produced based on the protocol of Keiwet et al [4]. (a). Optical microscope image (scale bar = 1 mm); (b). Scanning electron microscope image (scale bar = 200 μm); (c). Mastersizer laser diffraction particle size distribution.

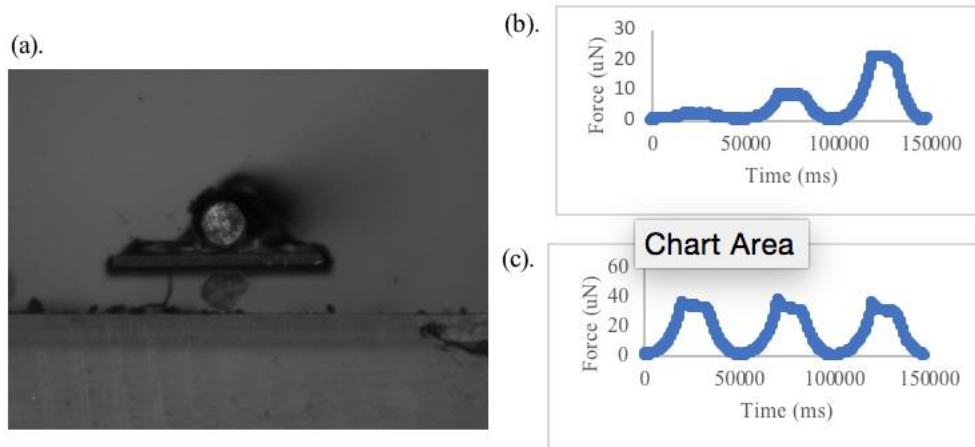


Figure 2.4 Mechanical properties of magnetic microgel beads as measured using the MicroSquisher. (a) Image of a magnetic microgel being compressed by a compression platen glued to a microbeam cantilever. (b) Time (ms) versus force (μN) following sequential 5%, 10%, and 15% compression of the magnetic microgel. (c) Time (ms) versus force (μN) following 3 repeated 10% compressions of the magnetic microgel.

Given that multiple factors including the emulsification method, quantity of emulsifier, stirring speed, and oil phase viscosity significantly influence the emulsion size [192][193], we first assessed the impact of changing the viscosity of the silicone oil (5 cst, 10 cst) or olive oil (~ 100 cst) used as the continuous phase. Magnetic microgel beads prepared with higher viscosity oils exhibited smaller sizes and lower aggregation, with microgels synthesized using the lowest viscosity 5 cst silicone oil exhibiting the worst stability and tending to form chunks of gel pieces. This result is consistent with the reduced diffusibility of the aqueous phase in higher viscosity oils, leading to reduced droplet coalescence prior to gel formation. Other factors such as the overall concentration of different components in the aqueous phase and the speed of adding water phase to the oil phase were also tested for their influence on the particle size. Slow

addition rates of the water phase and lower concentrations of components in water phase help to produce particles with smaller sizes but do not solve the aggregation issues.

Another hypothesis was that the hydrophilic magnetic microgel beads tend to clump together in oil such that the aggregation problems would be alleviated once surfactant and oil were washed off. However, while the microgel beads swelled as expected once they were separated and re-suspended in water, the aggregation problem persisted.

In the next set of experiments, the pH of the aqueous phase was adjusted to neutral (pH 7) prior to adding the aqueous phase to the oil phase, aiming to reduce aggregation by ionizing the co-polymerized carboxyl groups from the methacrylic acid residues in the microgel and thus enhancing electrosteric repulsion between the particles during polymerization. In addition, magnetic stirring was replaced with mechanical stirring to minimize any influence of the magnetization of the stirring bar in aggregating the magnetic particles. As shown in Figure 2.5, these changes significantly reduced aggregation, with both optical microscopy and laser diffraction particle sizing indicating the formation of magnetic beads with size $\sim 100 \mu\text{m}$. These magnetic beads can also be separated magnetically with the neodymium magnet in 10 minutes.

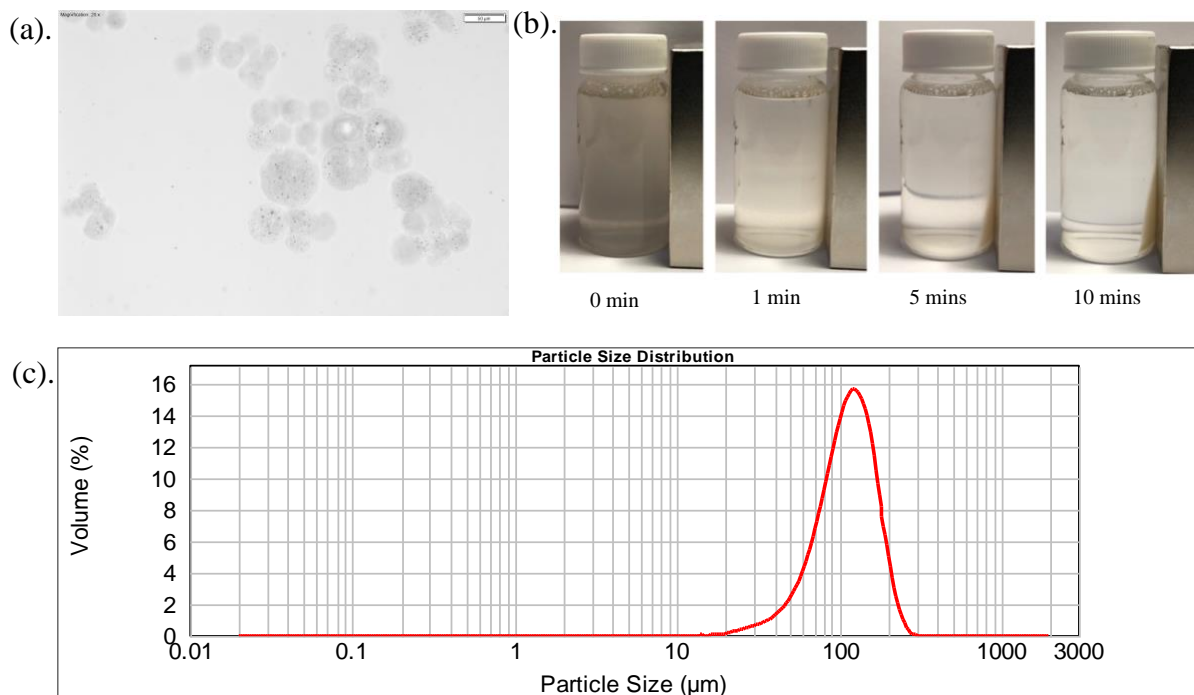


Figure 2.5 Magnetic beads produced by adjusting the pH of water phase to ~ 7 and using a mechanical stirrer. (a) Optical microscopy image ($50 \mu\text{m}$ scale bar). (b). Magnetic separation with time. A magnet was placed to the right of the scintillation vial. From left to right is the magnetic attraction of the microgel at 0, 1 5, and 10 minutes after exposure to the magnet. (c) Mastersizer analysis of the particle size distribution

Another important improvement to the original protocol was to change the washing process. Previous papers reported using centrifugation to separate microgels from oil and surfactant, albeit with the limitation of potential damage to microgels as well as aggravation of aggregations issues as the pellet is formed. Moreover, centrifugation is effective only when the density of the solvent is close to that of polymer [194]. Therefore, a phase inversion separation method was chosen over magnetic separation to improve the removal of the organic components from the synthesis procedure. Microgels were added to a separatory funnel which contains an equal volume of Milli-Q H_2O and hexane. Ideally, surfactant and oil will dissolve in the organic hexane phase while but microgels

will be retained in water. However, due to the presence of the surfactant, a large amount of oil bubbles or oil-in-water emulsions of size ~ 1 micron (as visualized by optical microscopy) were created during washing process that attached on the microgels and proved especially hard to remove. Washing the magnetic microgels with hexane three times before adding water helped remove most oil and surfactant and significantly reduced the possibility of forming oil bubbles.

The last optimization performed was to introduce a semi-batch feeding process. Aqueous phase, initiator, and surfactant were divided into three parts and were fed in three batches: (1) at the start of the polymerization (16% of the total aqueous volume); (2) 20 minutes after the first initiation (42% of the total aqueous volume); and (3) 40 minutes after the first initiation (42% of the total aqueous volume). The reaction was then allowed to proceed for 2 hours after the last feed was complete. Using the semi-batch process ensures stable chain growth throughout the whole polymerization process, previously noted to suppress aggregation and help achieve smaller particle sizes. This is because one feature of semi-batch polymerization process is that the growth rate of primary particles can be controlled by the rate of monomer feeding. In this case, the low aqueous phase volume at the start of polymerization (i.e. the volumetric ratio of water phase fed during the three stages is 1:2.5:2.5), increasing the number (and decreasing the diameter) of “seed” particles that can then be further grown as more aqueous phase is added, As shown in Figure 2.6e, magnetic microgel beads with size ~ 50 μm were synthesized and the size distribution of microgels was also significantly narrower. Semi-batch process

also makes the polymerization more controllable, so the reproducibility and repeatability of the protocol was much improved. However, the loading density of *E.coli* DNAzyme on these microgel magnetic beads was much lower than that of Dynabeads based on the electrochemical detection of redox signal of methylene blue from the hybridization of DNA barcodes and capture probes.

To address this loading problem, the degree of MAA functionalization was increased from 5 wt% to 30 wt% to provide more DNAzyme immobilization sites, otherwise using the same semi-batch protocol described above. As shown in Fig. 2.6f, the 30 wt% MAA functionalized magnetic beads were significantly smaller, with size of $\sim 5 \mu\text{m}$ that is more consistent with that of commercial magnetic beads, while avoiding any substantial aggregation. Scanning electron microscope measurements on the 30 wt% functionalized MAA also show relatively uniform iron oxide distribution inside microgel (Figure 2.6c), suggesting good dispersibility of the INPs inside the microgel phase. Magnetic beads synthesized with this protocol can also be separated magnetically from the suspension in 5 minutes (Figure 2.6d). Therefore, the 30 wt% functionalized MAA protocol was selected as the leading candidate to proceed with further characterization.

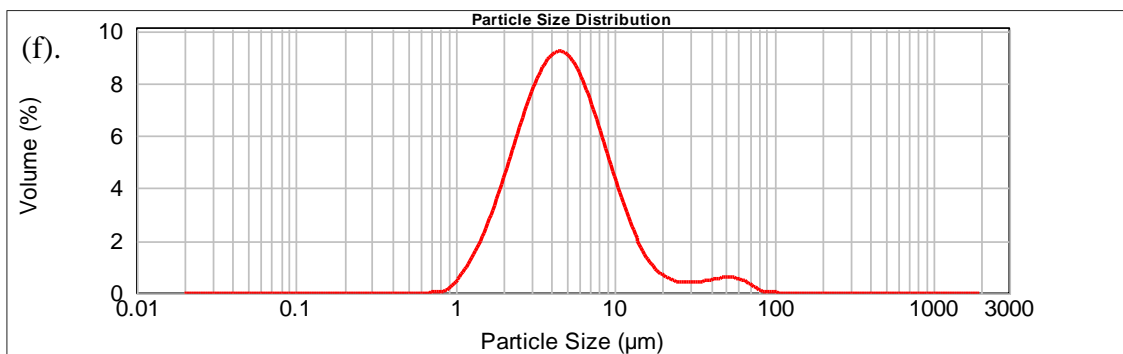
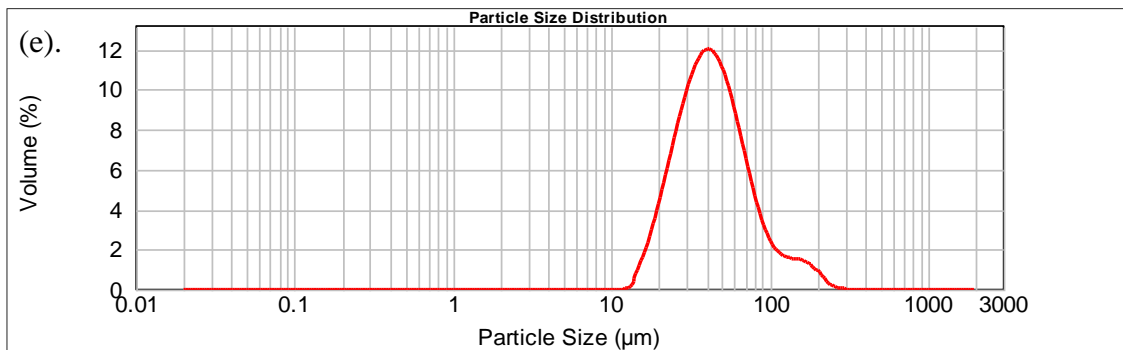
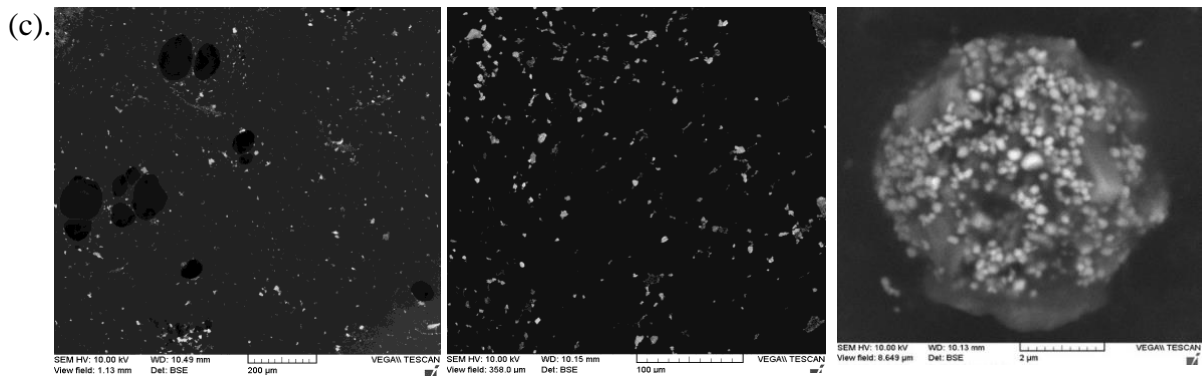
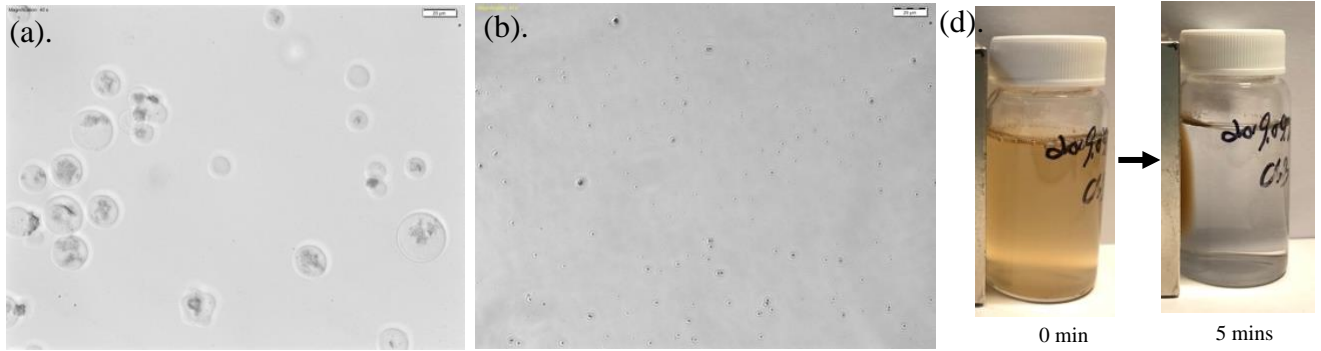


Figure 2.6 Comparison between 5 wt% MAA functionalized magnetic particle and 30 wt% MAA functionalized magnetic particles. (a) Optical microscope image of 5 wt% MAA functionalized magnetic particles (20 μm scale bar). (b) Optical microscope image of 30 wt% MAA functionalized magnetic particles (20 μm scale bar). (c) Scanning electron microscope images for 30 wt% MAA functionalized magnetic particle. From left to right, the scale bar is 200 μm , 100 μm , and 2 μm . (d) Magnetic separation with time. A magnet was mounted at the right of the scintillation vial. From left to right is the magnetic attraction of microgel at 0, 1 3, and 5 minutes after the magnet is mounted. (e). Mastersizer analysis shows the average particle size of 5 wt% MAA functionalized magnetic microgel is at $\sim 50 \mu\text{m}$. (f). Mastersizer analysis shows the average particle size of 30 wt% MAA functionalized magnetic microgel is at $\sim 5 \mu\text{m}$.

To assess whether aggregation can be further reduced by changing the total amount of surface-stabilizing emulsifier added to the synthesis, the amount of emulsifier added to the organic phase was increased from 2.5 mL surfactant mixture/42 mL oil to 4.5 mL surfactant mixture/42 mL oil, the results of which are shown in Figure 2.7.

Increasing the emulsifier concentration was found to minimally influence the particle size distribution, suggesting that the lower surfactant concentration is already sufficient to stabilize the total surface area generated in the emulsion. As such, the lower surfactant concentration was continued to be used for assay validation.

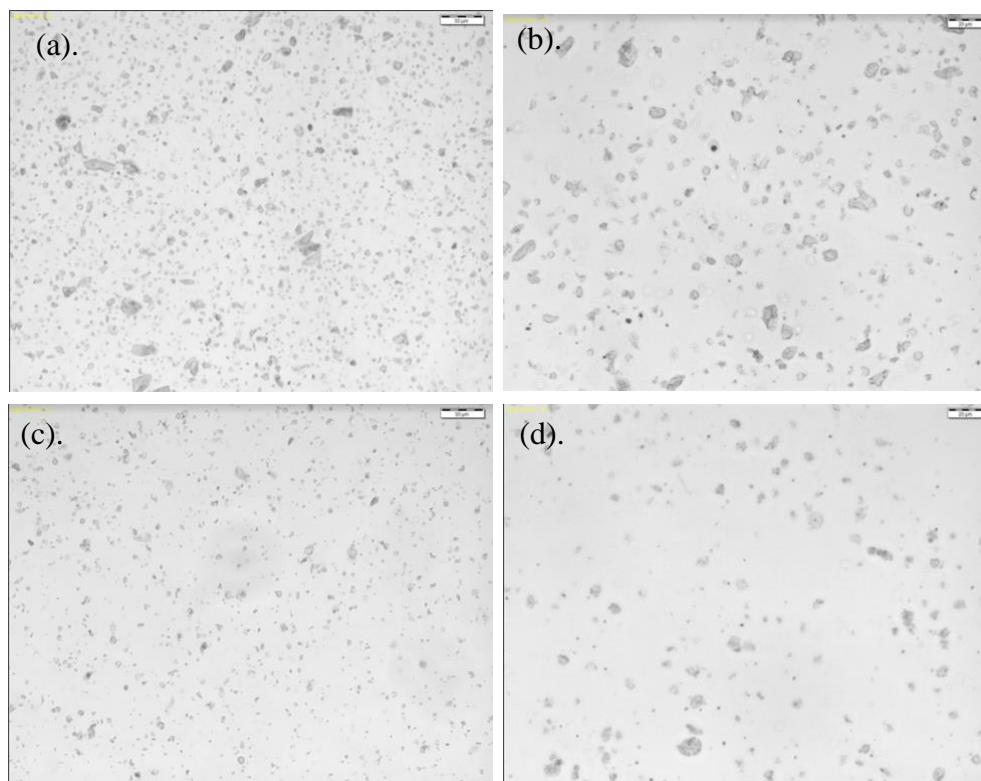


Figure 2.7 Optical microscope images for magnetic beads synthesized with different surfactant concentration. (a, b) 4.5 mL Span 80: Tween 80 surfactant mixture (75 v% : 25 v%) in 42 mL oil phase; (c, d) 2.5 mL Span 80: Tween 80 surfactant mixture (75 v% : 25 v%) in 42 mL oil phase. The scale bar for (a) and (c) is 50 μm and that for (b) and (d) is 20 μm .

2.4.2 Degree of surface functionalization

The surface of the magnetic microgels consists of a mixture of oligo(ethylene glycol) and carboxyl groups, the latter of which are derived from co-polymerized methacrylic acid and provide immobilization sites for amine-labelled *E.coli* DNAzymes. Therefore, the amount of carboxyl groups ultimately determines the loading density of magnetic beads while also contributing to their colloidal stability. The degree of methacrylic acid

functionalization was measured by conductometric base-into-acid titration. As seen in Figure 2.8, at the beginning of reaction, the pH of mixture was adjusted to ~ 2.75 such that there is a high concentration of highly mobile H^+ ions that resulted in a high conductivity. As sodium hydroxide was gradually added into the mixture, free H^+ ions were neutralized to form water and replaced by larger and less mobile sodium ions, so the conductivity decreased until all free hydrogen ions was consumed. At the pK_a of the carboxyl groups of the methacrylic acid residues, the carboxyl groups on the magnetic microgel beads are ionized, consuming added OH^- ions while introducing (very low mobility) COO^- ions and Na^+ ions; the net result of these changes is that the conductivity remains relatively constant, corresponding to the relatively flat region on the titration profile. After equivalence point when all carboxyl groups of polymer were ionized, further addition of sodium hydroxide introduces excess OH^- ions and Na^+ ions, increasing the conductivity again. Of note, the initial addition of acid to lower the pH prior to the titration resulted in some aggregations of the microgels due to the loss of electrosteric repulsion due to the presence of charged monomer residues. As such, sodium hydroxide first titrated carboxyl groups at the surface of the microgel aggregates and slowly redispersed the microgels during the titration as more $-COOH$ groups were ionized, consistent with the “step-wise” or “jagged” flat region observed on the curve.

The degree of carboxyl groups functionalization was calculated based on the equivalent amount of sodium hydroxide required for titration of the weak acid -COOH groups, corresponding to an experimental 24 wt% MAA functionalization for magnetic microgels, similar although slightly lower than the theoretical 30 wt% MAA content. This slight difference is likely attributable to the slow penetration of OH⁻ titrating ion into the microgels as they de-aggregate during titration, although the potential for some soluble polymer loss upon washing (given the high water solubility of any MAA-rich polymer chains) may also be a consideration.

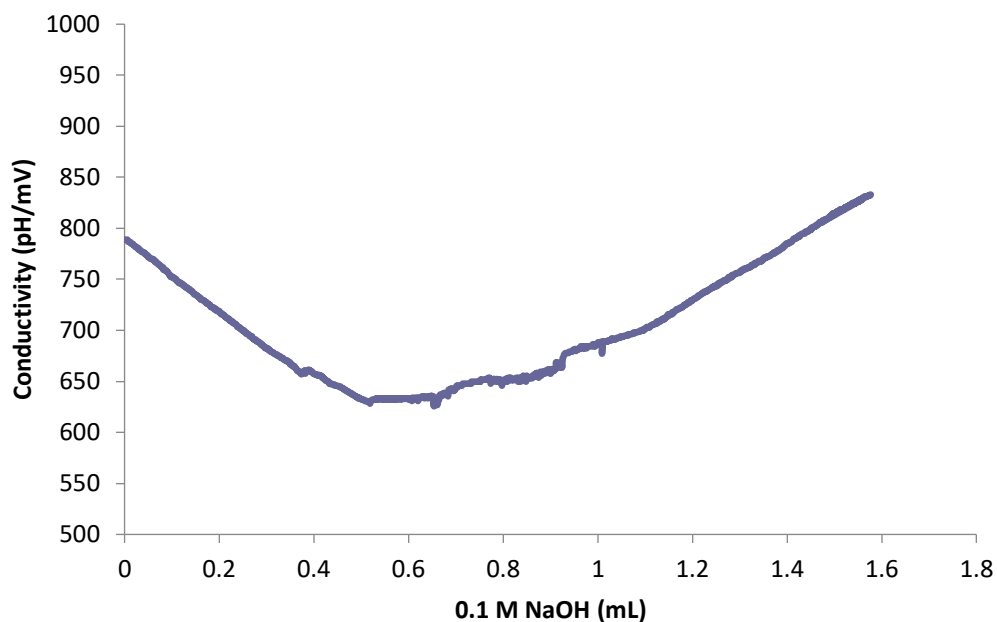


Figure 2.8 Base-into-acid conductometric titration curve. The x axis represents the amount of sodium hydroxide added while the y axis represents the conductivity of mixture.

2.4.3 Iron oxide content

The amount of iron oxide encapsulated inside the magnetic microgels regulates their magnetization. To assess the concentration of INPs encapsulated inside the microgels,

thermogravimetric analysis was used by conducting a three-stage heating cycle was conducted in which the sample was heated to 100 °C, held at 100 °C for 5 minutes to remove water residuals, and the temperature was ramped to 800 °C. The amount of mass lost from the heating stage of 100 °C to 800 °C was calculated as polymer mass, given that PEG decomposition begins at ~160 °C and is fully complete at 800 °C [195], [196]. Based on the curve, at temperatures below 200 °C, the weight loss was minimal (~2 wt%), attributable to the evaporation of chemically or physically absorbed water. The majority of the mass change occurs in the temperature range of 200-500°C, corresponding to the polymer mass; the remaining mass can be attribute to the iron oxide within the magnetic microgel, with the slight decrease in sample mass at ~700 °C attributable to the gradual oxidation of Fe₃O₄ into α -Fe₂O₃ [197]. Based on the TGA result (Figure 2.9a), the residual solids content was 22 wt%, much higher than the iron oxide concentration in the recipe which is only 1.5 wt%. This result suggests that there are many “white microgels” produced from the protocol with sufficiently low INP contents that they are not magnetically separable from the suspension, consistent with the limited turbidity maintained in the supernatant solution following the first magnetic separation cycle. However, as we tried to increase the iron oxide concentration from 1.5 wt% to 5.4 wt%, the electrochemical redox signal of methylene blue from the hybridization between DNA barcodes and capture probes decreased three-fold (Figure 2.9b), potentially due to the presence of more INPs reducing the beneficial swelling/porosity of the microgel bead. In the future, intermediate INP concentrations could be tested to see if magnetization could be improved to facilitate higher

magnetization or faster magnetic separation without sacrificing DNAzyme loading efficiency.

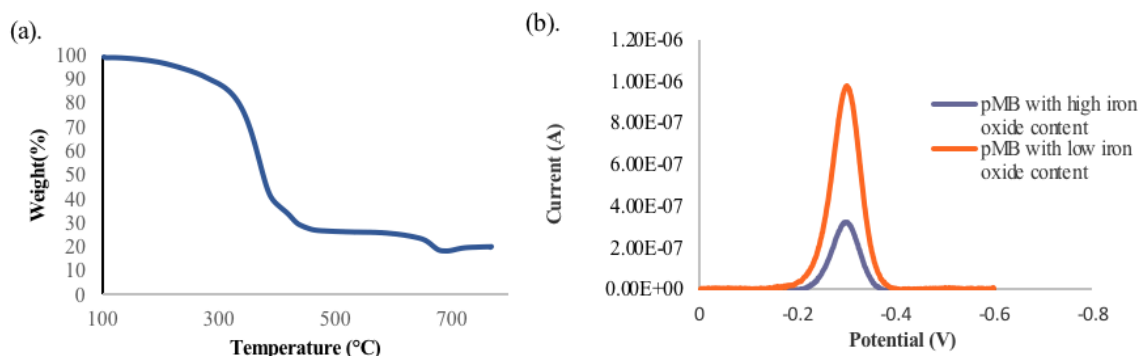


Figure 2.9 (a). Thermogravimetric analysis for 30 wt% MAA functionalized magnetic beads. (b). Electrochemical assay measuring the current associated with the methylene blue labeled DNA probe released from *E.coli* DNAzyme showing a 3-fold decrease in DNA probe signal for high iron oxide content beads compared to that from low iron oxide content beads.

2.4.4 Colloidal stability

Magnetic microgel beads can be stabilized both electrostatically by the presence of carboxyl groups on bead surface (from the MAA monomer residues) and sterically from the PEG side-chains of POEGMA [198]. The colloidal stability of magnetic microgel beads at room temperature was monitored by measuring the changes in the electrophoretic mobility (corresponding to the microgel charge) and the particle size over a one month period, the results of which are shown in Figure 2.10.

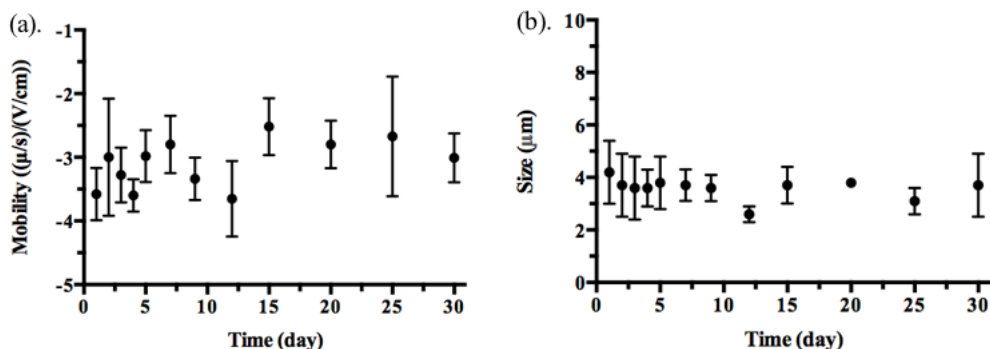


Figure 2.10 Particle stability over a one month period as tracked by changes in (a) electrophoretic mobility and (b) particle size measured via laser diffraction (sample stored at room temperature).

Both the electrophoretic mobility and the particle size remain essentially unchanged over the one month observation period, suggesting that the magnetic microgel maintain high colloidal and degradative stability over time (including extended storage times). Of note, while the conversion of electrophoretic mobility to zeta potential is theoretically questionable given the ion penetrability and soft nature of microgels [199][200], the electrophoretic mobilities measured correspond to zeta potential $>|30|$ mV, typically considered to be a threshold for electrostatic colloidal stability. The particle size result also clearly suggests minimal degradation of the magnetic microgels under normal storage conditions. As such, it is likely that the two possible mechanisms of degradation in the happen in magnetic microgels (i.e. hydrolysis of ester bonds within the EGDMA crosslinker and between the PEG side chain and the polymer backbone, Figure 2.11) do not occur, at least on the timescale of one month of storage. [201]–[203].

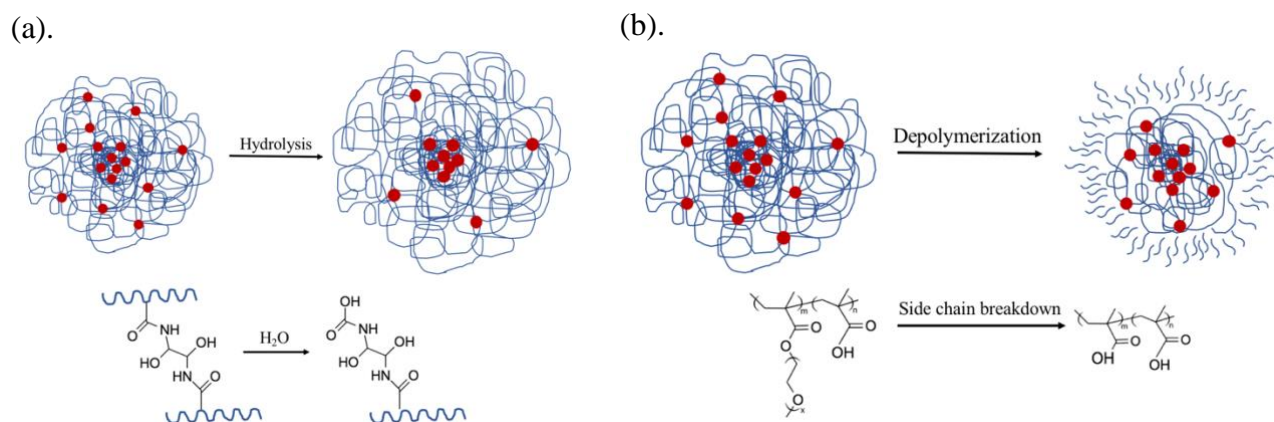


Figure 2.11 Illustration of two different possible pathways of magnetic microgel degradation. Left: the hydrolysis of crosslinkers EGDMA (red dots) lead to higher degree of swelling and larger hydrodynamic radius. Right: hydrolysis of the PEG side chains from the methacrylate backbone.

2.4.5 Reduction of non-specific protein adsorption/anti-fouling test

Magnetic microgels were designed to be used in untreated biological samples that contain multiple different types of interfering molecules that can sterically block access of the analyte to the surface and/or influence the alignment of analyte molecules on the surface, which is usually associated with their stability and functionality [204]. Consequently, magnetic particles for biological applications need to be modified to achieve minimal non-specific adsorption, most often through polymer coating, and most frequently with poly(ethylene glycol) [205]. However, the main polymer used to construct our magnetic microgel backbone is poly(oligo(ethylene glycol) methacrylate (POEGMA), which is a hydrophilic and non-ionic PEG-mimetic polymer that can bind a large amount of water to form a strong hydration layer at the surface [206]. As such, we do not anticipate the need

for any anti-fouling coating in this system, a significant advantage in the manufacturing of microgel magnetic beads relative to existing beads. The protein repellency of our magnetic microgel beads was thus compared to that of Dynabeads, which are coated with a hydrophilic layer of glycidyl ether to ensure low non-specific binding. Lysozyme, bovine serum albumin (BSA), immunoglobulin G (IgG), and fibrinogen were chosen to study the non-specific binding at the beads surface, chosen based on the prevalence of these proteins in biological samples and their broad range of shapes, molecular weight, and surface charges that represent different types of fouling present in clinical samples. Lysozyme is a globular enzyme existing abundantly in many types of secretions such as saliva, tears, and mucus with a net positive charge over a broad range of pH and a low molecular weight of ~14.3 kDa [207]. IgG, also a globular protein, is an antibody usually found in extracellular fluid and blood with a net anionic charge and relatively low molecular weight of ~20 kDa. Bovine serum albumin is a globular serum albumin protein with an intermediate molecular weight of 66.5 kDa and a net anionic charge at neutral pH, and moderate molecular weight. Lastly, fibrinogen is a glycoprotein with rod-like shape, net anionic charge at neutral pH, and a high molecular weight of 340 kDa. Proteins were dissolved in 1× PBS (pH 7.4) and incubated with magnetic microgel beads for 1 hour. Following three cycles of magnetic washing to remove loosely linked protein, the amount of protein left in supernatant was quantified by Pierce 660 nm colorimetric assay. According to Figure 2.12, both magnetic beads and Dynabeads showed good anti-fouling performance to BSA and IgG, both of which are globular proteins, and the worst anti-fouling performance towards fibrinogen, a rod-like protein, which is consistent with the

higher molecular weight of fibrinogen and its rod-like structure. Lysozyme adsorbs slightly more on the magnetic microgels is due to its net positive charge at physiological pH, promoting electrostatic interactions to the carboxyl groups on the magnetic microgel beads to a greater degree than the neutral Dynabeads [208]. However, overall, the magnetic microgels exhibit good anti-fouling properties that offer similar benefits in terms of preventing non-specific protein adsorption to the commercial Dynabeads.

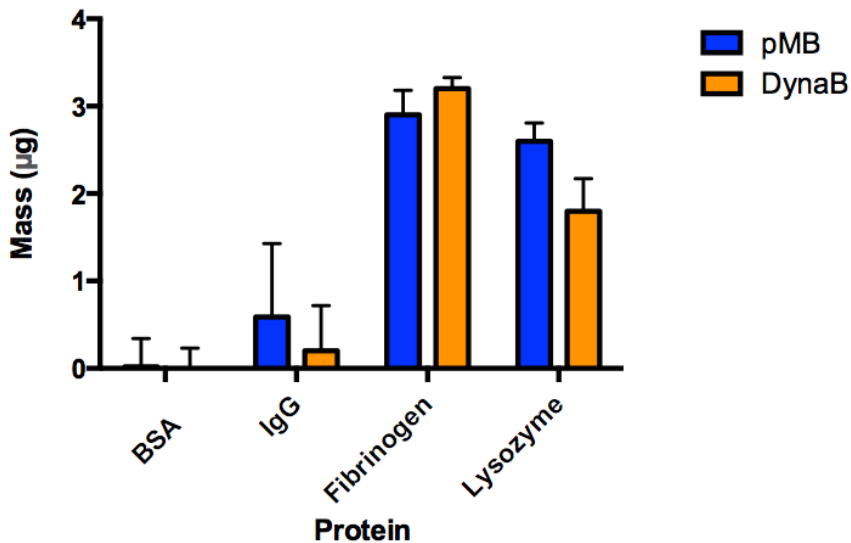


Figure 2.12 Anti-fouling/protein repellency test for POEGMA magnetic microgel beads (blue bar) and commercial Dynabeads (orange bar). For each measurement, 7.5 µg of protein was incubated with 20 µg magnetic beads and the amount of protein remaining in supernatant after washing was measured.

2.4.6 Loading efficiency test

The loading efficiency test compares the performance of *E.coli* DNAzyme immobilized magnetic microgel beads and Dynabeads in detecting *E.coli* targets by the release of DNA probes or DNA barcodes. Fluorescence and electrochemical detection were performed independently as complementary ways to verify the result. The amine-

terminated *E.coli* DNAzyme used for both tests has a similar sequence, such that the interaction of DNAzyme between targets and magnetic beads was kept consistent. As shown in Figure 2.13, using magnetic microgels with a low degree of MAA grafting (5 wt%), the current from the magnetic microgel beads was 170 times lower than that observed with Dynabeads; however, when the degree of MAA grafting was increased to 30 wt%, the hybridization signal from polymer magnetic beads was 6.3 times higher than that observed with Dynabeads. As such, the inherent flexibility of the chemistry of the microgel magnetic beads enables improved signal generation relative to leading commercial beads.

To assess the response of the magnetic microgel beads to varying *E.coli* CIM, 1 μM of aRCD was immobilized on both commercial and magnetic microgel beads and different concentrations of targets (*E.coli* CIM) were added. From Figure 2.14, the electrochemical signal increases systematically with the addition of more concentrated *E.coli* CIM, although the gradient in current gain is reduced as the concentration probably due to the saturation of magnetic beads with *E.coli* CIM. This advantage may not be as pronounced once both magnetic beads and Dynabeads are in high concentration of *E.coli* CIM. However, the magnetic microgel beads performed much better than commercial Dynabeads, with magnetic microgel beads demonstrating a 4.5 \times , 8.4 \times , and 12.2 \times increase in current output compared to Dynabeads at *E.coli* CIM concentrations of 10^6 , 10^4 , and 10^3 CFU/mL respectively. We attribute this result to one of two reasons: (1) the improved DNAzyme grafting efficiency enabled by increasing the degree of methacrylate

acid functionalization from 5 wt% to 30 wt% enables a higher capacity for signal generation upon exposure to the target; and/or (2) the porous gel surface and lack of a truly heterogeneous interface within the swollen magnetic microgels allows for higher accessibility of *E.coli* CIM to DNAzyme than Dynabeads, resulting in more efficient cleavage of DNA barcodes for the DNAzyme population that is present.

The electrochemical test was also used to compare the redox current generated by the hybridization of DNA barcodes released from magnetic beads with the capture probes in both buffer and in urine, the results of which were shown in Figure 2.15. In buffer, magnetic microgels demonstrated a 4.5× higher redox signal than that observed for Dynabeads upon the addition of *E.coli* CIM with a concentration of 10⁶ CFU/mL; in undiluted urine, the signal from the magnetic microgels was 97× higher than that from Dynabeads, suggesting particular benefits of the magnetic microgel beads for enhancing biosensor sensitivity in complex biological fluids. However, while the current measured in buffer was substantially better retained in urine using the magnetic microgels, a significant reduction in the redox current of DNA hybridization was still observed in urine for magnetic microgels. This result is most likely attributable to the presence of nucleases in the urine that can cleave the functional DNA barcodes or capture probes, preventing their hybridization and resulting in an overall low redox current.

The fluorescence test was performed as a complement to the electrochemical test by using fluorescently-labelled DNAzyme that releases a fluorescent marker upon probe

binding rather than the electrochemically-active methylene blue marker. Concentrations of 0, 0.1, 1, 10 μM of aRCD were immobilized on magnetic beads and incubated with *E.coli* CIM with the concentration of 10^5 CFU/mL, after which ungrafted aRCD in the supernatant was quantified to determine the loading efficiency; following, the aRCD immobilized magnetic beads were incubated with *E.coli* CIM and the cleaved DNA barcodes were quantified for cleavage efficiency. As shown in Figure 2.16, magnetic microgel beads show a significantly higher loading efficiency for aRCD at all concentrations and comparable cleavage efficiency. However, the difference in performance between commercial magnetic beads and magnetic microgel beads in terms of their cleavage efficiency is not as obvious as the result suggested by the electrochemical test. We hypothesize this result is due to the significantly lower sensitivity of the fluorescence test relative to the electrochemical test.

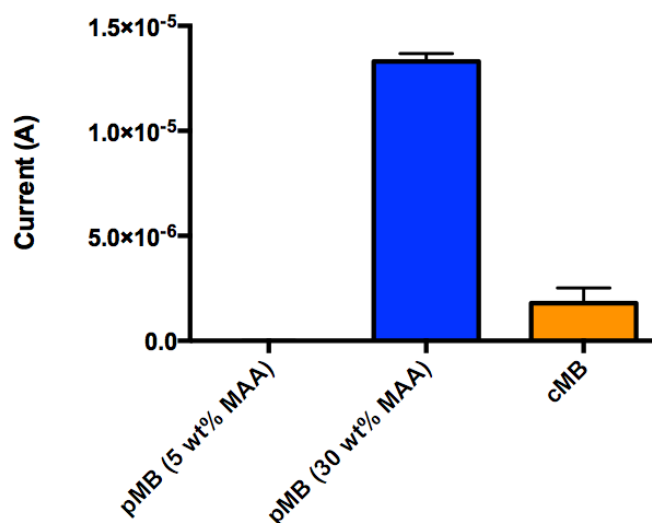


Figure 2.13 Electrochemical test comparing the performance of magnetic microgel beads (pMB) prepared with low and high degrees of MAA functionalization with commercial magnetic beads (cMB) exposed to 10^7 CFU/mL of *E.coli* CIM. The electrochemical signal was quantified by the redox current derived from released methylene blue following the hybridization of DNA barcodes with capture probes.

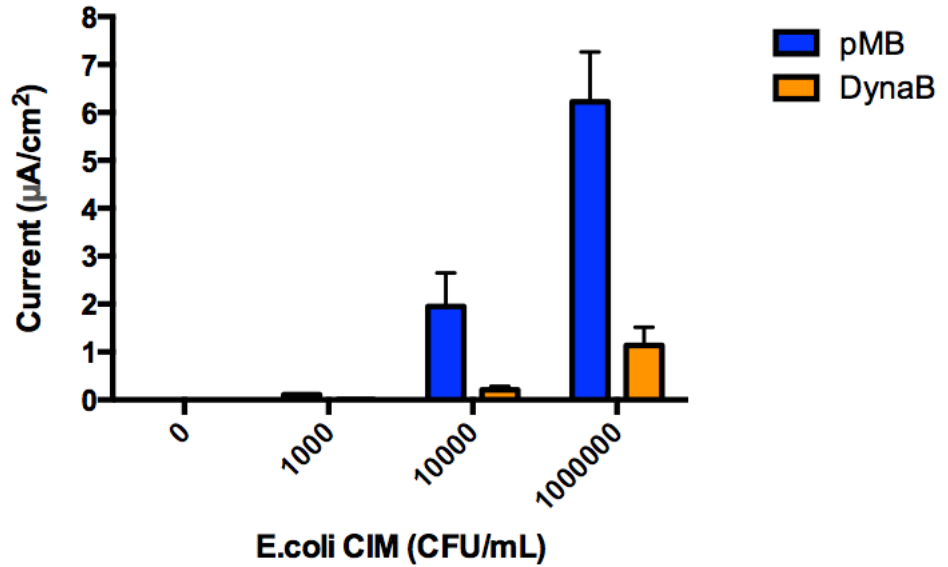


Figure 2.14 Electrochemical test comparing the performance of pMB and cMB with *E.coli* CIM of different concentrations. The electrochemical signal was quantified by the redox current released by released methylene blue following the hybridization of DNA barcodes with capture probes.

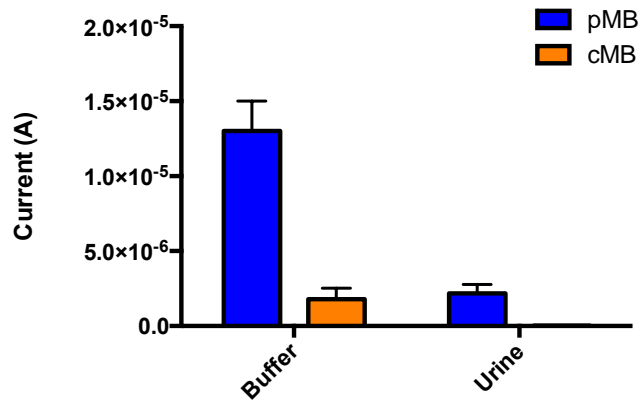


Figure 2.15 Electrochemical test comparing the performance of pMB and cMB in buffer and in urine. The electrochemical signal was quantified by the redox current from released methylene blue following the hybridization of DNA barcodes with capture probes.

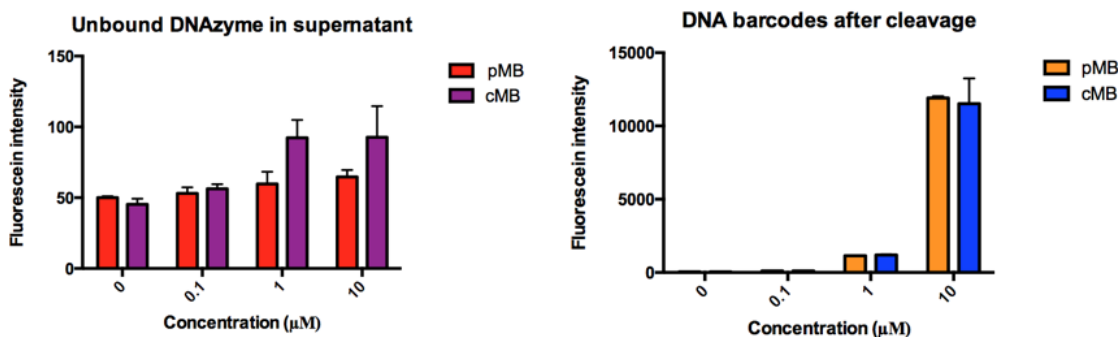


Figure 2.16 Fluorescence test showing the loading and cleavage efficiency of magnetic microgel beads (pMB) compared with commercial Dynabead magnetic beads (cMB) loaded with different amount of *E.coli* DNAzymes. Left: Fluorescence intensity of DNAzymes that are not grafted to the magnetic beads. Right: Florescence intensity of cleaved DNA probes after the addition of *E.coli* CIM.

Finally, the limit of detection for the *E.coli* DNAzyme-based biosensor in both buffer and urine using magnetic microgel beads as a DNAzyme immobilization platform was depicted in Figure 2.17. The lowest LOD that can be achieved by the electrochemical biosensor is 1 CFU/mL (i.e. a single bacteria in 1 mL of testing buffer), which indicates very high sensitivity; indeed, this high sensitivity is beyond even a clinically-useful detection limit since, when the target is present at such a low concentration, many aliquots of the target solution would not contain any bacteria. In undiluted urine, a still very low detection limit of 1000 CFU/mL was observed, an LOD directly relevant to the diagnosis of a possible urinary tract infection. A higher background signal was observed for the test done in urine compared to that done in buffer, likely due to the presence of redox-active compounds such as urea, citric acid, glucose, or proline in untreated urine samples [164] despite the higher salt concentration in urine that would otherwise result in higher ion conductivity and thus better sensitivity in urine compared to buffer.

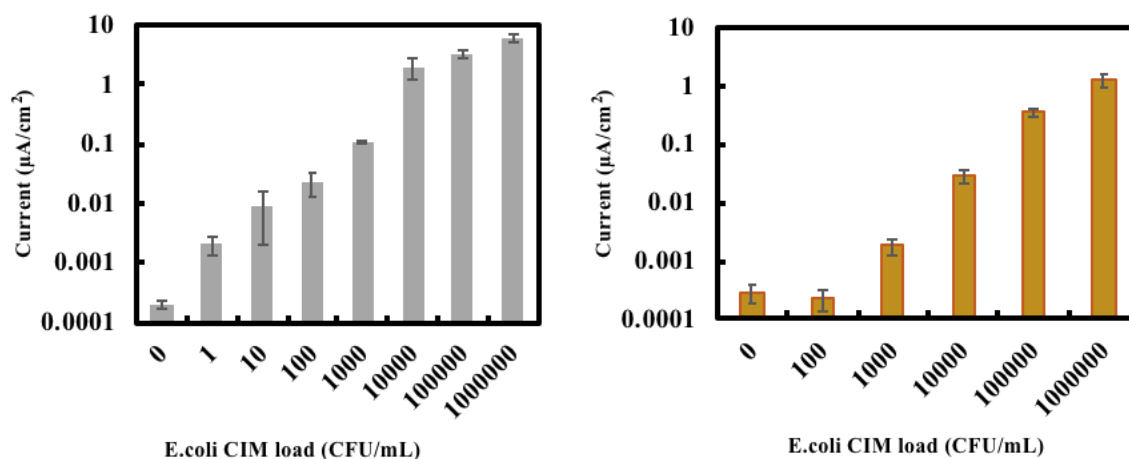


Figure 2.17 Limit of detection for designed electrochemical biosensors based on the use of magnetic microgel beads as an aRCD immobilization platform by performing the test in buffer (left) and in undiluted urine (right).

2.5 Conclusion

Magnetic microgel beads based on crosslinked poly(ethylene glycol) methyl ether methacrylate were fabricated using an inverse emulsion-templated polymerization strategy that enables physical encapsulation of iron oxide nanoparticles inside the beads. Methacrylate acid was copolymerized into the magnetic beads to provide functionalization sites for grafting amine-labeled *E. coli* RNA cleaving DNazymes. The synthesized particles contained 22 wt% iron oxide and showed long-term colloidal stability over at least one month. The magnetic microgel beads can be separated magnetically within 5-10 minutes in DIW and in <5 minutes in salt solution. Comparing the performance of the magnetic microgel beads to the commercial Dynabeads, electrochemical detection of the methylene blue signal from the hybridization of capture probes and cleaved DNA barcodes from DNzyme immobilized on polymer beads

results in a signal $6.3\times$ higher than that observed with commercial magnetic beads in buffer, and $97\times$ higher than that observed with commercial magnetic beads in urine, confirming the role of the highly hydrated and 3D gel morphology in improving the grafting density and ultimate activity of the grafted DNAzymes. Anti-fouling performance tests show that the magnetic microgel beads have comparable protein repellent properties to commercial Dynabeads. Finally, the designed biosensor using magnetic microgel beads as bio-recognition element immobilization site achieved a limit of detection of 1 CFU/mL in buffer and 1000 CFU/mL in undiluted urine, the latter in particular representing a highly clinically-relevant result. All of these demonstrated the potential of magnetic microgel beads for future commercialization.

Chapter 3: Water-Soluble Conductive Polymer Coatings to Reduce Non-Specific Adsorption on a Gold Electrode Surface

3.1 Introduction

Electrochemical biosensors are usually required to perform tests in untreated clinical samples such as blood, urine, and saliva that contain high concentrations of interfering molecules, resulting in high background signals. This becomes especially problematic when the sensor aims to detect low concentrations of targets or ligands, in which case the high signal-to-noise ratio for many biomedical diagnostics becomes particularly problematic. In the case of electrochemical biosensors, the presence of electrochemically active compounds such as glucose, urea, or dopamine may also impair the electrical conductivity, such that their contact with electrode surface should be avoided or at least minimized.

There are generally two ways to prevent the adsorption of biofoulants on substrates: active removal or passive blocking. Active removal techniques are relatively new in the biosensing field and aim to remove biofoulants on the electrode surface using either mechanical forces or acoustic waves, most often using the electrodes of an electrochemical biosensor as transducers. The fundamental concept behind this method is that biofoulants interact less strongly with electrodes than the targets, such that the applied shear force only removes non-specifically bound biofoulants. The active removal technique does not require any functionalization process or pose any chemical stability

issues but only works for biofoulants already adsorbed on the substrate surface; in addition, electrodes need to be specifically designed for creating shear forces.

Alternately, passive blocking methods involve introducing a layer of blocking molecules to the substrate surface through either chemical interaction or physical adsorption and are both more studied and more applicable to wider ranges of biofoulants. These molecules reduce biofouling through three major mechanisms - hydrophilic interactions, steric hindrance, or electrostatic repulsion - depending on the properties of coating materials and the surface chemistry of the substrates [172]. Most biofoulants adsorb to the substrate through hydrophobic interactions, such that the introduction of a hydrophilic polymer coating will reduce or prevent this interaction by forming a hydration layer at the interface. Some polymers (e.g. poly(ethylene glycol), PEG) can further reduce hydrophobic interactions by sterically excluding biofoulants from the near-electrode surface by virtue of their flexible hydrophilic polymeric side chains [176]. Zwitterionic polymers that contain a balanced number of cationic and anionic charges can interact with surrounding water molecules even more strongly through ionic water structuring, further improving anti-fouling properties [209].

While such passive coatings can reasonably reduce fouling for many types of sensors, the inherently insulating properties of such hydrophilic polymers can significantly reduce the charge transfer efficiency of electrodes in the context of electrochemical assays; conversely, most conductive polymers are hydrophobic and thus do not possess anti-

fouling properties. Therefore, there is substantial interest in designing a water-soluble anti-fouling polymer coating that could be easily grafted to gold electrode surface but does not compromise the conductivity of electrodes.

3.2 Objective

The main objective for this chapter is to design a water-soluble polymer with both anti-fouling and ion conducting properties that can readily adhere to the gold electrodes used for DNAzyme-based biosensing. Poly(ethylene glycol) methyl ether methacrylate based polymer and zwitterionic polymers were both screened as the polymer backbone and functionalized such that they can be retained on substrate by a simple coating and drying process. Multiple types of functionalizations and modifications were performed, after which the performance of the polymers as anti-fouling coatings for electrochemical biosensors was tested using a gold electrode surface.

3.3 Materials and experimental

3.3.1 Materials:

Oligo(ethylene glycol) methyl ether methacrylate (OEGMA, $M_n \sim 500$), methacrylic acid (MAA, 99%), thioglycolic acid (98%), aminoacetaldehyde dimethyl acetal (99%), 1,4-dioxane ($\geq 99\%$, ACS grade), sodium cyanoborohydrate (95%), 4-amino-2,2,6,6-tetramethyl-1-piperidinyloxy (4-amino-TEMPO, 98%), *N*-hydroxysuccinimide (NHS, 98%), cystamine dihydrochloride (96%), 1,4-dithiothreitol (DTT, $\geq 97\%$), EDTA disodium salt (99%-101%), sodium phosphate dibasic (ACS reagent, $\geq 99\%$), 5,5'-

dithiobis(2-nitrobenzoic acid) (DTNB, $\geq 98\%$), L-glutathione reduced (GSH, $\geq 98\%$), 2-(methacryloyloxy)ethyl]dimethyl-(3-sulfopropyl) ammonium hydroxide (DMAPS, 95%), 2-acrylamido-2-methyl-1-propanesulfonic acid (AMPS), bovine serum albumin ($\geq 96\%$, lyophilized powder), and fibrinogen from human plasma (50%-70% protein) were all purchased from Sigma Aldrich (Oakville, Canada). Inhibitors in oligo(ethylene glycol) methyl ether methacrylate (OEGMA), including 200 ppm BHT and 100 ppm MEHQ, were removed using an alumina oxide (Al_2O_3 , Thermo Scientific)-filled vertical glass column prior to use. 2,2-azobisisobutyric acid dimethyl ester (AIBMe, 98.5%) was purchase from Wako Chemicals (USA). N'-ethyl-N-(3-dimethylaminopropyl)-carbodiimide (EDC, commercial grade) was purchased from Carbosynth. Milli-Q grade distilled deionized water (Milli-Q H_2O) was used for all experiments. 1.0 N and 0.1 N hydrochloride acid solution (HCl) and 1.0 N and 0.1 N sodium hydroxide solution (NaOH) used for pH adjustment were purchased from VWR Analyticals (Canada).

3.3.2 Synthesis of POEGMA polymer backbone

Aldehyde-functionalized POEGMA (POEGMA-Ald) was synthesized by copolymerizing OEGMA₄₇₅ (8-9 repeat units) and aldehyde precursor monomer N-(2,2-dimethoxyethyl) methacrylate (DMAEMA, prepared in-house as previously reported [210]) through free radical polymerization with the protocol previously developed [211]. As a representative example for the 35 mol% aldehyde content polymer, 3 g of OEGMA, 0.58 g of DMAEMA, 45 mg AIBME, and 1 μL TGA were dissolved in 20 mL 1,4-dioxane, transferred to a single-neck round bottom flask, and purged with nitrogen for 30 minutes.

The flask was placed in a 75 °C oil bath for 4 hrs under nitrogen purging and magnetic stirring at 320 rpm to form the polymer. Following, the solvent was removed by using rotary evaporation, and 0.25 M HCl was added to hydrolyze the acetal protecting groups on the DMEMA monomer over a 24 hour reaction period. The polymer was then lyophilized and stored at 4 °C.

Carboxylic acid-functionalized POEGMA-Ald-MAA was synthesized using a similar strategy but adding methacrylic acid (MAA) as an additional comonomer. As a representative recipe for a polymer containing 30 mol% of aldehyde and 10 mol% MAA, 3g of OEGMA, 0.54g DMAEMA, 0.0905g MAA, 45 mg AIBME, and 1 μ L TGA were used as the raw ingredients, with the remaining workup as described for POEGMA-Ald.

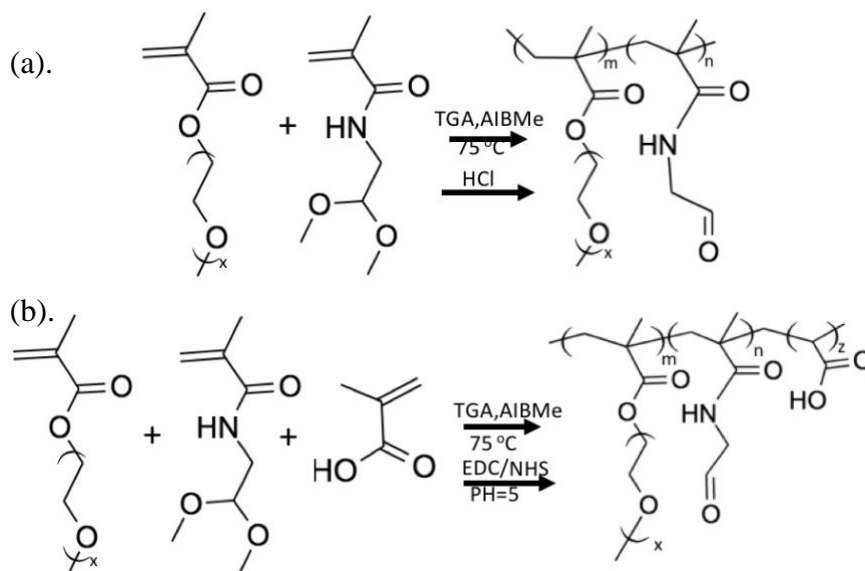


Figure 3.1 Illustration of the reaction pathways for synthesizing (a) POEGMA-Ald and (b) POGMA-Ald-MAA.

3.3.3 TEMPO-conjugated POEGMA

Lyophilized POEGMA-Ald or POEGMA-Ald-MAA were dissolved in Milli-Q H₂O to make a 20 wt% polymer solution. For POEGMA-Ald (35 mol%) with 5 mol% of amino-TEMPO grafting, 0.0832 g of 4-amino TEMPO was added to a 20 wt% polymer solution and left to react for 4 hours at pH 5 under continuous stirring at room temperature. After the reaction, the pH was adjusted back to 7. For POEGMA-Ald-MAA polymer, amino-TEMPO was conjugated to the carboxyl residues from MAA using carbodiimide chemistry with a 3× molar excess of EDC and NHS, targeting full conjugation of the incorporated MAA residues. The amount of TEMPO added depends on the molar concentration of MAA. For example, for PO-Ald-MAA (10 mol%), 0.661 g EDC and 0.714 g NHS were added to 20 wt% polymer solution, the pH was adjusted to 5.5, and the reagents were mixed for 20 minutes under magnetic stirring to create the NHS activated ester. Following, the pH was adjusted back to 7 and 0.18 g 4-amino TEMPO was added to the solution, subsequently being allowed to react for 3 hours. All polymers were dialyzed against Milli-Q H₂O for 6 cycles, lyophilized, and stored at 4 °C. The chemical structures of TEMPO-conjugated polymers are shown in Figure 3.2.

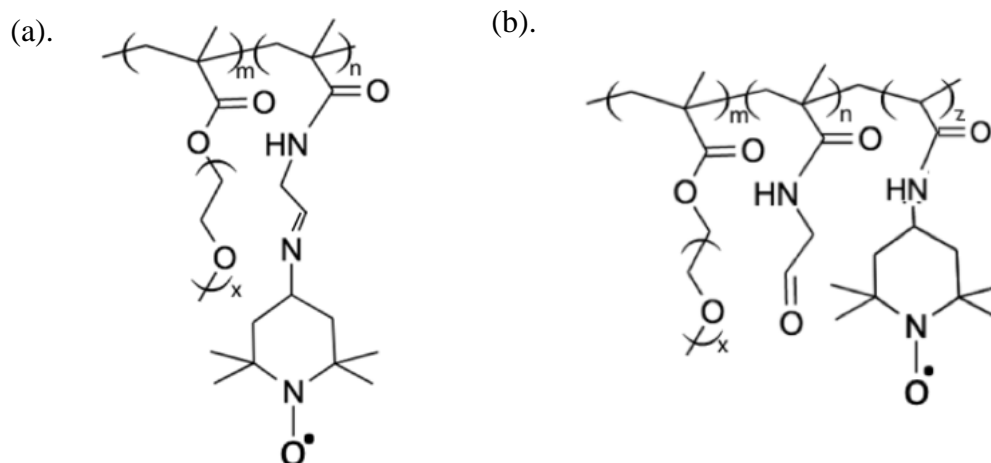


Figure 3.2. Chemical structures of (a) TEMPO-grafted POEGMA-Ald and (b) TEMPO-grafted POEGMA-Ald-MAA.

3.3.4 Conjugation of thiol groups to POEGMA-Ald-MAA

Thiolated polymer was synthesized by grafting cystamine to the carboxyl groups of MAA and subsequently reducing the disulfide bond in cystamine by adding DTT to generate monothiol groups. The degree of thiol functionalization was adjusted by changing the degree of functionalization of MAA. As a representative protocol for synthesizing POEGMA (35%)-Ald(10%)-MAA (55%), 3 g OEGMA, 0.309 g DMEMA, 0.854 g MAA, 45 mg AIBME, and 1 μ L TGA were dissolved in 20 mL of 1,4-dioxane and polymerized using the conditions previously described. The lyophilized polymer was then dissolved in 50 mL Milli-Q H₂O and 4.47g cystamine dihydrochloride (2 molar excess to the carboxyl groups incorporated into the polymer) was added, following by adjusting the pH of solution to 4.75. 3.8 g EDC was then added, and the reaction was allowed to proceed for 6 hours while keeping pH in the range of 4.5~5. The product was

dialyzed against Milli-Q H₂O for 6 cycles. Following, the pH was changed to 8 and 4.6 g DTT was added (1.5 molar excess to the carboxyl groups incorporated into the polymer). The reaction proceeded for another 6 hours while the pH was kept at 8~8.5. After the reaction, the pH was lowered back to 3.5, and the whole polymer solution was dialyzed against 0.1 M NaCl at pH 3.5 for 6 cycles. The final product was lyophilized and stored at 4 °C.

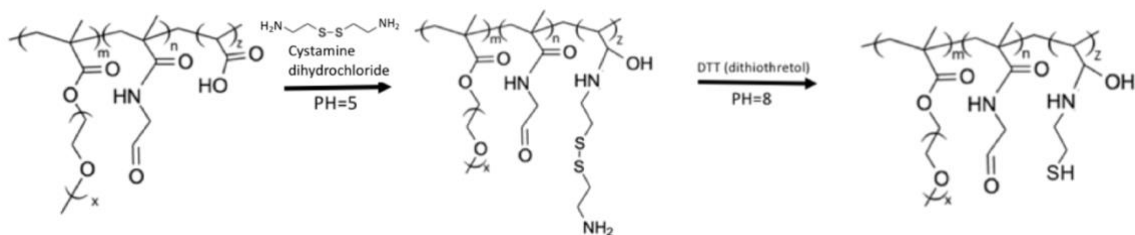


Figure 3.3 Synthesis pathway for grafting thiols to POEGMA-Ald-MAA.

3.3.5 Synthesis of zwitterionic DMAPS-Ald-MAA

[2-(Methacryloyloxy)ethyl]dimethyl-(3-sulfopropyl)ammonium hydroxide (DMAPS) is a hydrophilic, zwitterionic sulfobetaine monomer that contains both a cationic and anionic functional group in each monomer residue and was used in place of POEGMA to assess the benefits of using a zwitterionic rather than a neutral hydrophilic surface coating. As a representative example for the synthesis of DMAPS(65%)-Ald(15%)-MAA(20%), 3 g OEGMA, 0.42 g DMEMA, 0.28 g MAA, and 40 mg ammonium persulfate were dissolved in 20 mL water and polymerization was performed as described for the POEGMA-Ald-MAA polymer. Thiols were subsequently grafted to the MAA residues as described for POEGMA-Ald-MAA backbone; for example, to synthesize DMAPS(65%)-

Ald(15%)-MAA(20%), 2.87 g cystamine, 2.49 g EDC, and 0.76 g DTT were used. The final product was lyophilized and stored at 4 °C.

3.3.6 Synthesis of POEGMA-Ald-MAA-AMPS

2-Acrylamido-2-methylpropane sulfonic acid (AMPS) is hydrophilic comonomer that maintains an anionic charge over a wide range of pH values, hypothesized to promote ion transport. As such, the potential of using AMPS as a comonomer in a POEGMA-based surface coating was explored. As a representative example, POEGMA(40%)-Ald(15%)-MAA(20%)-AMPS(25%) was synthesized by dissolving 3 g OEGMA, 0.41 g DMEMA, 0.27 g MAA, 0.97 g AMPS, and 80 mg ammonium persulfate in 20 mL Milli-Q H₂O and polymerizing as described for the POEGMA-Ald-MAA polymer. Thiols were then grafted to the MAA residues of the polymer using the protocol described for POEMGA-Ald-MAA; for example, to synthesize POEGMA(40%)-Ald(15%)-MAA(20%)-AMPS(25%), 2.87 g cystamine, 2.49 g EDC, and 0.76 g DTT were used. The final product was lyophilized and stored at 4 °C.

3.3.7 Gel Permeation Chromatography

Polymer molecular weight was measured with gel permeation chromatography using a Waters 590 HPLC pump, three Waters Ultrastyrigel Linear Columns (30 cm x 7.8 mm (i.d.); HR2, HR3, HR4; <10 µm particles) at 40 °C, and a Water 410 refractive index detector at 35 °C. The eluent was prepared by dissolving 50 mM LiBr in N,N-dimethylformamide (DMF) and was run at a flow rate of 1 mL/min. The calibration was

performed by using Waters polyethylene glycol standards. All polymer samples were prepared by dissolving ~20 mg lyophilized polymer in 2 mL THF, following by filtering the polymer solution through a 0.2 μm PTFE membrane.

3.3.8 Base-into-acid conductometric titration

The degree of MAA incorporation and subsequent cystamine conjugation was determined by base-into-acid conductometric titration using Burivar-I2 automatic buret (Mantech) operating using PC titrate software. A 50 mg polymer sample was first dissolved in 50 mL of 3 mM NaCl. The polymer solution pH was manually adjusted to pH~2.75 before titration, after which 0.1 M NaOH injections were performed at a rate of 10 min/unit pH until the end point of pH 11.

3.3.9 Ellman's assay

An Ellman's assay was used to determine the free thiol concentration within the thiolated polymers. Ellman's reagent (5,5'-dithiobis(2-nitrobenzoic acid), DTNB) converts to a yellow color after reacting with free sulfhydryl groups, enabling the colorimetric detection of free thiol concentrations. 150 mL Ellman's assay buffer was first prepared by dissolving 55.8 mg of EDTA and 2.13 g of sodium phosphate dibasic in Milli-Q H₂O. The DTNB solution was then prepared by dissolving 4 mg of DTNB in 1 mL of Ellman's assay buffer; the dye converts into a yellow color when exposed to molecules containing free thiols that can be quantified colorimetrically. A calibration curve was built by dissolving reduced L-glutathione (GSH) in Ellman's assay buffer at concentrations of

4.40, 2.20, 1.47, 0.73, 0.37, 0.18, 0.092, and 0 mM. Following, to assess the free thiol content of the polymers, a lyophilized polymer sample was dissolved in Milli-Q H₂O to achieve a total polymer concentration of 5 mg/mL. The final assay solutions of both the GSH standards and the unknown sample were prepared by combining 1 mL of Ellman's assay buffer, 50 μ L of DTNB solution, and 250 μ L of either the GSH standard solution or the unknown sample. The reaction was allowed to proceed for 30 minutes at room temperature under shaking, after which the absorbance of the resulting solution was measured using a UV/vis plate reader operating at an absorbance of 412 nm.

3.3.10 Nuclear Magnetic Resonance

The structure of the POEGMA-based polymer backbone was verified with ¹H-NMR (nuclear magnetic resonance spectroscopy) using a Bruker AVANCE 600 MHz spectrometer and deuterated DMSO as solvent.

3.3.11 Protein anti-fouling test

The protein-repellent properties of the prepared polymers were tested by coating the polymers in the well of a polystyrene 96 well plate (aldehyde-functionalized polymers) or on a gold-coated vinyl sheet (thiol-functionalized polymers). Fluorescein isothiocyanate (FITC) labelled bovine serum albumin (BSA) and fibrinogen were selected as standards. 10 μ L of a 20 wt% polymer solution was air-dried on the tested surface followed by washing with 1 \times PBS to remove non-specifically adsorbed polymer. Following, 20 μ L of fluorescently-labeled protein solutions of different concentrations were incubated with

the polymer coating under gentle shaking in the dark for 2 hours. The supernatant was collected, and the surface was washed with 15 μL of $1\times$ PBS to remove excess or weakly-bound protein. The amount of unabsorbed protein inside the supernatant was quantified by measuring the fluorescence intensity using a plate reader (Tecan M200) operating at an excitation wavelength of 495 nm and an emission wavelength of 520 nm; the remaining amount of protein was considered to have adsorbed to the surface. The calibration curve between fluorescence intensity and protein concentration for each standard was built by preparing protein solutions with concentrations of 1000, 750, 500, 250, 125, 75, 50, 25, 10, 1 $\mu\text{g}/\text{mL}$.

3.3.12 X-Ray Photoelectron Spectroscopy (XPS)

XPS was performed on a Thermofisher Scientific Escalab 250 Xi (Thermofisher Scientific, UK) to confirm the success of coating polymer on the gold surface.

3.3.13 Electrochemical test

The performance of polymer drop-coated nanostructured electrodes was tested with cyclic voltammetry (CHI 420B, Austin, TX) in a 2 mM potassium ferro (II) cyanide (FOCN) solution using a potential range of 0-0.5V, a scan rate of 0.05V, and cycles of 2. The polymer-coated electrodes were deposited with 2 μM of capture probe solution for 6 hours, following by dropping 5 μM of methylene blue barcode solution on the electrodes for 30 minutes at 37 $^{\circ}\text{C}$. The methylene blue signal of the hybridization between methylene blue barcodes and capture probes was measured by square wave voltammetry

(CHI 420 B, Austin, TX) using a voltage range of 0 V to -0.6 V. The polymer-coated electrodes were compared with bare and capture probe-deposited electrodes using electrochemical impedance spectroscopy (EIS) (CHI 420B, Austin, TX) in 2 mM FOCN solution in 1× PBS. The conductivity of different polymer solutions was recorded using a Seven Excellence S470 conductivity meter using an InLab-731-ISM probe.

3.4 Results and Discussion

3.4.1 POEGMA polymer with TEMPO grafting

The first approach tested to enhance charge transfer with anti-fouling polymers is to graft 4-amino-2,2,6,6-tetramethylpiperidine-1-oxyl (4-amino TEMPO) on the POEGMA backbone. 4-amino TEMPO is a redox species with a stable free radical due to the presence of bulky substitute groups and has been demonstrated to facilitate electron transfer [212][213]. In the context of this application, TEMPO was hypothesized to catalyze charge transport through the polymer if enough TEMPO molecules are in close proximity, making the density of grafted TEMPO critical to creating a polymer film with good charge transfer properties.

Two POEGMA polymers containing adhesive aldehyde groups (POEGMA-Ald and POEGMA-Ald-MAA) were synthesized and tested for TEMPO grafting efficiency. For POEGMA-Ald, amino-TEMPO was grafted to aldehyde group through a Schiff base interaction to form imine. While Schiff base formation is reversible, imine formation is favoured at pH 5. The advantage of using POEGMA-Ald as backbone is that we simplify

the composition of the polymer; however, the disadvantage is that the aldehydes serve as both the grafting sites (for both TEMPO and DNA barcodes) and the adhesion sites, making control over grafting and adhesion more challenging. In contrast, for POEGMA-Ald-MAA, DNA barcodes can interact with the polymer through imine bonding but TEMPO molecules are grafted to the carboxyl groups of MAA via amide bond formation, a much more stable bond; furthermore, since the carboxyl groups are only used for TEMPO grafting, excesses of TEMPO can be used such that the grafting yield can be better controlled based on the mole fraction of MAA added to the copolymer.

We started with a low and a high degree of TEMPO grafting recipe, synthesizing POEGMA-Ald (35%) with 5 mol% TEMPO grafting and POEGMA-Ald (70%) with 40 mol% TEMPO grafting; both polymers are thus designed to have 30% aldehyde in excess for DNA grafting/adhesion purposes after TEMPO addition. As a comparison, POEGMA-Ald (30%)-MAA (5%) with 5 mol% TEMPO grafting and POEGMA-Ald (30%)-MAA (40%) with 40 mol% of TEMPO grafting were synthesized. The molecular weight and polydispersity index (PDI) of each polymer was tested with GPC, with the results summarized in Table 3.1. The results show that polymer was successfully synthesized, with all but the 70% POEGMA-Ald polymer exhibiting molecular weights in the 20-30 kDa range; the use of a high molar fraction of DMAEA in the recipe appears to limit the molecular weight of the polymer produced. The polydispersity index (PDI) is high for all polymers because free radical polymerization was used; however, for polymer

coatings, PDI is not an important property as long as a complete and uniform surface coverage can be achieved.

Table 3.1 Summary of molecular weight and PDI of POEGMA-Ald and POEGMA-Ald-MAA polymers synthesized.

<i>NAME</i>	<i>M_w (g/mol)</i>	<i>M_n (g/mol)</i>	<i>PDI</i>
<i>POEGMA-Ald(35%)</i>	28100	8800	3.2
<i>POEGMA-Ald(70%)</i>	8000	4500	1.8
<i>POEGMA-Ald(30%)-MAA(5%)</i>	24700	8600	2.9
<i>POEGMA-Ald(30%)-MAA(40%)</i>	28900	12900	4.6

The content of aldehyde in the polymer was determined by NMR, while the mole fraction of carboxyl groups was determined by base-into-acid conductometric titration. The theoretical and experimental aldehyde composition and moles of TEMPO grafted to aldehyde were summarized in Tables 3.2 and 3.3. The results indicate that the aldehyde group was not copolymerized with POEGMA effectively using the POEGMA-Ald recipe. For POEGMA-Ald with a 35% theoretical molar ratio of aldehyde, NMR result indicates only 3.2 mol% of aldehyde in the polymer; similarly, for POEGMA-Ald with a 70% theoretical molar ratio of aldehyde, only 8.4 mol% of aldehyde was detected. While the potential for aldehyde protons to exchange with water contaminants in the NMR solvent (and thus not be observed on the ¹H NMR) cannot be dismissed as a contributor to this apparently low aldehyde content, low TEMPO grafting efficiency is anticipated (and observed experimentally, Table 3.2) based on this result. Aldehyde copolymerization

efficiency is relatively better for polymer synthesized with the recipe of POEGMA-Ald-MAA. While amino-TEMPO can also react with aldehyde groups via Schiff base formation, the degree of grafting to aldehyde is relatively low compared to that to MAA based on the titration result (Table 3.3), consistent with the high reversibility of imines under the pH 7 conjugation condition. Therefore, POEGMA-Ald-MAA was chosen over POEGMA-Ald as the backbone to graft TEMPO. An attempt was also made to copolymerize TEMPO methacrylate acid directly with POEGMA polymer, but all runs resulted in a polymer with extremely high molecular weight and gel-like properties. We hypothesize this observation is a result of the stable free radicals in TEMPO exchanging with the polymeric radicals, prolonging the polymerization and producing high molecular weight products [214] [215]. However, using the methacrylic acid copolymer grafting approach, TEMPO contents of up to ~16 mol% of functional monomer residues can be achieved (Table 3.3)

Table 3.2 Summary of ¹H-NMR result on the degree of aldehyde copolymerization and degree of 4-amino TEMPO grafting to aldehyde groups.

<i>NAME</i>	<i>THEORETICAL (aldehyde)</i>	<i>EXPERIMENTAL (aldehyde)</i>	<i>EXPERIMENTAL (TEMPO)</i>	<i>Percentage of TEMPO grafting</i>
<i>POEGMA-Ald (35%)</i>	35 mol%	3.9 mol%	-	
<i>POEGMA-Ald (70%)</i>	70 mol%	8.4 mol%	-	
<i>POEGMA-Ald (35%) with TEMPO (5%)</i>	35 mol%	3.2 mol%	0.7 mol%	21.1 %
<i>POEGMA-Ald (70%) with TEMPO (40%)</i>	70 mol%	6.5 mol%	1.8 mol%	27.7 %
<i>POEGMA-Ald (30%)- MAA(5%)</i>	30 mol%	3.9 mol%	-	
<i>POEGMA-Ald (30%)- MAA(40%)</i>	30 mol%	12.0 mol%	-	
<i>POEGMA-Ald- MAA(5%) with TEMPO (5%)</i>	30 mol%	2.4 mol%	1.5 mol%	62.5 %
<i>POEGMA-Ald- MAA(40%) with TEMPO (40%)</i>	30 mol%	10.7 mol%	1.3 mol%	12.1 %

Table 3.3 Summary of base-into-acid conductometric titration results for the degree of MAA copolymerization and the degree of 4-amino TEMPO grafting to the carboxyl groups. The percentage of TEMPO grafting is calculated based on the percentage of MAA residues successfully grafted with TEMPO.

<i>NAME</i>	<i>THEORETICAL (MAA)</i>	<i>EXPERIMENTAL (MAA)</i>	<i>EXPERIMENTAL (TEMPO)</i>	<i>Percentage of TEMPO grafting</i>
<i>POEGMA-Ald (30%)-MAA(5%)</i>	5 mol%	3.3 mol%	-	-
<i>POEGMA-Ald (30%)-MAA(40%)</i>	40 mol%	33.3 mol%	-	-
<i>POEGMA-Ald-MAA(5%) with TEMPO (5%)</i>	5 mol%	1.4 mol%	1.9 mol%	38.0%
<i>POEGMA-Ald-MAA(10%) with TEMPO (10%)</i>	10 mol%	3.5 mol%	2.1 mol%	21.0 %
<i>POEGMA-Ald-MAA(20%) with TEMPO (20%)</i>	20 mol%	11.2 mol%	8.4 mol%	42.0 %
<i>POEGMA-Ald-MAA(40%) with TEMPO (40%)</i>	40 mol%	17.6 mol%	15.7 mol%	39.3 %

In the next step, TEMPO-grafted POEGMA-Ald-MAA with different degrees of TEMPO grafting was deposited on nanostructured electrodes by drying a drop of polymer solution on the electrode and then performing cyclic voltammetry (CV). The conductivities for 20 wt% solutions of POEGMA-Ald-MAA-TEMPO polymer with 10 mol%, 20 mol%, and 40 mol% TEMPO measured with ISM were 54.2, 83.5, 168.1 $\mu\text{S}/\text{cm}$, which falls into the

semi-conductive range but not the conductive range. Correspondingly, according to the result of Figure 3.4, the polymer coating of POEGMA-Ald-MAA with 5 mol% of TEMPO grafting greatly reduced the current on the electrodes to almost 0 A. While this result confirms that polymer was successfully coated on the electrode, the charge transfer ability for a polymer with 5 mol% TEMPO grafting is poor. POEGMA polymer with higher TEMPO grafting (10 mol% and 20 mol%) showed higher resulting current on electrodes, but the improvement was very limited, consistent with the improved but still low amount of TEMPO grafted to these polymers, as seen in Table 3.3. POEGMA polymer with higher TEMPO grafting. 40 mol% TEMPO polymers enabled a very high degree of TEMPO grafting; however, such a high degree of TEMPO grafting will lead to a low molar ratio of POEGMA, resulting in inferior anti-fouling properties. As such, achieving a sufficiently high TEMPO concentration to significantly enhance electrode conductivity compromised other desirable properties of the coating, leading us to explore alternative approaches.

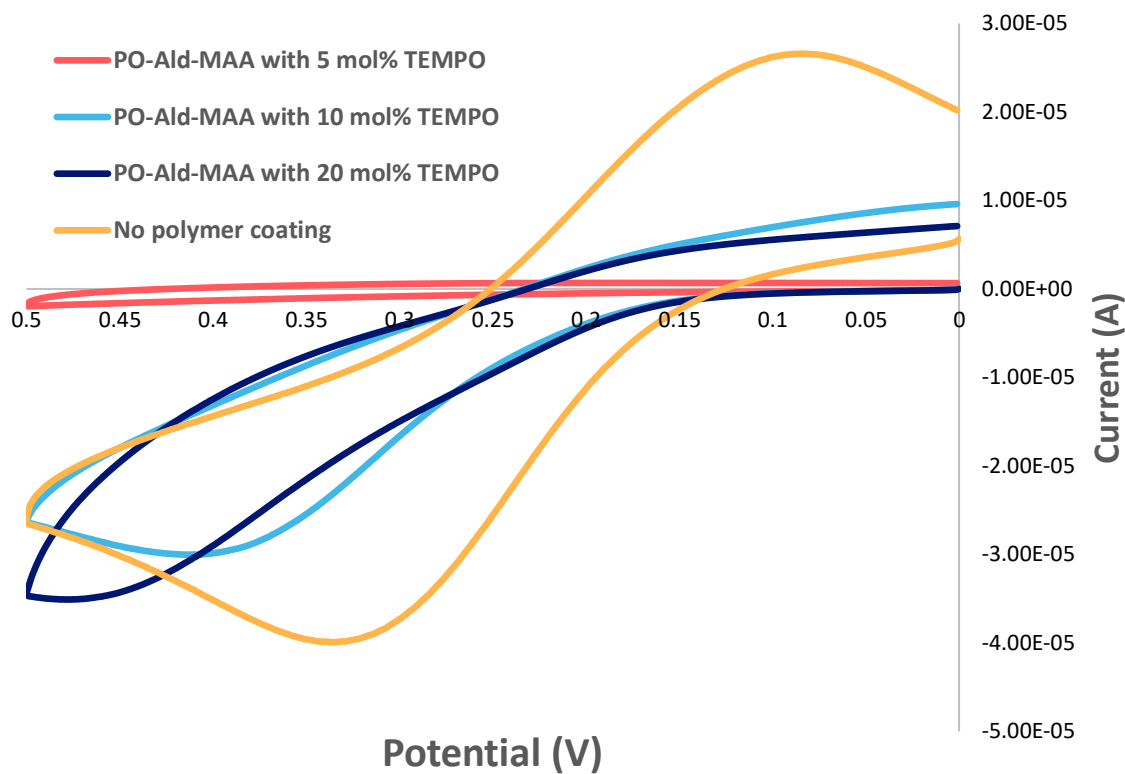


Figure 3.4 Cyclic voltammetry of nanostructured gold electrodes coated with POEGMA-Ald-MAA polymer grafted with different degrees of TEMPO compared to the bare electrode.

3.4.2 Thiolated POEGMA polymer

The interaction between electrodes and TEMPO-grafted POEGMA-Ald-MAA polymer was expected to be influenced by the cystamine coating on the electrode, which was used to immobilize polymer on electrodes by forming imine bonds with aldehyde groups on the polymer (as depicted in Figure 3.5a). As an alternative approach, we sought to decrease the thickness of the overall coating on the electrode by directly immobilizing polymer on the gold electrodes. Thiolated polymer can form self-assembled structures on gold electrodes because of the high affinity of thiols towards metals [216] (as shown in

Figure 3.5b). By omitting the use of cystamine, POEGMA polymer can be brought closer to the electrode surface and the interaction between polymer and electrodes (which governs the overall thickness of a given polymer coating) can be tuned by adjusting the degree of thiol functionalization of the polymer; higher thiol content polymer should form more interactions with the gold substrate and form a thinner coating layer.

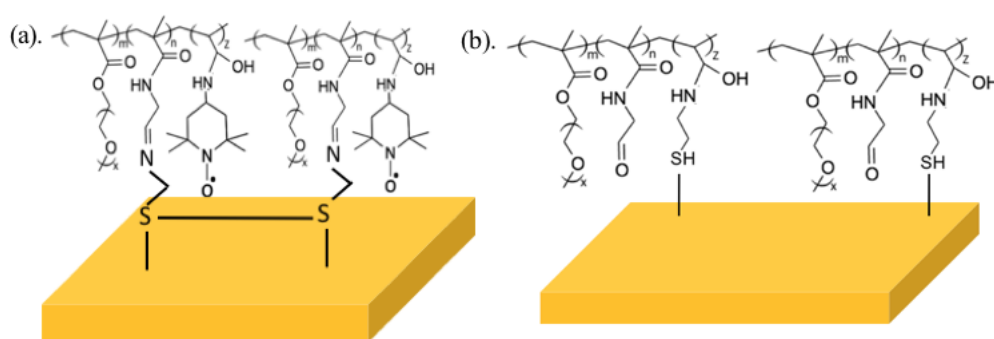


Figure 3.5 Illustration of the interaction between polymer and gold electrodes. (a) POEGMA-Ald-MAA with TEMPO grafting is grafted by first coating cystamine on the electrodes by forming imine bonds with the polymer-bound aldehyde; (b) thiolated POEGMA-Ald-MAA interacts directly with gold through Au-S bonds.

POEGMA-Ald-MAA polymers with 15 mol% and 55 mol% thiols were synthesized and characterized using GPC (to measure molecular weight) and base-into-acid conductometric titration before and after thiol grafting (to measure the degree of thiol functionalization). The results are summarized in Table 3.4. The thiol grafting efficiency was high for both recipes (~80%). However, because thiols tend to form disulfide bonds in aqueous solution and only free thiols are able to interact with gold, the percentage of free thiols on polymer was further determined with Ellman's assay; based on this assay, ~6-7% of total monomer residues in the POEGMA polymer with a targeted 15 mol%

total thiol content display a free thiol (irrespective of the content of aldehyde monomer in the polymer); correspondingly, ~20% of the total monomer residues in the POEGMA polymer with a targeted 55 mol% thiol content have a free thiol group. This significant drop in measured grafting efficiency between titration and the Ellman's assay indicates that a significant amount of thiols form disulfide bonds with each other, although the free thiol content is still appreciable in all polymers tested. However, disulfide bonds in the presence of a gold surface have been shown to favor dissociation to free thiols to form a stronger bond with gold surface, especially under slightly acidic conditions [217]. This was also demonstrated by the cyclic voltammetry result of electrodes deposited with thiolated polymer, the results of which are shown in Figure 3.6. The higher thiol content POEGMA polymer showed only a 33% decrease in current compared to the bare electrode, a substantially lower drop than that observed with the TEMPO-grafted polymers. However, when the hybridization between methylene blue labelled DNA barcodes and capture probes grafted to the polymer was tested by square wave voltammetry, only a small current (25 nA) of methylene blue was detected at the expected potential (-0.3V~-0.4V), as shown in Figure 3.7.

Table 3.4 Summary of the molecular weight, degree of thiol functionalization, and molar ratios of free thiols for thiolated POEGMA-Ald-MAA polymers synthesized

<i>Name</i>	<i>M_w</i>	<i>PDI</i>	<i>Theoretical mol %</i>	<i>Experimental mol%</i>	<i>Grafting efficiency</i>	<i>Free thiols mol%</i>
<i>POEGMA-Ald(5%)-MAA(15%) with thiols (15%)</i>	15738	2.4	15.0 %	12.2 %	81 %	5.9 %
<i>POEGMA-Ald(5%)-MAA(55%) with thiols (55%)</i>	16022	2.5	55.0 %	42.1 %	77 %	20 %
<i>POEGMA-Ald(15%)-MAA(15%) with thiols (15%)</i>	37296	3.3	15.0 %	12.9 %	86 %	6.4 %
<i>POEGMA-Ald(30%)-MAA(15%) with thiols (15%)</i>	30280	3.0	15.0 %	14.2 %	95 %	7.2 %

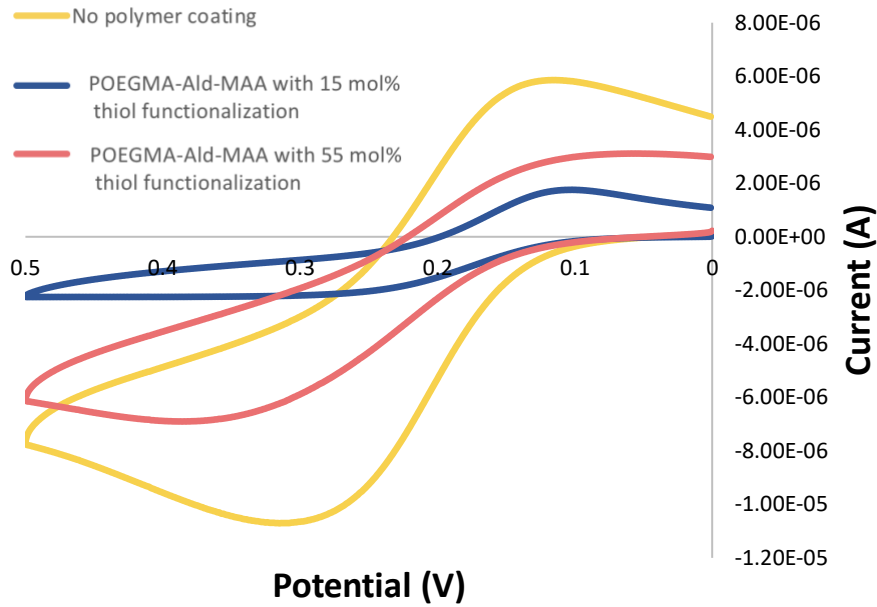


Figure 3.6. Cyclic voltammety result for nanostructured gold electrodes coated with POEGMA-Ald-MAA polymer functionalized with different degrees of thiolation compared to an uncoated electrode.

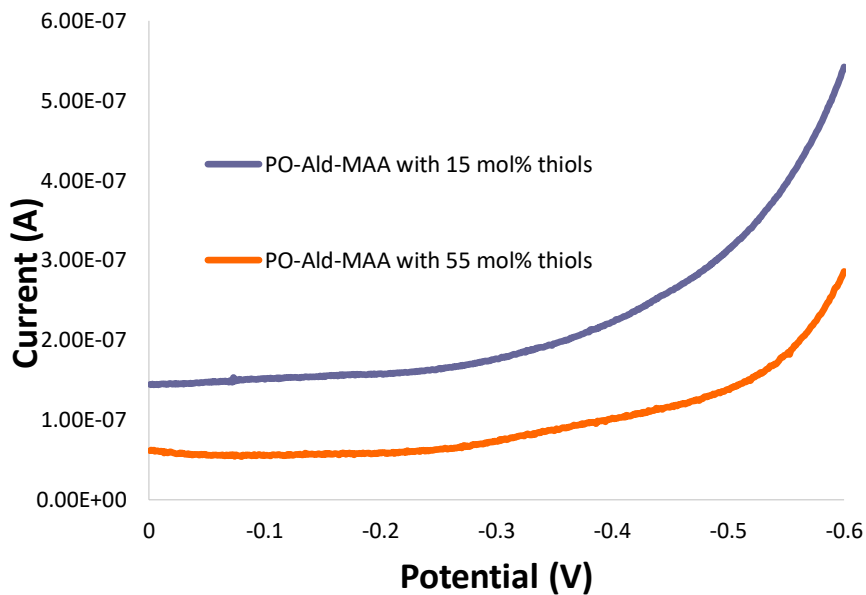


Figure 3.7 Square wave voltammety result for the redox current of methylene blue produced by the hybridization between methylene blue labelled DNA probes (barcodes) and capture probes immobilized on thiolated polymers.

Based on the relatively efficient charge transfer enabled by thiolated polymer, it was suspected that the low detection current was related to poor immobilization of the capture probes on the polymer. Two solutions were presented to solve the problem: (1) to increase the molar ratio of aldehyde groups in the recipe to provide more immobilization sites for capture probes; and (2) to reduce the imine bond between polymer and capture probes to amine with sodium cyanoborohydride, a reducing agent, to eliminate the reversibility of the linkage. For the first solution, the molar ratio of aldehyde was increased to 30 mol% while keeping the degree of thiol functionalization at 15 mol%, maintaining a sufficiently high POEGMA content in the recipe (>50 mol%) such that the anti-fouling properties were not compromised (see Table 3.4 for the physical properties of this polymer). The CV result shown in Figure 3.8 demonstrates that the charge transfer ability of polymer after the increase in aldehyde concentration remains reasonable, with an 41.2% decrease in current versus the bare electrode following drop-dry coating formation. As shown in Figure 3.9, while increasing the aldehyde content does enable a defined sensing peak related to methylene blue on the square wave voltammetry scan, the current detected following the hybridization of capture probes and DNA barcodes is only increased from 55 nA to 90 nA, a very small increase with only marginal utility in biosensing. Polymer reduced with sodium cyanoborohydride to ensure the irreversible retention of the capture probes on the polymer showed a similar minimal increase in current. Based on these results, the most likely explanation is that methylene blue cannot diffuse as well as the FOCN probe used in cyclic voltammetry, resulting in a good ion conductivity result in the CV test but a poor signal with the DNA probes.

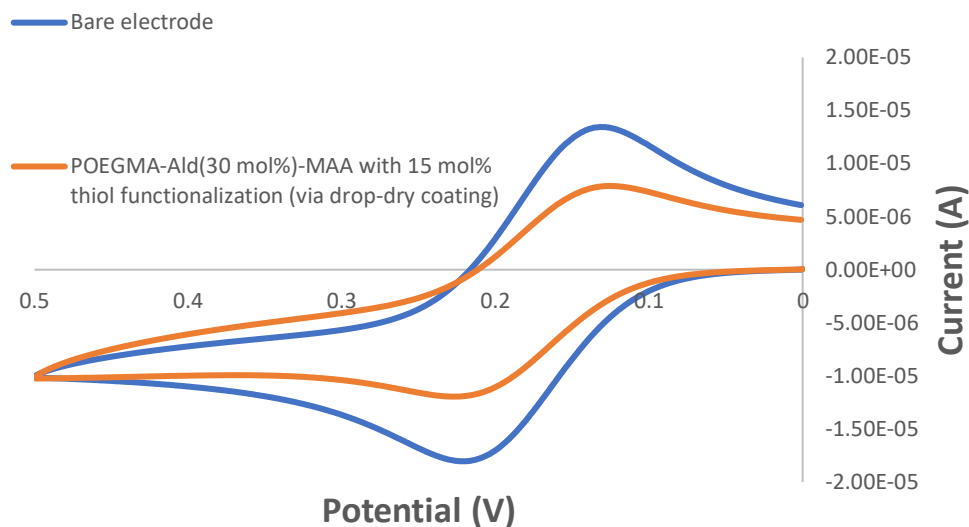


Figure 3.8 Cyclic voltammetry result for nanostructured gold electrodes coated with a 15 mol% thiolated POEGMA-Ald-MAA polymer with 30 mol% aldehyde functionalization compared to a bare gold electrode by using (a). Drop-dry coating method. (b) Spin coating method.

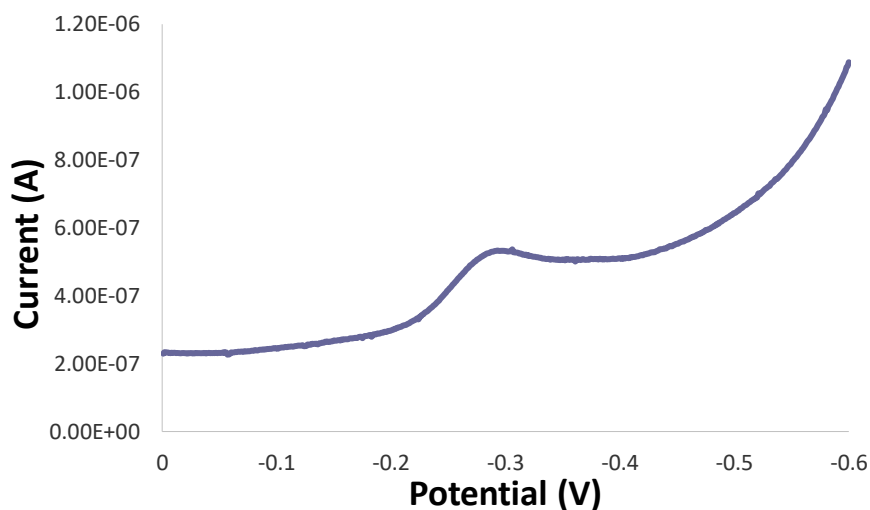


Figure 3.9 Square wave voltammetry result for the redox current of methylene blue produced by the hybridization between methylene blue labelled DNA probes (barcodes) and capture probes immobilized on a 15 mol% thiolated POEGMA-Ald-MAA polymer with 30 mol% aldehyde functionalization.

3.4.3. Charged Polymer

While POEGMA is an extremely good anti-fouling polymer, it is also completely neutral from a charge perspective and thus is a poor electrical and ion conductor. Instead, building on the promising results associated with probe grafting and surface adhesion acquired in the preceding data, we sought to leverage zwitterionic polymers as the backbone polymer as an alternative to POEGMA. Zwitterionic polymers contain both cationic and anionic groups (enabling charge transport and high water binding) but contain an overall neutral charge (enabling effective anti-fouling performance). Among the typical zwitterionic polymers types (sulfobetaines, phosphorylcholines, and carboxybetaines [209]), we selected the sulfobetaine monomer 2-(methacryloyloxy)ethyl]dimethyl-(3-sulfopropyl) ammonium hydroxide (DMAPS) as the backbone given its inexpensive commercial availability and demonstrated efficient anti-fouling properties [218][219]. The polymer DMAPS(65%)-Ald(15%)-MAA(20%) was synthesized containing similar functional groups to those already discussed above; the aldehyde fraction enables grafting of amine labeled capture probes through imine bond formation while the MAA residues are used to graft thiol groups to enable immobilization to the gold electrode. GPC indicated that the polymer product had a molecular weight of ~44 kDa and PDI of 1.98, with the molecular weight in particular somewhat higher than that measured for the POEGMA-based polymers; however, as described earlier, we do not believe molecular weight to be an important variable in this design provided the thiol content of the polymer is sufficiently high that it will primarily regulate the thickness of the coordinated polymer layer on the gold electrode. The thiol

grafting efficiency tested with conductometric titration is 50.0%, corresponding to ~10 mol% of the monomer residues in the polymer being functionalized with a thiol or disulfide group

The performance of the zwitterionic polymer coating was then assessed using cyclic voltammetry. Relative to the POEGMA-based polymers, electrodes coated with zwitterionic polymers surprisingly show similar charge transfer ability in the CV test, decreasing the redox current by 42.0 % compared to the bare electrode (Figure 3.10). As such, zwitterionic polymer coatings do not significantly improve charge transfer performance relative to POEGMA coatings.

In an attempt to further enhance charge transfer, another copolymer was synthesized that incorporated the negatively charged 2-acrylamido-2-methyl-1-propanesulfonic acid (AMPS); we hypothesized that the negative charge (which remains anionic over a large range of pH values) would enhance charge transfer beyond that achieved with the zwitterionic monomer alone, which contains charge but is net charge neutral. According to GPC, a product with molecular weight of ~39 kDa was synthesized. However, the ionic conductivity measured by the CV test (Figure 3.10) was reduced relative to the zwitterionic-only prepared without AMPS. We hypothesize that the repulsion between the sulfonic acid groups in AMPS induces swelling that alters the conformation of the polymer coating, leading to a thicker coating that may impair the charge transfer.

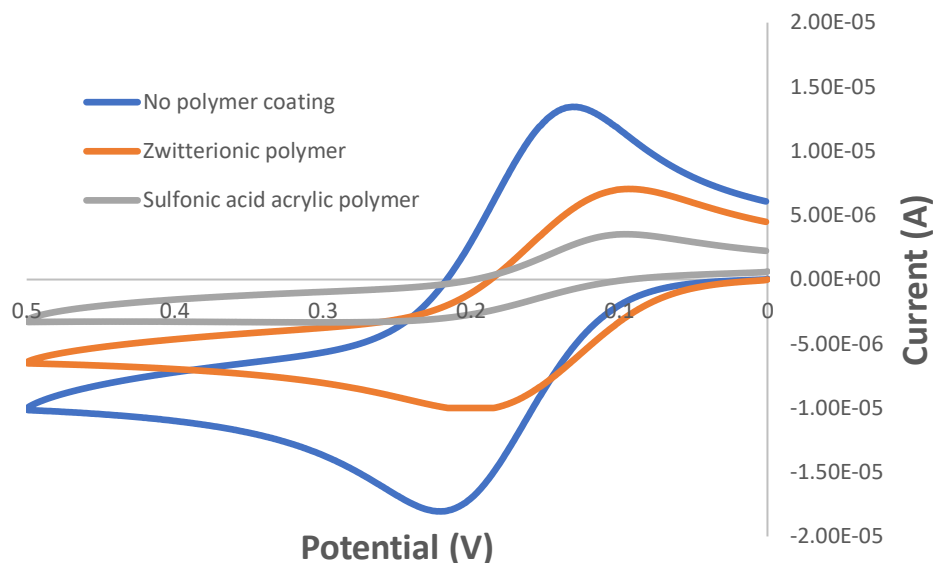


Figure 3.10 Cyclic voltammetry result for nanostructured gold electrodes with zwitterionic polymer and sulfonic acid acrylic polymer comparing to that without polymer coating.

3.4.4 Protein anti-fouling test

To assess the anti-fouling properties of polymer coatings, the polymers were drop-dry cast on polystyrene 96 well plates as a proof-of-concept experiment. 10 μL of a 20 wt% polymer solution was first air-dried at the surface of each well followed by washing with $1\times$ PBS and incubation with 20 μL of FITC-labelled BSA or fibrinogen at different concentrations for 2 hours. The amount of protein adsorbed on the polymer was determined by detecting the level of protein inside the supernatant. According to Figure 3.11, all of the thiolated POEGMA polymers that demonstrated the best charge transfer performance showed effective anti-fouling properties; for example, for thiolated POEGMA-Ald (5%)-MAA(15%) coatings incubated with 750 $\mu\text{g}/\text{mL}$ protein, a $35\times$ decrease in adsorbed fibrinogen density and a $37\times$ decrease in adsorbed BSA density was

observed compared to the surface without a coating. Repeating the same test on a gold surface produced by sputtering a 100 nm gold film on a polystyrene sheet using DC MagSput™, efficient protein repellency was also observed for all thiolated POEGMA polymers tested. XPS analysis confirmed the functionalization of the gold surface with the polymer, with a significant enhancement in the C and O signals and a reduction in the Au signal observed upon coating (Appendix Figure S.1). However, the degree of improvement observed was slightly lower on the gold substrate relative to the polystyrene alone; for example, surfaces coated with thiolated POEGMA-Ald(15 mol%)-MAA(15 mol%) show the best anti-fouling performance by exhibiting a ~40% decrease in protein adsorption at a protein concentration of 750 µg/mL compared to the surface without a polymer coating in Figure 3.12. We attribute this difference to experimental challenges exclusive to the gold electrode; in particular, compared to the anti-fouling test done in well plates, it is much harder to ensure the added protein solution stays entirely on the gold sheet without brimming over the edges, which would lead to an uneven coating of polymers (consistent with the larger error bars in the gold versus polystyrene well data) and result in a poorer anti-fouling performance. However, the best protein repellent property was observed for zwitterionic polymer, which enables a ~67% decrease in protein adsorption at the gold surface in the presence of 750 µg/mL protein relative to the bare gold surface. In the future, this experiment may be improved if a higher concentration (i.e. higher viscosity) of polymer solution was coated on the gold surface to ensure improved retention on the gold surface. However, even with these experimental

challenges, the data clearly indicate the benefit of POEGMA or (in particular) zwitterionic polymer coatings for reducing non-specific protein adsorption.

While higher POEGMA concentration in the polymer should in theory improve its anti-fouling performance, no clear difference was observed in the protein repellency between the 15 mol% and 55 mol% thiol-functionalized polymers despite their very significant difference in PEG concentrations. We hypothesize that the length of the brush (n=7-8 ethylene oxide repeat units) coupled with the presence of that brush on every OEGMA monomer residue results in the incorporation of a sufficient number of short PEG groups to orient in a reasonably close-packed configuration at the electrode interface and thus effectively suppress protein adsorption even for lower PEG content coatings.

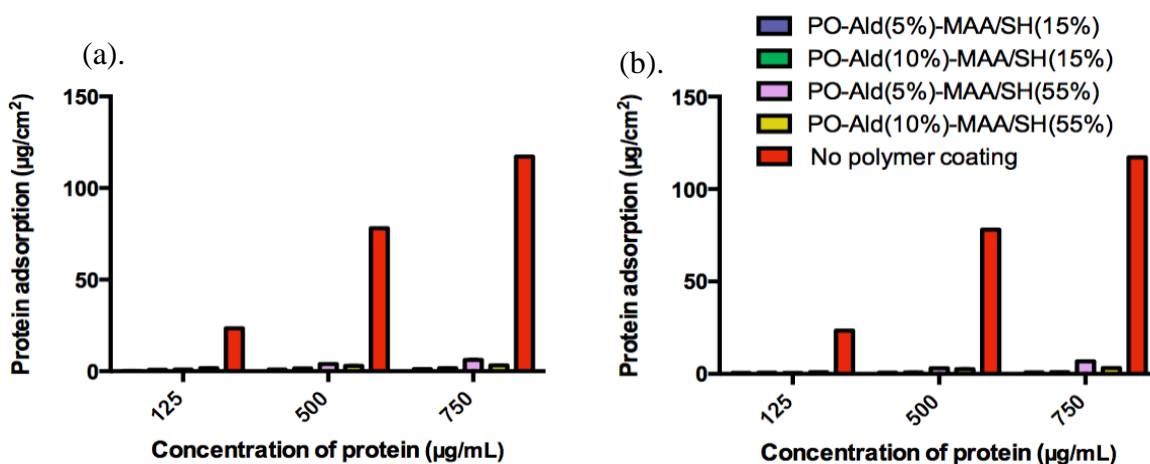


Figure 3.11 Anti-fouling test for thiolated POEGMA polymers coated on a polystyrene surface: (a) Anti-fouling test for POEGMA-Ald-MAA against FITC-labelled BSA. (b) Anti-fouling test for POEGMA-Ald-MAA against FITC-labelled fibrinogen.

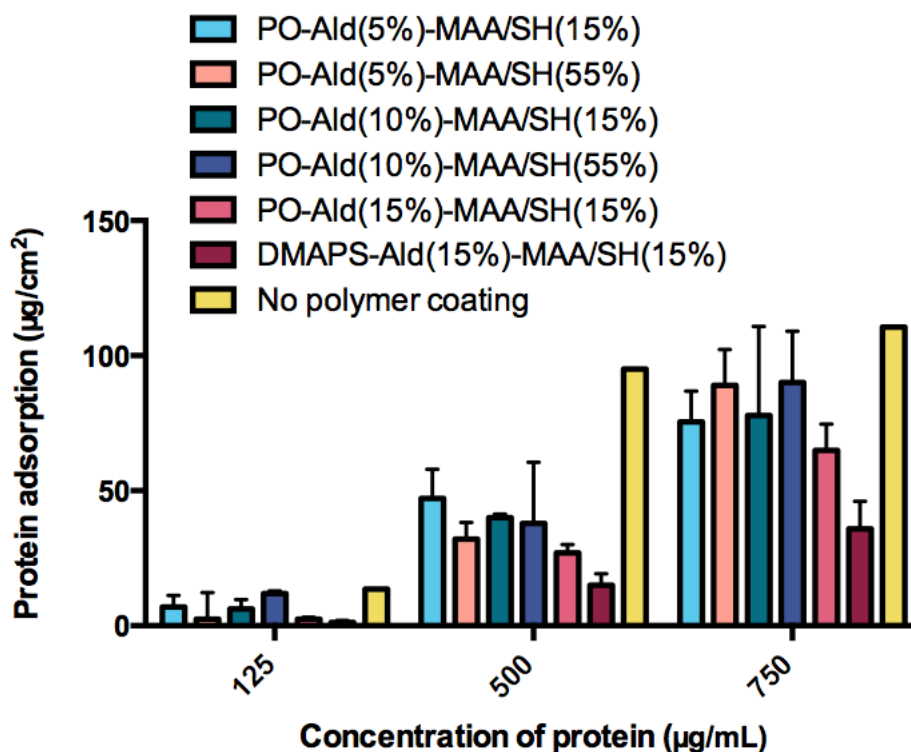


Figure 3.12 Anti-fouling test for various thiolated POEGMA polymers and thiolated zwitterionic polymer coated on a sputter-coated gold electrode interface by using FITC-labelled BSA as model protein.

3.5 Conclusion

Four different types of polymers based on a POEGMA backbone, including POEGMA-Ald with TEMPO grafting, POEGMA-Ald-MAA with TEMPO grafting, POEGMA-Ald-MAA with thiol grafting, and POEGMA-Ald-MAA-AMPS with thiol grafting, in addition to one thiolated zwitterionic polysulfobetaine polymer (DMAPS) were synthesized and characterized as polymer coatings for gold electrodes, aiming to reduce non-specific fouling in clinical samples without compromising the conductivity at the electrode. For POEGMA polymer with TEMPO grafting, a significant reduction in

charge transfer was observed with polymer-coated electrodes based on cyclic voltammetry, with easily synthetically accessible TEMPO grafting contents not significantly aiding in conductivity enhancement. Thiolated polymer allows for sufficient charge transfer between electrolytes and gold electrodes but reduced methylene blue signal from the hybridization of DNA barcodes and capture probes immobilized on the coating. The increase in the number of potential capture probe immobilization sites by increasing the concentration of aldehyde in polymer from 5 mol% to 30 mol% improves the methylene blue signal from 55 nA to 90 nA, but this increase is not significant enough for practical biosensing utility. Finally, zwitterionic polymer DMAPS exhibits good charge transfer ability, and the hybridization of DNA barcodes and capture probes can be tested in the future to see whether zwitterionic polymer allows better methylene blue diffusion than POEGMA polymer.

Chapter 4 – Conclusions and Recommendations

The incorporation of polymer into an electrochemical biosensor could benefit its performance in many ways, including improving its sensitivity, limit of detection, automation, real-time responses, and capacity for in-field testing [15][31][68]. In particular, polymer microparticles provide higher surface areas compared to traditional two-dimensional surfaces such that more bio-recognition elements can be immobilized per unit mass of microparticle to realize higher biosensor sensitivity [14]. When magnetic materials such as iron oxides were encapsulated inside the polymer microparticles, these particles can be simply collected or removed with magnet, amenable to in-field processing. Comparing to traditional methods to separate biomolecules, magnetic separation is easier to manipulate, less harmful to samples, and is able to realize complete separation [67] [133][141]. The optimized polymer magnetic particles synthesized in this project have a diameter of $\sim 5 \mu\text{m}$ and can be separated magnetically in 5-10 minutes suspended in water, and less than 5 minutes if suspended in salt solution. These particles also show good long-term stability so that they can maintain the properties for end-use even after storage. Because these microparticles are synthesized based on poly(ethylene glycol) methacrylate acid, a highly protein-repellent hydrophilic polymer with long side chains, they also exhibit good anti-fouling properties without the need for additional functionalization [176], especially for small globular proteins such as BSA and IgG. Finally, the performance of a magnetic microgel-based *E.coli* DNAzyme electrochemical biosensor indicated that the methylene blue signal generated from DNA barcodes released from polymer magnetic beads upon target binding was $6.3\times$ higher than that

from *Dynabeads* (a leading commercial bead for this purpose) when analyzed in buffer and 97× higher methylene blue signal was observed using polymer magnetic beads relative to *Dynabeads* if the same experiment was conducted in undiluted urine. A similar experiment comparing the cleavage efficiency of polymer magnetic beads and *Dynabeads* using fluorescence labeled *E.coli* DNAzymes indicated a slightly higher DNAzyme grafting efficiency to the magnetic microgels and comparable cleavage efficiency between *Dynabeads* and magnetic microgel beads, the latter attributed to the inherently lower sensitivity of fluorescence test relative to the electrochemical test.

The size distribution of polymer magnetic beads synthesized from current protocols may be improved using one or both of two approaches: (1) replacing methacrylic acid with the sodium salt of acrylic acid (NaAA), as suggested by Hwee Peng et al. [43] or (2) further adjusting the emulsifier type/concentration to better stabilize the interface. Alternately, more shear-controlled strategies such as jetting microfluidics (which can in theory reach a similar particle size) could be used, although based on the current results we believe the current polydispersity of bead size is not practically problematic for applications in biosensing.

To prepare magnetic particles with a more uniform iron oxide distribution, iron oxides can be pre-treated with stabilizers such as oleic acid [44][68]. Also, iron oxide nanoparticles can be synthesized with more controllable process such as thermal decomposition rather than precipitation that typically result in narrower size distributions

and smaller sizes [37]. Finally, the stability and anti-fouling performances of magnetic beads may be further improved if longer oligo(ethylene glycol) side chain brushes were used; for example, an n=20 OEGMA monomer (compared to n=7-8 in the current design) is commercially available and may provide even better surface steric stability.

As for the polymer coating designed for reducing the fouling on the electrodes of the electrochemical sensor, POEGMA-Ald-MAA showed higher efficiency aldehyde copolymerization than POEGMA-Ald, such that POEGMA-Ald-MAA was chosen as the polymer backbone for further functionalization. POEGMA-Ald-MAA functionalized with TEMPO reduced the charge transfer between electrolyte and the electrodes by >80% and fell into the semi-conductive range. In comparison, POEGMA-Ald-MAA with thiols grafting and zwitterionic DMAPS-Ald-MAA with thiols grafting exhibited good charge transfer ability, yielding only 30-40% decreases in charge transfer. However, the methylene blue signal from the hybridization of the released DNA barcodes and capture probes was low for POEGMA-Ald-MAA. Increasing the concentration of the aldehyde inside the recipe from 5 mol% to 30 mol% to provide for more DNAzyme binding sites enables an increase in the redox signal from 50 nA to 90 nA; however, this is still a low signal that would lead to a relatively poor-resolution biosensor.

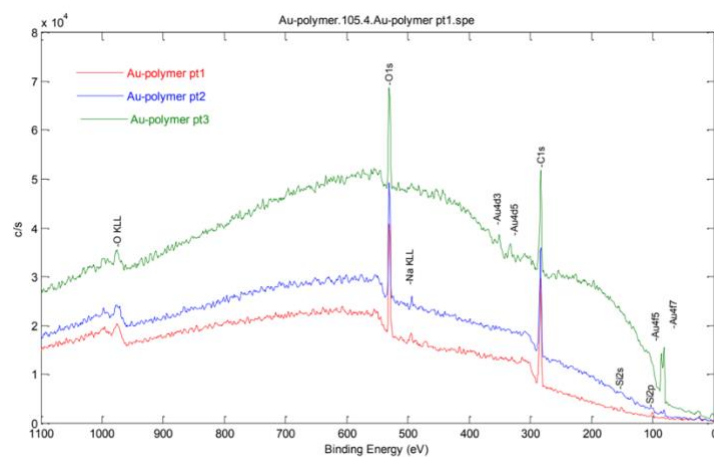
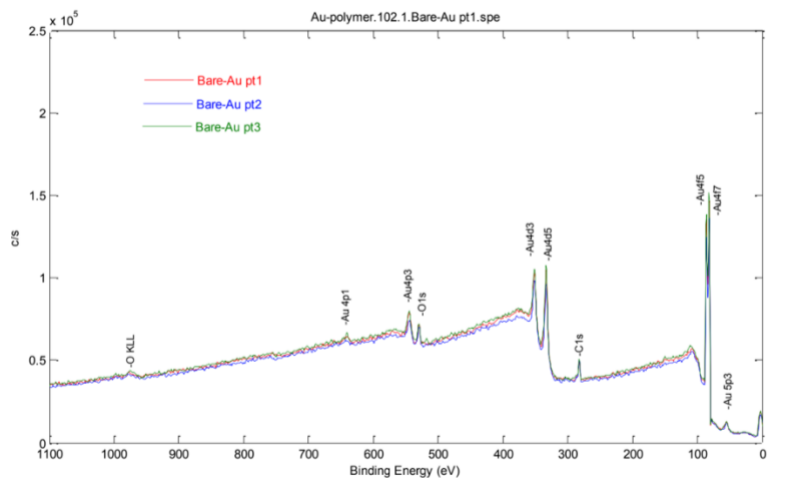
Moving forward, to improve the signal, multiple experiments could be attempted. If the capture probes are immobilized on the polymer in an incorrect or inefficient orientation (i.e. not stand-up conformation), pre-treatment of the polymer-coated electrode with a

layer of blocking molecules may help promote the stand-up position of the capture probes, allowing more efficient interaction between captures probes and DNA barcodes. For example, González-Fernández et al. tested the anti-fouling performance of a ternary SAM formed by PEG of different lengths in an electrochemical biosensor with or without inserting backfillers in the pre-formed SAM. While the chain length of PEG did not strongly correlate to the probe accessibility and limit of detection, a PEG SAM blocked with BSA showed significantly better anti-fouling abilities [220]. Similar results were shown with a zwitterionic peptide-based SAM system in an electrochemical DNA biosensor designed by Cui et al. The carboxylated zwitterionic peptides with the sequence of EKEKEKE-PPPPC were first immobilized on gold electrode, after which the amino-terminated capture probes were functionalized to the peptide. The introduction of 6-Mercaptohexanol (MCH) in this system not only improved the anti-fouling performance (due to the incorporation of dense hydroxyl interfacial groups from MCH self-assembly) but also promoted effective hybridization between oligonucleotides and polymer layers to achieve a low detection limit of 0.3 fM for breast cancer detection [221]. Thus, by combining the thiolated polymer with a more traditional surface blocking approach, improved performance may be achieved without significantly compromising conductivity, although any orientation change that results in a thicker polymer layer must be first tested to ensure the conductivity is not excessively affected by the coating. The limited DNA hybridization signal could also due to the presence of the long side chains of POEGMA polymer, which can not only block foulants but also sterically disrupt the interaction of DNA barcodes with the capture probes. This could be tested by replacing

long chain OEGMA monomer (7-9 repeating units) with short chain monomer (3-4 repeating units), such that the polymer is less sterically inhibiting but still not thermoresponsive and thus less protein-repellent under physiological conditions.

Overall, the designed biosensing system can be made more automated by introducing a microfluidics system, which allows the interaction of DNAzymes with targets, the release of DNA barcodes, and the hybridization of capture probes and DNA barcodes all on a single chip. Magnetic separation of the magnetic beads can also be implemented directly on-chip. This will greatly reduce the cost of each test and enable the in-field and real-time detection.

Appendix



%	C	O	Au
pt1	45.61	18.65	35.74
pt2	49.73	20.67	29.6
pt3	47.78	19.25	32.97
Mean	47.71	19.52	32.77

%	C	O	Na	Si	Au
pt1	71.06	26.65	0.81	1.27	0.21
pt2	69.89	27.8	0.51	1.42	0.39
pt3	66.88	25.03	0.98	3.75	3.36
Mean	69.27	26.49	0.76	2.15	1.32

Figure S.1 XPS scan for gold surface before coating (left) and after polymer coating (right) with POEGMA-Ald (30 mol%)-MAA with 15 mol% thiol functionalization. The higher percentage of oxygen and carbon level, and low percentage of gold level was detected indicates the successful coating of polymer.

Reference

- [1] M. A. M. Gijs, “Magnetic bead handling on-chip: New opportunities for analytical applications,” *Microfluidics and Nanofluidics*. 2004, doi: 10.1007/s10404-004-0010-y.
- [2] A. N. M. B. El-hoshoudy, “Emulsion Polymerization Mechanism,” in *Recent Research in Polymerization*, InTech, 2018.
- [3] S. A. and N. Duc, “Organic–Inorganic Mesoporous Silica Nanotube Hybrid Anodic Alumina Membranes for Ultrafine Filtration of Noble Metal Nanoparticles,” in *Noble Metals*, 2012.
- [4] B. Kriwet, E. Walter, and T. Kissel, “Synthesis of bioadhesive poly(acrylic acid) nano- and microparticles using an inverse emulsion polymerization method for the entrapment of hydrophilic drug candidates,” *J. Control. Release*, vol. 56, no. 1–3, pp. 149–158, Dec. 1998, doi: 10.1016/S0168-3659(98)00078-9.
- [5] L. Gong *et al.*, “DNAzyme-based biosensors and nanodevices,” *Chemical Communications*. 2015, doi: 10.1039/c4cc06855f.
- [6] M. Hollenstein, “DNA catalysis: The chemical repertoire of DNAzymes,” *Molecules*. 2015, doi: 10.3390/molecules201119730.
- [7] S. W. Santoro and G. F. Joyce, “A general purpose RNA-cleaving DNA enzyme,” *Proc. Natl. Acad. Sci. U. S. A.*, 1997, doi: 10.1073/pnas.94.9.4262.
- [8] M. Liu, D. Chang, and Y. Li, “Discovery and Biosensing Applications of Diverse RNA-Cleaving DNAzymes,” *Acc. Chem. Res.*, 2017, doi: 10.1021/acs.accounts.7b00262.

- [9] H. Peng *et al.*, “DNAzyme-Mediated Assays for Amplified Detection of Nucleic Acids and Proteins,” *Analytical Chemistry*. 2018, doi: 10.1021/acs.analchem.7b04926.
- [10] J. Zhang, “RNA-cleaving DNAzymes: Old catalysts with new tricks for intracellular and in vivo applications,” *Catalysts*. 2018, doi: 10.3390/catal8110550.
- [11] L. C. Clark and C. Lyons, “ELECTRODE SYSTEMS FOR CONTINUOUS MONITORING IN CARDIOVASCULAR SURGERY,” *Ann. N. Y. Acad. Sci.*, 1962, doi: 10.1111/j.1749-6632.1962.tb13623.x.
- [12] S. Dzyadevych and N. Jaffrezic-Renault, “Conductometric biosensors,” in *Biological Identification: DNA Amplification and Sequencing, Optical Sensing, Lab-On-Chip and Portable Systems*, 2014.
- [13] K. Nakazato, “BioCMOS LSIs for portable gene-based diagnostic inspection system,” in *ISCAS 2012 - 2012 IEEE International Symposium on Circuits and Systems*, 2012, doi: 10.1109/ISCAS.2012.6271750.
- [14] S. Liébana and G. A. Drago, “Bioconjugation and stabilisation of biomolecules in biosensors,” *Essays Biochem.*, 2016, doi: 10.1042/EBC20150007.
- [15] M. Holzinger, A. Le Goff, and S. Cosnier, “Nanomaterials for biosensing applications: A review,” *Frontiers in Chemistry*. 2014, doi: 10.3389/fchem.2014.00063.
- [16] O. Philippova, A. Barabanova, V. Molchanov, and A. Khokhlov, “Magnetic polymer beads: Recent trends and developments in synthetic design and applications,” in *European Polymer Journal*, 2011, doi:

- 10.1016/j.eurpolymj.2010.11.006.
- [17] P. Allia and G. Barrera, “Fundamentals of magnetism,” in *Ultra-High-Density Magnetic Recording: Storage Materials and Media Designs*, 2016.
- [18] K. M. Krishnan and K. M. Krishnan, “Introduction to Magnetism and Magnetic Materials,” in *Fundamentals and Applications of Magnetic Materials*, 2016.
- [19] “Magnetism: fundamentals,” *Choice Rev. Online*, 2005, doi: 10.5860/choice.42-3481.
- [20] B. D. Cullity and C. D. Graham, *Introduction to Magnetic Materials*. 2008.
- [21] A. P. Guimarães, “Magnetic domains,” in *NanoScience and Technology*, 2017.
- [22] R. L. Stamps, “Magnetism,” in *Springer Proceedings in Physics*, 2013.
- [23] M. Trainer, “Ferroelectrics and the Curie-Weiss law,” *Eur. J. Phys.*, 2000, doi: 10.1088/0143-0807/21/5/312.
- [24] V. Marghussian, “Magnetic Properties of Nano-Glass Ceramics,” in *Nano-Glass Ceramics*, Elsevier, 2015, pp. 181–223.
- [25] M. Abe *et al.*, “Preparation and medical application of magnetic beads conjugated with bioactive molecules,” *J. Magn. Magn. Mater.*, 2009, doi: 10.1016/j.jmmm.2008.11.086.
- [26] T. L. Hawkins, T. O’connor-morin, A. Roy, and C. Santillan, “DNA purification and isolation using a solid-phase,” *Nucleic Acids Res.*, 1994, doi: 10.1093/nar/22.21.4543.
- [27] H. Sequencing and P. O. Kit, “Multiplexed Sequencing with the Illumina Genome Analyzer System,” *Analyzer*, 2008, doi: 10.1101/pdb.prot5448.

- [28] N. M. Karabacak *et al.*, “Microfluidic, marker-free isolation of circulating tumor cells from blood samples,” *Nat. Protoc.*, 2014, doi: 10.1038/nprot.2014.044.
- [29] D. L. Leslie-Pelecky and R. D. Rieke, “Magnetic properties of nanostructured materials,” *Chemistry of Materials*. 1996, doi: 10.1021/cm960077f.
- [30] K. Nishio *et al.*, “Identification of a chemical substructure that is immobilized to ferrite nanoparticles (FP),” *Colloids Surfaces B Biointerfaces*, 2007, doi: 10.1016/j.colsurfb.2006.10.039.
- [31] P. Oberacker *et al.*, “Bio-On-Magnetic-Beads (BOMB): Open platform for high-throughput nucleic acid extraction and manipulation,” *PLOS Biol.*, vol. 17, no. 1, p. e3000107, Jan. 2019, doi: 10.1371/journal.pbio.3000107.
- [32] S. E. Khalafalla and G. W. Reimers, “Preparation of dilution-stable aqueous magnetic fluids,” *IEEE Trans. Magn.*, 1980, doi: 10.1109/TMAG.1980.1060578.
- [33] R. Massart, “Preparation of aqueous ferrofluids without using surfactant; behavior as a function of pH and counterions,” *Comptes Rendus des Seances l’Academie des Sci. Ser. C Sci. Chim.*, 1980.
- [34] T. Sugimoto and E. Matijević, “Formation of uniform spherical magnetite particles by crystallization from ferrous hydroxide gels,” *J. Colloid Interface Sci.*, 1980, doi: 10.1016/0021-9797(80)90187-3.
- [35] A. K. Gupta and S. Wells, “Surface-Modified Superparamagnetic Nanoparticles for Drug Delivery: Preparation, Characterization, and Cytotoxicity Studies,” *IEEE Trans. Nanobioscience*, 2004, doi: 10.1109/TNB.2003.820277.
- [36] S. Sun and H. Zeng, “Size-controlled synthesis of magnetite nanoparticles,” *J. Am.*

- Chem. Soc.*, 2002, doi: 10.1021/ja026501x.
- [37] T. Hyeon, Su Seong Lee, J. Park, Y. Chung, and Hyon Bin Na, “Synthesis of highly crystalline and monodisperse maghemite nanocrystallites without a size-selection process,” *J. Am. Chem. Soc.*, 2001, doi: 10.1021/ja016812s.
- [38] C. Xu and A. S. Teja, “Continuous hydrothermal synthesis of iron oxide and PVA-protected iron oxide nanoparticles,” *J. Supercrit. Fluids*, 2008, doi: 10.1016/j.supflu.2007.09.033.
- [39] Y. Hao and A. S. Teja, “Continuous hydrothermal crystallization of α -Fe₂O₃ and Co₃O₄ nanoparticles,” *J. Mater. Res.*, 2003, doi: 10.1557/JMR.2003.0053.
- [40] H. Hayashi and Y. Hakuta, “Hydrothermal Synthesis of metal oxide nanoparticles in supercritical water,” *Materials*. 2010, doi: 10.3390/ma3073794.
- [41] P. Hugounenq *et al.*, “Iron oxide monocrystalline nanoflowers for highly efficient magnetic hyperthermia,” *J. Phys. Chem. C*, 2012, doi: 10.1021/jp3025478.
- [42] J. Xu *et al.*, “Preparation and magnetic properties of magnetite nanoparticles by sol-gel method,” *J. Magn. Magn. Mater.*, 2007, doi: 10.1016/j.jmmm.2006.07.037.
- [43] H. P. Khng, D. Cunliffe, S. Davies, N. A. Turner, and E. N. Vulfson, “The synthesis of sub-micron magnetic particles and their use for preparative purification of proteins,” *Biotechnol. Bioeng.*, 1998, doi: 10.1002/(SICI)1097-0290(19981120)60:4<419::AID-BIT3>3.0.CO;2-P.
- [44] S. Kniajanski *et al.*, “Synthesis of highly loaded and well-controlled magnetic beads via emulsion polymerization,” *J. Appl. Polym. Sci.*, 2013, doi: 10.1002/app.38857.

- [45] C. Ménager, O. Sandre, J. Mangili, and V. Cabuil, “Preparation and swelling of hydrophilic magnetic microgels,” *Polymer (Guildf)*, 2004, doi: 10.1016/j.polymer.2004.02.018.
- [46] D. Müller-Schulte and T. Schmitz-Rode, “Thermosensitive magnetic polymer particles as contactless controllable drug carriers,” *J. Magn. Magn. Mater.*, 2006, doi: 10.1016/j.jmmm.2005.05.043.
- [47] Q. Zhang, H. Zhang, G. Xie, and J. Zhang, “Effect of surface treatment of magnetic particles on the preparation of magnetic polymer microspheres by miniemulsion polymerization,” *J. Magn. Magn. Mater.*, 2007, doi: 10.1016/j.jmmm.2006.11.181.
- [48] L. Ngaboni Okassa *et al.*, “Development and characterization of sub-micron poly(D,L-lactide-co- glycolide) particles loaded with magnetite/maghemite nanoparticles,” *Int. J. Pharm.*, vol. 302, no. 1–2, pp. 187–196, Sep. 2005, doi: 10.1016/j.ijpharm.2005.06.024.
- [49] L. Zang, J. Qiu, X. Wu, W. Zhang, E. Sakai, and Y. Wei, “Preparation of magnetic chitosan nanoparticles as support for cellulase immobilization,” *Ind. Eng. Chem. Res.*, 2014, doi: 10.1021/ie404072s.
- [50] C. S. Chern, “Emulsion polymerization mechanisms and kinetics,” *Progress in Polymer Science (Oxford)*. 2006, doi: 10.1016/j.progpolymsci.2006.02.001.
- [51] A. Pich, S. Bhattacharya, A. Ghosh, and H. J. P. Adler, “Composite magnetic particles: 2. Encapsulation of iron oxide by surfactant-free emulsion polymerization,” *Polymer (Guildf)*, 2005, doi: 10.1016/j.polymer.2005.01.017.

- [52] T. Jamshaid *et al.*, “Tailoring of carboxyl-decorated magnetic latex particles using seeded emulsion polymerization,” *Polym. Adv. Technol.*, 2017, doi: 10.1002/pat.4001.
- [53] F. Montagne, O. Mondain-Monval, C. Pichot, and A. Elaïssari, “Highly magnetic latexes from submicrometer oil in water ferrofluid emulsions,” *J. Polym. Sci. Part A Polym. Chem.*, 2006, doi: 10.1002/pola.21391.
- [54] G. L. Rempel and H. Wang, “Microemulsion Polymerization,” in *Encyclopedia of Polymeric Nanomaterials*, Springer Berlin Heidelberg, 2015, pp. 1241–1250.
- [55] K. D. Hermanson and E. W. Kaler, “Transition from microemulsion to emulsion polymerization: Mechanism and final properties,” *J. Polym. Sci. Part A Polym. Chem.*, 2004, doi: 10.1002/pola.20340.
- [56] E. Chiellini, F. Chiellini, P. Cinelli, and V. I. Ilieva, “Biobased Polymeric Materials for Agriculture Applications,” in *Biodegradable Polymers and Plastics*, Springer US, 2003, pp. 185–210.
- [57] S. Demirci and N. Sahiner, “Microemulsion Polymerization,” in *Encyclopedia of Polymer Science and Technology*, Wiley, 2019, pp. 1–24.
- [58] J. M. Asua, “Miniemulsion Polymerization,” in *Encyclopedia of Polymeric Nanomaterials*, Springer Berlin Heidelberg, 2015, pp. 1267–1275.
- [59] F. J. Schork, Y. Luo, W. Smulders, J. P. Russum, A. Butté, and K. Fontenot, “Miniemulsion polymerization,” *Adv. Polym. Sci.*, vol. 175, pp. 129–255, Feb. 2005, doi: 10.1007/b100115.
- [60] A. N. M. B. El-hoshoudy, “Emulsion Polymerization Mechanism,” in *Recent*

- Research in Polymerization*, InTech, 2018.
- [61] L. P. Ramírez and K. Landfester, “Magnetic polystyrene nanoparticles with a high magnetite content obtained by miniemulsion processes,” *Macromol. Chem. Phys.*, vol. 204, no. 1, pp. 22–31, Jan. 2003, doi: 10.1002/macp.200290052.
- [62] I. Csetneki, M. K. Faix, A. Szilágyi, A. L. Kovács, Z. Németh, and M. Zrinyi, “Preparation of magnetic polystyrene latex via the miniemulsion polymerization technique,” *J. Polym. Sci. Part A Polym. Chem.*, 2004, doi: 10.1002/pola.20300.
- [63] Y. Deng, L. Wang, W. Yang, S. Fu, and A. Elaïssari, “Preparation of magnetic polymeric particles via inverse microemulsion polymerization process,” *J. Magn. Mater.*, 2003, doi: 10.1016/S0304-8853(02)00987-3.
- [64] J. Ramos and J. Forcada, “Surfactant-free miniemulsion polymerization as a simple synthetic route to a successful encapsulation of magnetite nanoparticles,” *Langmuir*, 2011, doi: 10.1021/la200786k.
- [65] J. W. VANDERHOFF, E. B. BRADFORD, H. L. TARKOWSKI, J. B. SHAFFER, and R. M. WILEY, “Inverse Emulsion Polymerization,” 1962, pp. 32–51.
- [66] C. Mayoux, J. Dandurand, A. Ricard, and C. Lacabanne, “Inverse suspension polymerization of sodium acrylate: synthesis and characterization,” *J. Appl. Polym. Sci.*, 2000, doi: 10.1002/1097-4628(20000919)77:12<2621::AID-APP90>3.0.CO;2-X.
- [67] Z. Ma and H. Liu, “Synthesis and surface modification of magnetic particles for application in biotechnology and biomedicine,” *China Particuology*, 2007, doi: 10.1016/j.cpart.2006.11.001.

- [68] Z. Y. Ma, Y. P. Guan, X. Q. Liu, and H. Z. Liu, "Preparation and characterization of micron-sized non-porous magnetic polymer microspheres with immobilized metal affinity ligands by modified suspension polymerization," *J. Appl. Polym. Sci.*, 2005, doi: 10.1002/app.21688.
- [69] M. Sari, S. Akgöl, M. Karataş, and A. Denizli, "Reversible immobilization of catalase by metal chelate affinity interaction on magnetic beads," *Ind. Eng. Chem. Res.*, 2006, doi: 10.1021/ie0507979.
- [70] Y. Zhang, R. Liu, Y. Hu, and G. Li, "Microwave heating in preparation of magnetic molecularly imprinted polymer beads for trace triazines analysis in complicated samples," *Anal. Chem.*, 2009, doi: 10.1021/ac8018262.
- [71] Y. Zhang, Y. Li, Y. Hu, G. Li, and Y. Chen, "Preparation of magnetic indole-3-acetic acid imprinted polymer beads with 4-vinylpyridine and β -cyclodextrin as binary monomer via microwave heating initiated polymerization and their application to trace analysis of auxins in plant tissues," *J. Chromatogr. A*, 2010, doi: 10.1016/j.chroma.2010.09.059.
- [72] Z. Zhang, W. Tan, Y. Hu, G. Li, and S. Zan, "Microwave synthesis of gibberellin acid 3 magnetic molecularly imprinted polymer beads for the trace analysis of gibberellin acids in plant samples by liquid chromatography-mass spectrometry detection," *Analyst*, 2012, doi: 10.1039/c2an16001c.
- [73] Z. Zhang, Y. Zhang, W. Tan, G. Li, and Y. Hu, "Preparation of styrene-co-4-vinylpyridine magnetic polymer beads by microwave irradiation for analysis of trace 24-epibrassinolide in plant samples using high performance liquid

- chromatography,” *J. Chromatogr. A*, 2010, doi: 10.1016/j.chroma.2010.08.052.
- [74] R. J. Ansell and K. Mosbach, “Magnetic molecularly imprinted polymer beads for drug radioligand binding assay,” *Analyst*, 1998, doi: 10.1039/a801903g.
- [75] Y. Hu, R. Liu, Y. Zhang, and G. Li, “Improvement of extraction capability of magnetic molecularly imprinted polymer beads in aqueous media via dual-phase solvent system,” *Talanta*, 2009, doi: 10.1016/j.talanta.2009.04.029.
- [76] X. Kan, Z. Geng, Y. Zhao, Z. Wang, and J. J. Zhu, “Magnetic molecularly imprinted polymer for aspirin recognition and controlled release,” *Nanotechnology*, 2009, doi: 10.1088/0957-4484/20/16/165601.
- [77] R. Arshady, “Suspension, emulsion, and dispersion polymerization: A methodological survey,” *Colloid Polym. Sci.*, 1992, doi: 10.1007/BF00776142.
- [78] K. E. J. Barrett and H. R. Thomas, “Kinetics of dispersion polymerization of soluble monomers. I. Methyl methacrylate,” *J. Polym. Sci. Part A-1 Polym. Chem.*, 1969, doi: 10.1002/pol.1969.150070913.
- [79] D. Horák and N. Bedyk, “Magnetic poly(glycidyl methacrylate) microspheres prepared by dispersion polymerization in the presence of electrostatically stabilized ferrofluids,” *J. Polym. Sci. Part A Polym. Chem.*, 2004, doi: 10.1002/pola.20406.
- [80] Z. Ma, Y. Guan, and H. Liu, “Synthesis and characterization of micron-sized monodisperse superparamagnetic polymer particles with amino groups,” *J. Polym. Sci. Part A Polym. Chem.*, 2005, doi: 10.1002/pola.20803.
- [81] S. M. Joscelyne and G. Trägårdh, “Membrane emulsification - A literature

- review,” *J. Memb. Sci.*, 2000, doi: 10.1016/S0376-7388(99)00334-8.
- [82] G. T. Vladislavljević, I. Kobayashi, and M. Nakajima, “Production of uniform droplets using membrane, microchannel and microfluidic emulsification devices,” *Microfluidics and Nanofluidics*. 2012, doi: 10.1007/s10404-012-0948-0.
- [83] W. Liu, X.-L. Yang, and W. S. W. Ho, “Preparation of Uniform-Sized Multiple Emulsions and Micro/ Nano Particulates for Drug Delivery by Membrane Emulsification,” *J Pharm Sci*, vol. 100, pp. 75–93, 2010, doi: 10.1002/jps.22272.
- [84] S. Omi, A. Kanetaka, Y. Shimamori, A. Supsakulchai, M. Nagai, and G. H. Ma, “Magnetite (Fe₃O₄) microcapsules prepared using a glass membrane and solvent removal,” *J. Microencapsul.*, 2001, doi: 10.1080/02652040110055252.
- [85] J. Ma, S. M. Y. Lee, C. Yi, and C. W. Li, “Controllable synthesis of functional nanoparticles by microfluidic platforms for biomedical applications-a review,” *Lab on a Chip*. 2017, doi: 10.1039/C6LC01049K.
- [86] D. K. Hwang, D. Dendukuri, and P. S. Doyle, “Microfluidic-based synthesis of non-spherical magnetic hydrogel microparticles,” *Lab Chip*, 2008, doi: 10.1039/b805176c.
- [87] A. M. Schmidt, “The synthesis of magnetic core-shell nanoparticles by surface-initiated ring-opening polymerization of ε-caprolactone,” *Macromol. Rapid Commun.*, 2005, doi: 10.1002/marc.200400426.
- [88] Y. Yang *et al.*, “An overview of pickering emulsions: Solid-particle materials, classification, morphology, and applications,” *Frontiers in Pharmacology*. 2017, doi: 10.3389/fphar.2017.00287.

- [89] P. J. Colver, C. A. L. Colard, and S. A. F. Bon, “Multilayered nanocomposite polymer colloids using emulsion polymerization stabilized by solid particles,” *J. Am. Chem. Soc.*, 2008, doi: 10.1021/ja807242k.
- [90] C. Wang, C. Zhang, Y. Li, Y. Chen, and Z. Tong, “Facile fabrication of nanocomposite microspheres with polymer cores and magnetic shells by Pickering suspension polymerization,” *React. Funct. Polym.*, 2009, doi: 10.1016/j.reactfunctpolym.2009.06.003.
- [91] A. Werner, V. Schmitt, G. Sèbe, and V. Héroguez, “Convenient Synthesis of Hybrid Polymer Materials by AGET-ATRP Polymerization of Pickering Emulsions Stabilized by Cellulose Nanocrystals Grafted with Reactive Moieties,” *Biomacromolecules*, 2019, doi: 10.1021/acs.biomac.8b01482.
- [92] F. Liu and C. H. Tang, “Soy glycinin as food-grade Pickering stabilizers: Part. III. Fabrication of gel-like emulsions and their potential as sustained-release delivery systems for β -carotene,” *Food Hydrocoll.*, 2016, doi: 10.1016/j.foodhyd.2016.01.002.
- [93] J. Peng, Q. Liu, Z. Xu, and J. Masliyah, “Synthesis of interfacially active and magnetically responsive nanoparticles for multiphase separation applications,” *Adv. Funct. Mater.*, 2012, doi: 10.1002/adfm.201102156.
- [94] J. Tang, P. J. Quinlan, and K. C. Tam, “Stimuli-responsive Pickering emulsions: Recent advances and potential applications,” *Soft Matter*. 2015, doi: 10.1039/c5sm00247h.
- [95] H. Singh, P. E. Laibinis, and T. A. Hatton, “Rigid, superparamagnetic chains of

- permanently linked beads coated with magnetic nanoparticles. Synthesis and rotational dynamics under applied magnetic fields,” *Langmuir*, 2005, doi: 10.1021/la0517843.
- [96] W. Chen and T. J. McCarthy, “Layer-by-layer deposition: A tool for polymer surface modification,” *Macromolecules*, 1997, doi: 10.1021/ma961096d.
- [97] S. Pedroso-Santana and N. Fleitas-Salazar, “Ionotropic gelation method in the synthesis of nanoparticles/microparticles for biomedical purposes,” *Polym. Int.*, vol. 69, no. 5, pp. 443–447, May 2020, doi: 10.1002/pi.5970.
- [98] D. Y. Lee, Y. Il Oh, D. H. Kim, K. M. Kim, K. N. Kim, and Y. K. Lee, “Synthesis and performance of magnetic composite comprising barium ferrite and biopolymer,” in *IEEE Transactions on Magnetics*, 2004, doi: 10.1109/TMAG.2004.829177.
- [99] E. B. Denkbaş, E. Kiliçay, C. Birlikseven, and E. Öztürk, “Magnetic chitosan microspheres: Preparation and characterization,” *React. Funct. Polym.*, 2002, doi: 10.1016/S1381-5148(01)00115-8.
- [100] S. Roger, D. Talbot, and A. Bee, “Preparation and effect of Ca²⁺ on water solubility, particle release and swelling properties of magnetic alginate films,” *J. Magn. Magn. Mater.*, 2006, doi: 10.1016/j.jmmm.2006.01.005.
- [101] T. G. Park and H. K. Choi, “Thermally induced core-shell type hydrogel beads having interpenetrating polymer network (IPN) structure,” *Macromol. Rapid Commun.*, 1998, doi: 10.1002/marc.1998.030190401.
- [102] P. M. Xulu, G. Filipcsei, and M. Zrínyi, “Preparation and responsive properties of

- magnetically soft poly(N-isopropylacrylamide) gels,” *Macromolecules*, 2000, doi: 10.1021/ma990967r.
- [103] W. S. Prestvik, A. Berge, P. C. Mørk, P. M. Stenstad, and J. Ugelstad, “Preparation and Application of Monosized Magnetic Particles in Selective Cell Separation,” in *Scientific and Clinical Applications of Magnetic Carriers*, 1997.
- [104] J. Ugelstad *et al.*, “Preparation and application of new monosized polymer particles,” *Progress in Polymer Science*. 1992, doi: 10.1016/0079-6700(92)90017-S.
- [105] a Berge, T. Ellingsen, O. Helgee, and J. Ugelstad, “Magnetic polymer particles and process for the preparation thereof,” *US Patent 4,654,267*. 1987.
- [106] V. L. Covolani, L. H. Innocentini Mei, and C. L. Rossi, “Chemical modifications on polystyrene latex: Preparation and characterization for use in immunological applications,” *Polym. Adv. Technol.*, 1997, doi: 10.1002/(SICI)1099-1581(199701)8:1<44::AID-PAT613>3.0.CO;2-1.
- [107] V. T. Kemtchou, M. Schäfer, and U. A. Peuker, “Synthesis of Functionalized Magnetic Beads Using Spray Drying,” 2014.
- [108] H. Y. Huang, Y. T. Shieh, C. M. Shih, and Y. K. Twu, “Magnetic chitosan/iron (II, III) oxide nanoparticles prepared by spray-drying,” *Carbohydr. Polym.*, vol. 81, no. 4, pp. 906–910, Jul. 2010, doi: 10.1016/j.carbpol.2010.04.003.
- [109] S. Wei, Q. Wang, J. Zhu, L. Sun, H. Lin, and Z. Guo, “Multifunctional composite core-shell nanoparticles,” *Nanoscale*. 2011, doi: 10.1039/c1nr11000d.
- [110] L. Shen, P. E. Laibinis, and T. Alan Hatton, “Bilayer Surfactant Stabilized

- Magnetic Fluids: Synthesis and Interactions at Interfaces,” *Langmuir*, 1999, doi: 10.1021/la9807661.
- [111] I. Karimzadeh, M. Aghazadeh, T. Doroudi, M. R. Ganjali, and P. H. Kolivand, “Superparamagnetic iron oxide (Fe₃O₄) nanoparticles coated with PEG/PEI for biomedical applications: A facile and scalable preparation route based on the cathodic electrochemical deposition method,” *Adv. Phys. Chem.*, vol. 2017, 2017, doi: 10.1155/2017/9437487.
- [112] D. K. Kim *et al.*, “Starch-Coated Superparamagnetic Nanoparticles as MR Contrast Agents,” *Chem. Mater.*, 2003, doi: 10.1021/cm031104m.
- [113] L. Shan, *Superparamagnetic iron oxide nanoparticles (SPION) stabilized by alginate*. 2004.
- [114] H. Unterweger *et al.*, “Dextran-coated superparamagnetic iron oxide nanoparticles for magnetic resonance imaging: Evaluation of size-dependent imaging properties, storage stability and safety,” *Int. J. Nanomedicine*, 2018, doi: 10.2147/IJN.S156528.
- [115] S. Khoee and A. Kavand, “A new procedure for preparation of polyethylene glycol-grafted magnetic iron oxide nanoparticles,” *J. Nanostructure Chem.*, 2014, doi: 10.1007/s40097-014-0111-4.
- [116] W. Brullot *et al.*, “Versatile ferrofluids based on polyethylene glycol coated iron oxide nanoparticles,” *J. Magn. Magn. Mater.*, 2012, doi: 10.1016/j.jmmm.2012.01.032.
- [117] S. García-Jimeno and J. Estelrich, “Ferrofluid based on polyethylene glycol-coated

- iron oxide nanoparticles: Characterization and properties,” *Colloids Surfaces A Physicochem. Eng. Asp.*, 2013, doi: 10.1016/j.colsurfa.2012.12.022.
- [118] K. G. Paul, T. B. Frigo, J. Y. Groman, and E. V. Groman, “Synthesis of Ultrasmall Superparamagnetic Iron Oxides Using Reduced Polysaccharides,” *Bioconjug. Chem.*, 2004, doi: 10.1021/bc034194u.
- [119] C. Saikia, A. Hussain, A. Ramteke, H. K. Sharma, and T. K. Maji, “Carboxymethyl starch-chitosan-coated iron oxide magnetic nanoparticles for controlled delivery of isoniazid,” *J. Microencapsul.*, vol. 32, no. 1, pp. 29–39, Feb. 2015, doi: 10.3109/02652048.2014.940015.
- [120] P. Tartaj and C. J. Serna, “Synthesis of Monodisperse Superparamagnetic Fe/Silica Nanospherical Composites,” *J. Am. Chem. Soc.*, vol. 125, no. 51, pp. 15754–15755, Dec. 2003, doi: 10.1021/ja0380594.
- [121] S. Santra, R. Tapeç, N. Theodoropoulou, J. Dobson, A. Hebard, and W. Tan, “Synthesis and characterization of silica-coated iron oxide nanoparticles in microemulsion: The effect of nonionic surfactants,” *Langmuir*, 2001, doi: 10.1021/la0008636.
- [122] X. Liu, Z. Ma, J. Xing, and H. Liu, “Preparation and characterization of amino-silane modified superparamagnetic silica nanospheres,” *J. Magn. Magn. Mater.*, 2004, doi: 10.1016/j.jmmm.2003.07.006.
- [123] A. A. Oladipo and M. Gazi, “Hydroxyl-enhanced magnetic chitosan microbeads for boron adsorption: Parameter optimization and selectivity in saline water,” *React. Funct. Polym.*, 2016, doi: 10.1016/j.reactfunctpolym.2016.09.005.

- [124] P. D. Rye, “Sweet and sticky: Carbohydrate-coated magnetic beads,” *Nat. Biotechnol.*, vol. 14, no. 2, pp. 155–157, 1996, doi: 10.1038/nbt0296-155.
- [125] X. Liu, Y. Guan, Z. Ma, and H. Liu, “Surface modification and characterization of magnetic polymer nanospheres prepared by miniemulsion polymerization,” *Langmuir*, 2004, doi: 10.1021/la0491908.
- [126] X. Li, J. Huang, Y. Zhang, M. Guo, and H. Yan, “Preparation of magnetic microspheres with polymer brushes containing epoxide and amino groups and immobilization of penicillin G acylase on them,” *Acta Polym. Sin.*, 2008, doi: 10.3724/SP.J.1105.2008.00697.
- [127] M. M. Rahman and A. Elaissari, “Temperature and magnetic dual responsive microparticles for DNA separation,” *Sep. Purif. Technol.*, 2011, doi: 10.1016/j.seppur.2011.07.030.
- [128] X. Sun *et al.*, “The Hydroxyl-Functionalized Magnetic Particles for Purification of Glycan-Binding Proteins,” *Curr. Pharm. Biotechnol.*, vol. 10, no. 8, pp. 753–760, Nov. 2009, doi: 10.2174/138920109789978720.
- [129] N. Nakajima and Y. Ikada, “Mechanism of Amide Formation by Carbodiimide for Bioconjugation in Aqueous Media,” *Bioconjug. Chem.*, 1995, doi: 10.1021/bc00031a015.
- [130] D. Sehgal and I. K. Vijay, “A method for the high efficiency of water-soluble carbodiimide-mediated amidation,” *Anal. Biochem.*, 1994, doi: 10.1006/abio.1994.1144.
- [131] C. Mateo, G. Fernández-Lorente, O. Abian, R. Fernández-Lafuente, and J. M.

- Guisán, “Multifunctional epoxy supports: A new tool to improve the covalent immobilization of proteins. The promotion of physical adsorptions of proteins on the supports before their covalent linkage,” *Biomacromolecules*, 2000, doi: 10.1021/bm000071q.
- [132] M. Eliasson *et al.*, “Chimeric IgG-binding receptors engineered from staphylococcal protein A and streptococcal protein G,” *J. Biol. Chem.*, 1988.
- [133] M. Uhlen, “Magnetic separation of DNA,” *Nature*. 1989, doi: 10.1038/340733a0.
- [134] M. A. Vijayalakshmi, “Pseudo-Biospecific Affinity Ligand Chromatography,” in *Molecular Interactions in Bioseparations*, Springer US, 1993, pp. 257–275.
- [135] Z. Ma, Y. Guan, and H. Liu, “Superparamagnetic silica nanoparticles with immobilized metal affinity ligands for protein adsorption,” *J. Magn. Magn. Mater.*, 2006, doi: 10.1016/j.jmmm.2005.07.027.
- [136] J. J. Hubbuch and O. R. T. Thomas, “High-gradient magnetic affinity separation of trypsin from porcine pancreatin,” *Biotechnol. Bioeng.*, 2002, doi: 10.1002/bit.10285.
- [137] A. Mierczynska-Vasilev, P. Boyer, K. Vasilev, and P. A. Smith, “A novel technology for the rapid, selective, magnetic removal of pathogenesis-related proteins from wines,” *Food Chem.*, 2017, doi: 10.1016/j.foodchem.2017.04.050.
- [138] S. Centi, S. Tombelli, M. Minunni, and M. Mascini, “Aptamer-based detection of plasma proteins by an electrochemical assay coupled to magnetic beads,” *Anal. Chem.*, 2007, doi: 10.1021/ac061879p.
- [139] C. Albretsen, K. H. Kalland, B. I. Haukanes, L. S. Håvarstein, and K. Kleppe,

- “Applications of magnetic beads with covalently attached oligonucleotides in hybridization: Isolation and detection of specific measles virus mRNA from a crude cell lysate,” *Anal. Biochem.*, 1990, doi: 10.1016/0003-2697(90)90041-7.
- [140] R. S. M. S. Karumanchi, S. N. Doddamane, C. Sampangi, and P. W. Todd, “Field-assisted extraction of cells, particles and macromolecules,” *Trends in Biotechnology*. 2002, doi: 10.1016/S0167-7799(01)01847-9.
- [141] S. Berensmeier, “Magnetic particles for the separation and purification of nucleic acids,” *Applied Microbiology and Biotechnology*. 2006, doi: 10.1007/s00253-006-0675-0.
- [142] J. Křížová, A. Španová, B. Rittich, and D. Horák, “Magnetic hydrophilic methacrylate-based polymer microspheres for genomic DNA isolation,” in *Journal of Chromatography A*, 2005, doi: 10.1016/j.chroma.2004.12.014.
- [143] J. Stadler, R. Lemmens, and T. Nyhammar, “Plasmid DNA purification,” *Journal of Gene Medicine*. 2004, doi: 10.1002/jgm.512.
- [144] R. M. Satokari, K. Kataja, and H. Söderlund, “Multiplexed quantification of bacterial 16S rRNA by solution hybridization with oligonucleotide probes and affinity capture,” *Microb. Ecol.*, 2005, doi: 10.1007/s00248-004-0136-1.
- [145] T. Hultman, S. Stahl, E. Homes, and M. Uhlén, “Direct solid phase sequencing of genomic and plasmid DNA using magnetic beads as solid support,” *Nucleic Acids Res.*, 1989, doi: 10.1093/nar/17.13.4937.
- [146] E. Blanco, H. Shen, and M. Ferrari, “Principles of nanoparticle design for overcoming biological barriers to drug delivery,” *Nature Biotechnology*. 2015, doi:

10.1038/nbt.3330.

- [147] B. Y. S. Kim, J. T. Rutka, and W. C. W. Chan, “Nanomedicine,” *N. Engl. J. Med.*, vol. 363, no. 25, pp. 2434–2443, Dec. 2010, doi: 10.1056/NEJMra0912273.
- [148] S. Kralj and D. Makovec, “Magnetic Assembly of Superparamagnetic Iron Oxide Nanoparticle Clusters into Nanochains and Nanobundles,” *ACS Nano*, 2015, doi: 10.1021/acsnano.5b02328.
- [149] C. Wang *et al.*, “Iron oxide @ polypyrrole nanoparticles as a multifunctional drug carrier for remotely controlled cancer therapy with synergistic antitumor effect,” *ACS Nano*, 2013, doi: 10.1021/nn4017179.
- [150] M. H. Pablico-Lansigan *et al.*, “Magnetic nanobeads as potential contrast agents for magnetic resonance imaging,” *ACS Nano*, vol. 7, no. 10, pp. 9040–9048, Oct. 2013, doi: 10.1021/nn403647t.
- [151] Y. Cheng, R. A. Morshed, B. Auffinger, A. L. Tobias, and M. S. Lesniak, “Multifunctional nanoparticles for brain tumor imaging and therapy,” *Advanced Drug Delivery Reviews*. 2014, doi: 10.1016/j.addr.2013.09.006.
- [152] M. A. McAteer *et al.*, “In vivo magnetic resonance imaging of acute brain inflammation using microparticles of iron oxide,” *Nat. Med.*, 2007, doi: 10.1038/nm1631.
- [153] P. Foroozandeh and A. A. Aziz, “Insight into Cellular Uptake and Intracellular Trafficking of Nanoparticles,” *Nanoscale Research Letters*. 2018, doi: 10.1186/s11671-018-2728-6.
- [154] Y. J. Li, M. Dong, F. M. Kong, and J. P. Zhou, “Folate-decorated anticancer drug

- and magnetic nanoparticles encapsulated polymeric carrier for liver cancer therapeutics,” *Int. J. Pharm.*, 2015, doi: 10.1016/j.ijpharm.2015.04.028.
- [155] V. Singh and V. Banerjee, “Hysteresis in a magnetic bead and its applications,” *Appl. Phys. Lett.*, 2011, doi: 10.1063/1.3567732.
- [156] D. Chang *et al.*, “Biologically targeted magnetic hyperthermia: Potential and limitations,” *Frontiers in Pharmacology*. 2018, doi: 10.3389/fphar.2018.00831.
- [157] H. S. Huang and J. F. Hainfeld, “Intravenous magnetic nanoparticle cancer hyperthermia,” *Int. J. Nanomedicine*, 2013, doi: 10.2147/IJN.S43770.
- [158] X. Liu *et al.*, “Comprehensive understanding of magnetic hyperthermia for improving antitumor therapeutic efficacy,” *Theranostics*, 2020, doi: 10.7150/thno.40805.
- [159] L. Kafrouni and O. Savadogo, “Recent progress on magnetic nanoparticles for magnetic hyperthermia,” *Prog. Biomater.*, 2016, doi: 10.1007/s40204-016-0054-6.
- [160] J. Y. Lichtenberg, Y. Ling, and S. Kim, “Non-specific adsorption reduction methods in biosensing,” *Sensors (Switzerland)*. 2019, doi: 10.3390/s19112488.
- [161] M. Sun *et al.*, “A correlation study of protein adsorption and cell behaviors on substrates with different densities of PEG chains,” *Colloids Surfaces B Biointerfaces*, 2014, doi: 10.1016/j.colsurfb.2014.06.041.
- [162] Y. Inoue and K. Ishihara, “Reduction of protein adsorption on well-characterized polymer brush layers with varying chemical structures,” *Colloids Surfaces B Biointerfaces*, 2010, doi: 10.1016/j.colsurfb.2010.07.030.
- [163] P. S. Liu, Q. Chen, S. S. Wu, J. Shen, and S. C. Lin, “Surface modification of

- cellulose membranes with zwitterionic polymers for resistance to protein adsorption and platelet adhesion,” *J. Memb. Sci.*, 2010, doi: 10.1016/j.memsci.2010.01.015.
- [164] N. Bunyakul and A. J. Baeumner, “Combining electrochemical sensors with miniaturized sample preparation for rapid detection in clinical samples,” *Sensors (Switzerland)*. 2015, doi: 10.3390/s150100547.
- [165] F. Fang and I. Szleifer, “Kinetics and thermodynamics of protein adsorption: A generalized molecular theoretical approach,” *Biophys. J.*, 2001, doi: 10.1016/S0006-3495(01)76228-5.
- [166] T. A. Horbett and J. L. Brash, “Proteins at Interfaces: Current Issues and Future Prospects,” vol. 22, UTC, 1987, pp. 1–33.
- [167] M. Rabe, D. Verdes, and S. Seeger, “Understanding protein adsorption phenomena at solid surfaces,” *Advances in Colloid and Interface Science*. 2011, doi: 10.1016/j.cis.2010.12.007.
- [168] F. Höök, M. Rodahl, B. Kasemo, and P. Brzezinski, “Structural changes in hemoglobin during adsorption to solid surfaces: Effects of pH, ionic strength, and ligand binding,” *Proc. Natl. Acad. Sci. U. S. A.*, 1998, doi: 10.1073/pnas.95.21.12271.
- [169] P. Parhi, A. Golas, N. Barnthip, H. Noh, and E. A. Vogler, “Volumetric interpretation of protein adsorption: Capacity scaling with adsorbate molecular weight and adsorbent surface energy,” *Biomaterials*, 2009, doi: 10.1016/j.biomaterials.2009.09.005.

- [170] J. E. Contreras-Naranjo and O. Aguilar, “Suppressing non-specific binding of proteins onto electrode surfaces in the development of electrochemical immunosensors,” *Biosensors*. 2019, doi: 10.3390/bios9010015.
- [171] K. C. Dee, D. A. Puleo, and R. Bizios, “Protein-Surface Interactions,” in *An Introduction To Tissue-Biomaterial Interactions*, 2003.
- [172] P. H. Lin and B. R. Li, “Antifouling strategies in advanced electrochemical sensors and biosensors,” *Analyst*. 2020, doi: 10.1039/c9an02017a.
- [173] S. Pan, H. Zhang, W. Liu, Y. Wang, W. Pang, and X. Duan, “Biofouling Removal and Protein Detection Using a Hypersonic Resonator,” *ACS Sensors*, 2017, doi: 10.1021/acssensors.7b00298.
- [174] J. Sabaté del Río, O. Y. F. Henry, P. Jolly, and D. E. Ingber, “An antifouling coating that enables affinity-based electrochemical biosensing in complex biological fluids,” *Nat. Nanotechnol.*, 2019, doi: 10.1038/s41565-019-0566-z.
- [175] J. J. Gooding, “Finally, a simple solution to biofouling,” *Nature Nanotechnology*. 2019, doi: 10.1038/s41565-019-0573-0.
- [176] S. Chen, L. Li, C. Zhao, and J. Zheng, “Surface hydration: Principles and applications toward low-fouling/nonfouling biomaterials,” *Polymer*, vol. 51, no. 23. Elsevier Ltd, pp. 5283–5293, 29-Oct-2010, doi: 10.1016/j.polymer.2010.08.022.
- [177] E. S. Gil and S. M. Hudson, “Stimuli-responsive polymers and their bioconjugates,” *Progress in Polymer Science (Oxford)*. 2004, doi: 10.1016/j.progpolymsci.2004.08.003.

- [178] C. Leng *et al.*, “Probing the Surface Hydration of Nonfouling Zwitterionic and PEG Materials in Contact with Proteins,” *ACS Appl. Mater. Interfaces*, 2015, doi: 10.1021/acsami.5b05627.
- [179] J. B. Schlenoff, “Zwitteration: Coating surfaces with zwitterionic functionality to reduce nonspecific adsorption,” *Langmuir*. 2014, doi: 10.1021/la500057j.
- [180] V. Chechik, R. M. Crooks, and C. J. M. Stirling, “Reactions and reactivity in self-assembled monolayers,” *Adv. Mater.*, 2000, doi: 10.1002/1521-4095(200008)12:16<1161::AID-ADMA1161>3.0.CO;2-C.
- [181] H. Kitano and Y. Taira, “Inclusion of bisphenols by a self-assembled monolayer of thiolated cyclodextrin on a gold electrode,” *Langmuir*, 2002, doi: 10.1021/la020155f.
- [182] W. P. Wuelfing, S. M. Gross, D. T. Miles, and R. W. Murray, “Nanometer gold clusters protected by surface-bound monolayers of thiolated poly(ethylene glycol) polymer electrolyte [16],” *Journal of the American Chemical Society*. 1998, doi: 10.1021/ja983183m.
- [183] T. Goda, M. Tabata, M. Sanjoh, M. Uchimura, Y. Iwasaki, and Y. Miyahara, “Thiolated 2-methacryloyloxyethyl phosphorylcholine for an antifouling biosensor platform,” *Chem. Commun.*, 2013, doi: 10.1039/c3cc44357d.
- [184] T. Goda and Y. Miyahara, “Electrodeposition of Zwitterionic PEDOT Films for Conducting and Antifouling Surfaces,” *Langmuir*, 2019, doi: 10.1021/acs.langmuir.8b01492.
- [185] E. J. Calvo, C. Danilowicz, C. M. Lagier, J. Manrique, and M. Otero,

- “Characterization of self-assembled redox polymer and antibody molecules on thiolated gold electrodes,” *Biosens. Bioelectron.*, 2004, doi: 10.1016/j.bios.2003.11.017.
- [186] B. Lu, E. I. Iwuoha, M. R. Smyth, and R. O’Kennedy, “Development of an ‘electrically wired’ amperometric immunosensor for the determination of biotin based on a non-diffusional redox osmium polymer film containing an antibody to the enzyme label horseradish peroxidase,” *Anal. Chim. Acta*, 1997, doi: 10.1016/S0003-2670(97)00083-4.
- [187] M. A. Pellitero, A. Shaver, and N. Arroyo-Currás, “Critical Review—Approaches for the Electrochemical Interrogation of DNA-Based Sensors: A Critical Review,” *J. Electrochem. Soc.*, 2020, doi: 10.1149/2.0292003jes.
- [188] J. Chen, B. Liu, X. Gao, and D. Xu, “A review of the interfacial characteristics of polymer nanocomposites containing carbon nanotubes,” *RSC Advances*, vol. 8, no. 49, Royal Society of Chemistry, pp. 28048–28085, 02-Aug-2018, doi: 10.1039/c8ra04205e.
- [189] S. P. Schwaminger, P. Fraga-García, M. Eigenfeld, T. M. Becker, and S. Berensmeier, “Magnetic separation in bioprocessing beyond the analytical scale: From biotechnology to the food industry,” *Frontiers in Bioengineering and Biotechnology*. 2019, doi: 10.3389/fbioe.2019.00233.
- [190] J. C. Rife, M. M. Miller, P. E. Sheehan, C. R. Tamanaha, M. Tondra, and L. J. Whitman, “Design and performance of GMR sensors for the detection of magnetic microbeads in biosensors,” *Sensors Actuators, A Phys.*, vol. 107, no. 3, pp. 209–

- 218, Nov. 2003, doi: 10.1016/S0924-4247(03)00380-7.
- [191] M. A. M. Gijs, “Magnetic bead handling on-chip: New opportunities for analytical applications,” *Microfluidics and Nanofluidics*, vol. 1, no. 1. Springer, pp. 22–40, 02-Nov-2004, doi: 10.1007/s10404-004-0010-y.
- [192] F. Li, W. Zhu, T. Zhao, D. Dai, and F. Yang, “Factors influencing droplet size of silicone oil emulsion with high solid content,” *China Pet. Process. Petrochemical Technol.*, 2011.
- [193] A. N. I. Anisa and A. H. Nour, “Affect of Viscosity and Droplet Diameter on water-in-oil (w/o) Emulsions: An Experimental Study,” Feb. 2010, doi: 10.5281/ZENODO.1328970.
- [194] T. R. CROMPTON, “POLYBUTADIENE,” in *The Analysis of Plastics*, Elsevier, 1984, pp. 308–347.
- [195] J. R. Conder, N. A. Fruitwala, and M. K. Shingari, “Thermal decomposition of polyethylene glycol 20m and essential oils in gas-liquid chromatography and the effect of traces of oxygen,” *J. Chromatogr. A*, 1983, doi: 10.1016/S0021-9673(01)90800-3.
- [196] “Chapter 2 Thermal decomposition of polymers,” *Tech. Instrum. Anal. Chem.*, vol. 25, no. C, pp. 31–107, Jan. 2005, doi: 10.1016/S0167-9244(05)80003-4.
- [197] E. T. Tenório-Neto *et al.*, “TGA and magnetization measurements for determination of composition and polymer conversion of magnetic hybrid particles,” *Polymers for Advanced Technologies*. 2015, doi: 10.1002/pat.3562.
- [198] D. H. Napper, “Colloid Stability,” *Ind. Eng. Chem. Prod. Res. Dev.*, vol. 9, no. 4,

- pp. 467–477, 1970, doi: 10.1021/i360036a005.
- [199] T. Hoare and R. Pelton, “Electrophoresis of functionalized microgels: Morphological insights,” in *Polymer*, 2005, doi: 10.1016/j.polymer.2004.11.055.
- [200] M. J. Vold, “Zeta potential in colloid science. Principles and applications,” *J. Colloid Interface Sci.*, 1982, doi: 10.1016/0021-9797(82)90296-x.
- [201] N. Welsch and L. A. Lyon, “Oligo(ethylene glycol)-sidechain microgels prepared in absence of cross-linking agent: Polymerization, characterization and variation of particle deformability,” *PLoS One*, vol. 12, no. 7, p. e0181369, Jul. 2017, doi: 10.1371/journal.pone.0181369.
- [202] J. K. Pandey, K. Raghunatha Reddy, A. Pratheep Kumar, and R. P. Singh, “An overview on the degradability of polymer nanocomposites,” *Polym. Degrad. Stab.*, 2005, doi: 10.1016/j.polymdegradstab.2004.09.013.
- [203] S. Saxena, C. E. Hansen, and L. A. Lyon, “Microgel mechanics in biomaterial design,” *Acc. Chem. Res.*, vol. 47, no. 8, pp. 2426–2434, Aug. 2014, doi: 10.1021/ar500131v.
- [204] C. W. Hung, T. R. P. Holoman, P. Kofinas, and W. E. Bentley, “Towards oriented assembly of proteins onto magnetic nanoparticles,” *Biochem. Eng. J.*, 2008, doi: 10.1016/j.bej.2007.06.017.
- [205] X. Cao, D. Horák, Z. An, and Z. Plichta, “Raft polymerization of N,N-dimethylacrylamide from magnetic poly(2-hydroxyethyl methacrylate) microspheres to suppress nonspecific protein adsorption,” *J. Polym. Sci. Part A Polym. Chem.*, 2016, doi: 10.1002/pola.27939.

- [206] B. Rattier, A. Hoffman, F. Schoen, and J. Lemons, “Biomaterials Science: An Introduction to Materials in Medicine,” *J. Clin. Eng.*, 1997, doi: 10.1097/00004669-199701000-00009.
- [207] D. E. Kuehner, J. Engmann, F. Fergg, M. Wernick, H. W. Blanch, and J. M. Prausnitz, “Lysozyme net charge and ion binding in concentrated aqueous electrolyte solutions,” *J. Phys. Chem. B*, 1999, doi: 10.1021/jp983852i.
- [208] S. J. Attwood, R. Kershaw, S. Uddin, S. M. Bishop, and M. E. Welland, “Understanding how charge and hydrophobicity influence globular protein adsorption to alkanethiol and material surfaces,” *J. Mater. Chem. B*, 2019, doi: 10.1039/c9tb00168a.
- [209] L. Zheng, H. S. Sundaram, Z. Wei, C. Li, and Z. Yuan, “Applications of zwitterionic polymers,” *Reactive and Functional Polymers*, vol. 118. Elsevier B.V., pp. 51–61, 01-Sep-2017, doi: 10.1016/j.reactfunctpolym.2017.07.006.
- [210] D. Sivakumaran, E. Bakaic, S. B. Campbell, F. Xu, E. Mueller, and T. Hoare, “Fabricating degradable thermoresponsive hydrogels on multiple length scales via reactive extrusion, microfluidics, self-assembly, and electrospinning,” *J. Vis. Exp.*, 2018, doi: 10.3791/54502.
- [211] N. M. B. Smeets, E. Bakaic, M. Patenaude, and T. Hoare, “Injectable and tunable poly(ethylene glycol) analogue hydrogels based on poly(oligoethylene glycol methacrylate),” *Chem. Commun.*, 2014, doi: 10.1039/c3cc48514e.
- [212] J. R. Fish, S. G. Swarts, M. D. Sevilla, and T. Malinski, “Electrochemistry and spectroelectrochemistry of nitroxyl free radicals,” *J. Phys. Chem.*, 1988, doi:

10.1021/j100324a012.

- [213] M. Tsunaga, C. Iwakura, and H. Tamura, “Electrode reactions of nitroxide radicals at platinum in acetonitrile,” *Electrochim. Acta*, 1973, doi: 10.1016/0013-4686(73)80020-9.
- [214] Z. Wang, J. He, Y. Tao, L. Yang, H. Jiang, and Y. Yang, “Controlled chain branching by RAFT-based radical polymerization,” *Macromolecules*, 2003, doi: 10.1021/ma025673b.
- [215] J. E. Nutting, M. Rafiee, and S. S. Stahl, “Tetramethylpiperidine N-Oxyl (TEMPO), Phthalimide N-Oxyl (PINO), and Related N-Oxyl Species: Electrochemical Properties and Their Use in Electrocatalytic Reactions,” *Chemical Reviews*. 2018, doi: 10.1021/acs.chemrev.7b00763.
- [216] T. Bürgi, “Properties of the gold-sulphur interface: from self-assembled monolayers to clusters,” *Nanoscale*, 2015, doi: 10.1039/c5nr03497c.
- [217] H. Grönbeck, A. Curioni, and W. Andreoni, “Thiols and disulfides on the Au(111) surface: The headgroup-gold interaction,” *J. Am. Chem. Soc.*, 2000, doi: 10.1021/ja993622x.
- [218] T. Cai, X. Li, C. Wan, and T. S. Chung, “Zwitterionic polymers grafted poly(ether sulfone) hollow fiber membranes and their antifouling behaviors for osmotic power generation,” *J. Memb. Sci.*, 2016, doi: 10.1016/j.memsci.2015.09.037.
- [219] H. Ren, Z. Mei, Y. Chen, S. Chen, Z. Ge, and J. Hu, “Synthesis of zwitterionic acrylamide copolymers for biocompatible applications,” *J. Bioact. Compat. Polym.*, 2018, doi: 10.1177/0883911517707776.

- [220] E. González-Fernández, M. Staderini, N. Avlonitis, A. F. Murray, A. R. Mount, and M. Bradley, “Effect of spacer length on the performance of peptide-based electrochemical biosensors for protease detection,” *Sensors Actuators, B Chem.*, 2018, doi: 10.1016/j.snb.2017.09.128.
- [221] M. Cui, Y. Wang, H. Wang, Y. Wu, and X. Luo, “A label-free electrochemical DNA biosensor for breast cancer marker BRCA1 based on self-assembled antifouling peptide monolayer,” *Sensors Actuators, B Chem.*, 2017, doi: 10.1016/j.snb.2017.01.060.